POWER QUALITY AND INVERTER-GENERATOR INTERACTIONS IN MICROGRIDS

A Thesis
Presented to
The Academic Faculty

by

Andrew Paquette

In Partial Fulfillment
of the Requirements for the Degree
Doctor of Philosophy in the
School of Electrical and Computer Engineering

Georgia Institute of Technology
May 2014

Copyright © 2014 by Andrew D. Paquette

POWER QUALITY AND INVERTER-GENERATOR INTERACTIONS IN MICROGRIDS

Approved by:

Dr. Deepak Divan, Advisor
School of Electrical and Computer Engineering
Georgia Institute of Technology

Dr. Douglas Williams
School of Electrical and Computer Engineering
Georgia Institute of Technology

Dr. Ronald Harley
School of Electrical and Computer Engineering
Georgia Institute of Technology

Dr. Rhett Mayor
School of Mechanical Engineering
Georgia Institute of Technology

Dr. Santiago Grijalva
School of Electrical and Computer Engineering
Georgia Institute of Technology

Date Approved: 01/07/2014

ACKNOWLEDGEMENTS

I would like to thank my advisor, Dr. Divan, for his guidance throughout the PhD program. I have learned important skills from him such as focusing on the storyline and the importance of figuring out the right questions to ask. These soft skills are even more valuable than the technical expertise I have gained from him.

I would like to thank Dr. Harley for all of his support and guidance throughout my time at Georgia Tech. I would also like to thank the rest of my committee members, Dr. Grijalva, Dr. Williams, and Dr. Mayor, for their valuable input and for taking the time to review my thesis.

I have appreciated all the conversations with my lab mates, bouncing ideas off each other and talking about life. So, thank you in particular to Dustin Howard, Diogenes Molina, Rohit Moghe, Matthew Reno and Yi Du.

My wife is awesome and has been a huge help and encouragement throughout the program – thank you. I would like to thank my son for providing all the entertainment we could want since his arrival in my last year of graduate school. I love you two! Finally, I'm thankful to God for his goodness to me and for sustaining me through this time.

TABLE OF CONTENTS

Page

LIST OF TABLES

Page

LIST OF FIGURES

Page

LIST OF SYMBOLS AND ABBREVIATIONS

AVR	Automatic voltage regulator
CERTS	Consortium for Electric Reliability Technology Solutions
CHP	Combined heat and power
DER	Distributed-energy resource
DQ	Direct-quadrature
DSP	Digital signal processor
DVR	Dynamic voltage restorer
DySC	Dynamic sag corrector
FPGA	Field-programmable gate-array
GSGFm	Grid-supporting-grid-forming
GSGFd	Grid-supporting-grid-feeding
HIL	Hardware in the loop
IGBT	Insulated-gate bipolar transistor
IM	Induction motor
NG	Natural gas
PCC	Point of common coupling
PF	Power factor
PI	Proportional-integral
PID	Proportional-integral-derivative
PLL	Phase-locked loop
pu	Per-unit
PV	Photovoltaic
PWM	Pulse width modulation
RMS	Root-mean-square
SG	Synchronous generator
UPS	Uninterruptible power supply

SUMMARY

Microgrids have attracted attention in recent years for their role in the integration of distributed-energy resources (DER), delaying transmission investments by adding generation near load centers, and providing islanded operation during outages. Three main value propositions have been identified for microgrids in this work: improving reliability through islanded operation during outages; providing revenue in grid-connected operation; and improving power quality by rapidly islanding during utility disturbances and outages. Providing improved power quality through seamless islanding is challenging and costly when trying to compete with existing power-quality solutions. However, in most cases the added cost of providing seamless islanding is unnecessary and energy arbitrage or backup are all that is required. This research provides design considerations for microgrids that focus on each of the three main value propositions, enabling solutions that provide the desired functionality without adding unnecessary cost.

Synchronous generators are the most common type of DER, and this research focuses on interactions between inverter based DER and synchronous generators in microgrids. When voltage controlled inverters are operated in parallel with synchronous generators, the inverters exhibit poor transient load sharing, where the inverter picks up the majority of any load step. This restricts the rating of the inverter relative to the largest load step, increases strain on the inverter, and negatively impacts battery life in battery energy-storage inverters. Differences in the frequency regulation characteristics of inverters and synchronous generators are identified as the cause of the poor transient load sharing characteristics. It is shown that equal transient load sharing can be provided by using the inverter to emulate a synchronous generator. Virtual impedance and transient droop are proposed to allow control over the degree of power sharing, and control over the tradeoff between power sharing and power quality.

Instead of mitigating inverter overloads by providing equal transient load sharing, and thus allowing larger voltage and frequency transients, it is often preferable to allow the inverter to provide as much support as possible, and simply current limit when necessary. Current limiting in the presence of other grid-forming DER is complicated for voltage controlled inverters. The use of simple current reference saturation is shown to cause instability. Virtual impedance current limiting is proposed to provide improved transient stability during current limiting with overloads and faults. Current limiting performance during faults in islanded mode is investigated, and it is shown that virtual impedance current limiting provides improved transient stability during current limiting in the presence of synchronous generators compared to traditional current limiting methods.

While the problems associated with poor transient load sharing between voltage controlled inverters and synchronous generators could be avoided by choosing a sufficiently large inverter capable of supplying the largest possible transient, cost constraints will often prohibit microgrid designers from doing so. As the inverter ratings are reduced as much as possible, the transient load sharing problems explored in this thesis will be encountered. The methods proposed in this thesis for mitigating inverter overloads and faults will allow for more reliable and cost effective application of inverter based DER with synchronous generators in microgrids.

CHAPTER 1: INTRODUCTION

1.1. Problem Statement

Microgrids offer many benefits to the grid, and to end customers. Many of the new types of distributed energy resources (DER) are inverter based, such as photovoltaics (PV), wind, microturbines, and fuel cells. Inverters with energy storage enable new functionality such as peak shaving, energy arbitrage, and seamless islanding, i.e. UPS functionality. However, since internal combustion engine driven synchronous generators (SGs) are the most common type of DER with a combined installed capacity exceeding 100,000 MW [1], mostly in backup power applications, it is expected that synchronous generators will play a major role in microgrid installations. It is therefore important to investigate the performance of microgrids when operated with a combination of synchronous generators and inverter based DER.

Voltage controlled inverters with energy storage can operate in grid-connected or islanded mode, and can operate with other grid-forming sources or stand-alone. The need for mode transitions between grid-connected and islanded operation is therefore eliminated. Eliminating mode transitions is beneficial, as experience suggests that most problems occur during mode transitions.

Voltage controlled inverters exhibit poor transient load sharing with synchronous generators in islanded operation. The inverter tends to initially pick up the majority of any load step. This poor transient load sharing restricts the inverter rating relative to the largest load steps, increases stress on the inverter, and decreases battery life by subjecting the battery to larger and more frequent load steps. While transient load sharing problems could be mitigated by selecting a very large inverter, cost constraints would often prohibit this. Cost constraints may force the designer to choose the smallest inverter possible, in which case transient load sharing becomes a significant concern. Voltage controlled

inverters can operate in any mode, but they can be more difficult to control during transients. This research looks at the behavior of voltage controlled inverters during overloads and during current limiting when in parallel with synchronous generators.

1.2. Research Scope and Objectives

The objective of this research is to mitigate inverter overloads caused by poor transient load sharing between inverters and synchronous generators in islanded microgrids. The cause of the poor transient load sharing characteristics are investigated, and the use of virtual impedance and transient droop are proposed to control the transient load sharing characteristics. Inverter current-limiting in the presence of synchronous generators is investigated and virtual impedance current limiting is proposed to provide stable current limiting during overloads. Finally, current limiting during three-phase faults is investigated.

1.3. Outline of Chapters

In Chapter 2, the motivations for microgrid development are described, and a literature survey on the state of the art in control of inverters and generators in microgrids is provided. In Chapter 3, analysis of the value propositions of microgrids is provided, and challenges to providing UPS functionality with microgrids are described. A case study outlines design considerations for microgrids focused on different value propositions. The cause of poor-transient load sharing between inverters and synchronous generators is identified in Chapter 4. In Chapter 5, it is shown that by using an inverter to emulate a synchronous generator, equal transient load sharing is achieved, and overloads are reduced. However, equal transient load sharing comes at the expense of increased voltage and frequency transients. In Chapter 6, the use of virtual impedance and transient droop is proposed to control the degree of transient load sharing. The challenges involved with current limiting in the presence of synchronous generators are described in Chapter 7, and virtual impedance current limiting is proposed to provide stable current limiting

during overloads and three-phase faults. Finally, conclusions, contributions, and topics for future work are described in Chapter 8.

CHAPTER 2: BACKGROUND AND LITERATURE SURVEY

2.1. Introduction

Microgrids have attracted attention in recent years for their role in integration of distributed-energy resources (DER), delaying transmission investments by adding generation near load centers, and providing islanded operation during outages. A microgrid can be defined as a group of sources and loads that have the ability to operate in parallel with, or intentionally separate from the utility. A conceptual microgrid architecture is shown in Fig. 1. Microgrids can simplify the integration of large numbers of DER with the grid by aggregating the control of multiple DER and allowing the utility to interface with the microgrid as a single entity. By operating in islanded mode, DER have the ability to improve reliability by operating in islanded mode during grid disturbances and outages.

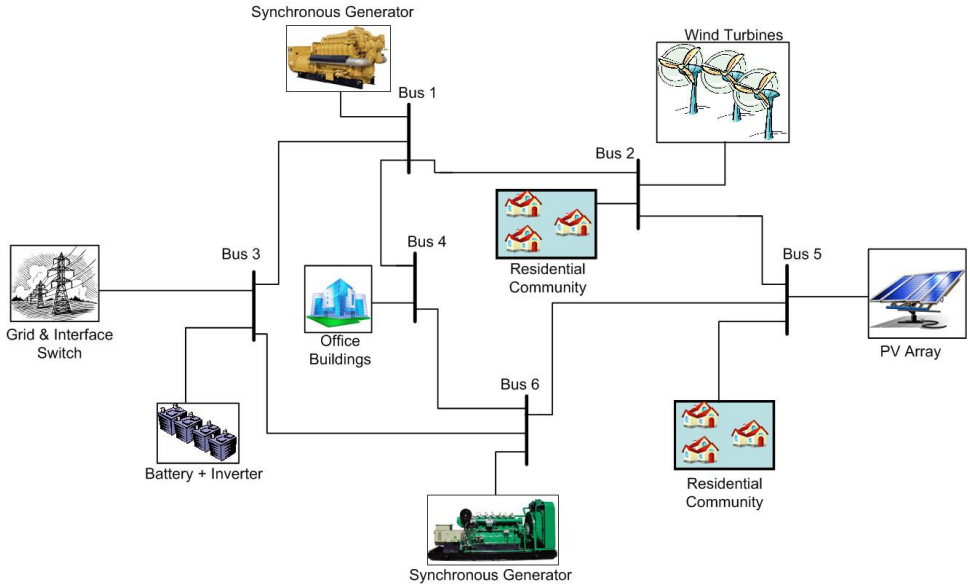

Fig. 1: Conceptual microgrid architecture.

Microgrids have many potential benefits to both utilities and customers [2-10]. Due to continued load growth and minimal investment in transmission infrastructure, existing transmission and distribution systems are becoming increasingly strained. Microgrids, and DER in general, can help meet load growth by placing generation assets

near loads. Placing generation near loads improves efficiency by reducing transmission losses. One of the biggest efficiency improvements can be made by combined heat and power (CHP), where the DER utilizes the waste heat which is normally just dissipated. CHP can improve efficiency from the 30 % – 40 % range to over 90 % [11]. The presence of DER on the distribution system can be used for ancillary services such as voltage regulation and demand response. From a utility perspective, microgrids may be helpful with the integration of large numbers of DER by aggregating multiple DER and controllable loads and interacting with the utility as a single entity, reducing the control burden on the utility [5-7, 9, 12]. Microgrids may also help with integration of large amounts of renewables by using controllable DER for load tracking and smoothing renewables variability. One of the primary benefits of microgrids is improving reliability by operating in islanded mode during grid outages. This may be desirable for a utility or distribution system operator to improve the reliability of a problematic feeder or remote location, or for a customer to provide backup for critical loads. There is also the possibility of rapidly islanding during utility disturbances or faults in order to provide uninterruptible power supply (UPS) functionality.

Based on the different benefits from a utility and customer perspective, there can be different types of microgrids. A utility would typically be interested in distribution microgrids that utilize the general benefits of DER, and possibly utilize islanded operation to improve reliability to meet reliability standards or as a value added service. Customers would be interested in DER's potential to reduce the electricity cost, and to improve reliability or provide UPS functionality. Customers such as the military may also be interested in operating a microgrid in islanded mode for extended periods of time [10], or for permanent off-grid applications in remote areas or physical islands. Based on these requirements, different types of microgrids may include distribution system microgrids, campus microgrids, and microgrids designed for extended islanded operation.

Many types of renewables and distributed generation such as photovoltaics (PV), wind, microturbines, fuel cells, and energy storage interface to the grid through DC/AC inverters. Therefore much of the existing microgrid literature assumes that microgrids will be dominated by inverter-based sources. However, since internal combustion engine driven synchronous generators (SGs) are the most common type of DER, it is expected that synchronous generators will play a major role in microgrid installations. Thus it is important to carefully consider the interaction between inverters and generators.

For stable islanded operation a microgrid requires at least one source that is able to regulate voltage and frequency and respond quickly to changes in load. This requires some form of energy storage or a fast-responding, dispatchable power source. For microgrids the practical choices are generators, or inverters with energy storage. When inverters in voltage control mode operate in parallel with generators, the inverters will transiently supply the majority of any load step. This lack of transient load sharing constrains the inverters to be rated to handle the entirety of the largest possible load step, which may be problematic with high inrush loads, and it negatively impacts battery life in battery energy-storage inverters by increasing the size of transients seen by the inverter. While inverters have short duration overload capabilities, these overloads may not be acceptable for the energy source, with absorbing large negative load steps being especially problematic.

2.2. Control of Inverters in Microgrids

2.2.1. Four Basic Types of Inverter Control

Inverter controls can be categorized into the four basic types [13, 14] shown in Fig. 2, grid-forming, grid-feeding, grid-supporting-grid-forming (GSGFm), and grid-supporting-grid-feeding (GSGFd).

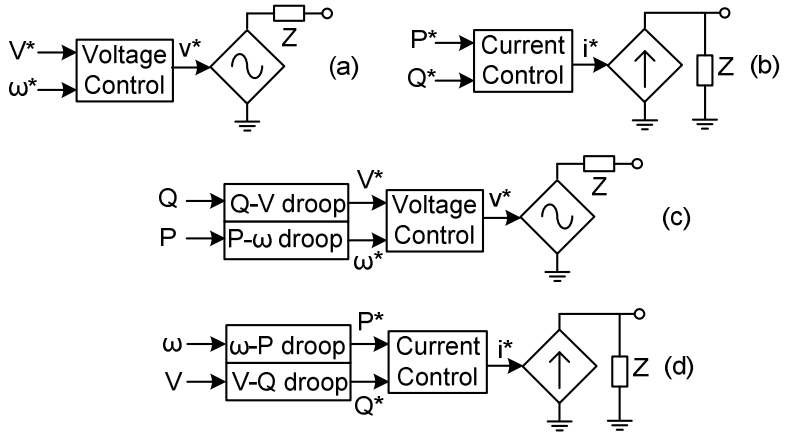

Fig. 2: Four basic types of inverter control (a) grid-forming, (b) grid-feeding, (c) grid-supporting-grid-forming, (d) grid-supporting-grid-feeding.

Grid-forming control acts as a fixed voltage source, and thus is not suitable for paralleling with other grid-forming sources. Small variations in voltage and frequency references would cause the voltage sources to fight against each other, causing large circulating currents and ultimately, instability. Grid-forming sources are typically applied in standalone applications, as they cannot be operated in parallel with the utility.

Grid-feeding control acts as a fixed current source, and the current control typically uses a phase-locked-loop (PLL) to follow the grid voltage. Therefore grid-feeding control is not suitable for operation in microgrids without a grid-forming source to regulate the voltage and does not contribute to voltage and frequency regulation [13, 14]. Many types of renewables such as wind and PV typically use grid-feeding control.

Grid-supporting control supports the grid by adjusting its set points based on the grid conditions. Grid-supporting control can be realized by modification of grid-feeding or grid-forming control.

Grid-supporting-grid-feeding control is a modification of grid-feeding control that acts as a droop controlled current source, where the real and reactive power references are adjusted based on measured voltage and frequency. Grid-supporting-grid-feeding control also typically uses a PLL driven current control, and thus does not work reliably without another source to regulate voltage and frequency. If another voltage source is not

always available, then an inverter with this control must switch to grid-forming or grid-supporting-grid-forming control upon transition to islanding.

Grid-supporting-grid-forming control is a modification of grid-forming control that acts as a droop controlled voltage source, where the voltage and frequency references are adjusted based on measured real and reactive power. This method is capable of operating in parallel with other voltage sources, as the droop control provides stable real and reactive power sharing with other droop controlled voltage or current sources, or stable real and reactive power output in parallel with a fixed voltage source. Using grid-supporting-grid-forming control eliminates the need for rapid mode switching between current and voltage control when generator(s) transition on and off, or when switching from grid-connected to islanded mode. Elimination of mode transitions is a significant benefit, as experience suggests that most problems occur during mode transitions. This thesis focuses on grid-supporting-grid-forming control.

2.2.2. **Droop Control**

Droop control is a popular means of providing stable real and reactive power sharing without communications. Droop control uses voltage and frequency as a means of communication, by allowing the voltage and frequency to sag with increasing power output.

2.2.2.1. Basic Formulation

The basic concept of voltage and frequency droop is based on the power flow between two voltage sources across an inductor, as illustrated in Fig. 3.

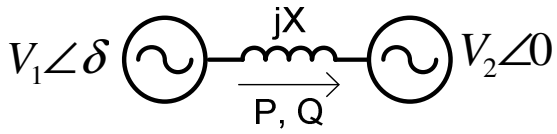

Fig. 3: Power flow between two voltage sources across an inductive impedance.

The real power flow across the inductor is given by:

$$P=\frac{V_1V_2\sin\delta}{X}\approx\frac{V_1V_2\delta}{X}\propto f\,. \tag{1}$$

Assuming that the angle δ is small, sinδ ≈ δ, and the approximation in (1) can be made. Since δ is the integral of the frequency difference between the two voltage sources, the power flow can be controlled by adjusting the frequency. The reactive power flow across the inductor is given by:

$$Q=\frac{V_2(V_2-V_1\cos\delta)}{X}\approx\frac{V_2(V_2-V_1)}{X}\propto V\,, \tag{2}$$

and is proportional to the voltage difference across the inductor. Therefore the reactive power can be controlled by adjusting the voltage.

Equations (1)- (2) lead to the basic idea of droop control: provide reactive power sharing by drooping the voltage in response to reactive power output, and provide real power sharing by drooping the frequency in response to real power output. Voltage and frequency droop are illustrated in Fig. 4, and the voltage and frequency references are given in (3)-(4). In (3)-(4), ω^* is the frequency reference, ω_0 is the nominal frequency, m_P is the frequency droop slope, P is the real power, V^* is the voltage reference, V_0 is the nominal voltage, m_Q is the voltage droop slope, and Q is the reactive power. More thorough treatments of voltage and frequency droop can be found in [14-17], including derivations showing the relative power sharing as a function of the droop parameters.

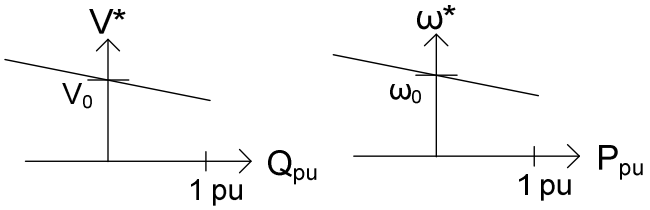

Fig. 4: Voltage and frequency droop.

$$\omega^*=\omega_0-m_PP\,, \tag{3}$$

$$V^*=V_0-m_QQ\,. \tag{4}$$

The primary purpose of droop control is to provide stable real and reactive power sharing without communication [15]. Other control schemes such as isochronous control,

cross-current compensation, and average current sharing have been used, but these require communications for stable operation, and thus are not robust in case of communications failure. Without communication, droop control only provides *stable* power sharing. Any desired optimization, such as monitoring, turning sources on/off, adjusting relative power sharing, adjusting setpoints to restore voltage and frequency to rated values, etc., requires communication. While any practical microgrid would include communication, basic functionality is robust against communications failure, and thus is preferred for microgrids.

2.2.2.2. Variations

The performance of traditional droop control degrades when non idealities are considered. Much of the microgrid literature consists of variations on droop control to address problems such as resistive line impedance, unbalanced line impedance, and harmonic current sharing [13, 17-22].

Droop control is based on the power flow across an inductor, but in the presence of significant resistance, coupling is introduced between the real and reactive power control. The real and reactive power across an impedance Z = R+jX are given by:

$$P=\frac{V_1}{R^2+X^2}\left(R(V_1-V_2\cos\delta)+XV_2\sin\delta\right), \tag{5}$$

$$Q=\frac{V_1}{R^2+X^2}\left(-RV_2\sin\delta+X(V_1-V_2\cos\delta)\right). \tag{6}$$

Resistive line impedance introduces coupling between real and reactive power control, such that adjusting the voltage causes a change in real power, and adjusting frequency causes a change in reactive power. This coupling between the voltage and frequency controls tends to de-stabilize the droop controls, leading to instability in some cases. Common methods to deal with resistive impedance are to add a degree of coupling between the voltage and frequency references to account for the line X/R ratio [18], or to add a large inductor or virtual output impedance to make the overall output impedance

predominantly inductive [17]. In the case of low-voltage cables, where the impedance is predominantly resistive, the control variables can be reversed, since for highly resistive lines real power is primarily a function of voltage and reactive power is primarily a function of frequency [20]. Based on resistive line impedance, [20] proposed to use resistive virtual output impedance and P-V, Q-ω droop, i.e.

$$\omega^* = \omega_0 + m_Q Q\,, \tag{7}$$

$$V^* = V_0 - m_P P\,. \tag{8}$$

Droop control provides equal real power sharing, since frequency is the same at all points in steady state. However, equal reactive power sharing is not guaranteed since the voltage varies throughout the microgrid due to voltage drop across line impedances. Reactive power sharing can be degraded significantly with unbalanced line impedances, i.e. different impedance between two sources and a load bus, such as when one source is closer to a load bus than another source. The main solutions for improving reactive power sharing are virtual output impedance or adaptive droop [19, 23]. Harmonic current sharing is typically achieved with harmonic droops, or virtual output impedance to give each inverter similar output impedance at harmonic frequencies [22].

In this work the traditional droop control is used, because in the author's opinion, it is preferable to use the simplest control strategy that works acceptably well. Even though the impedance in the low voltage experimental microgrid setup used in this thesis has an X/R ratio less than one, traditional droop control gives acceptable performance.

2.2.3. **Inverter Plant Model**

The circuit diagram for a three-phase, three-wire, voltage-source inverter with an LC filter is shown in Fig. 5. Three-phase four-wire inverters that have a neutral wire connected either to the DC bus midpoint or a fourth inverter leg are possible, but are not considered in this research. If it is necessary to supply single-phase loads with a three-

wire inverter, an output delta-wye transformer can be used. The differential equations governing the inductor current and output voltage are given in (9) and (10).

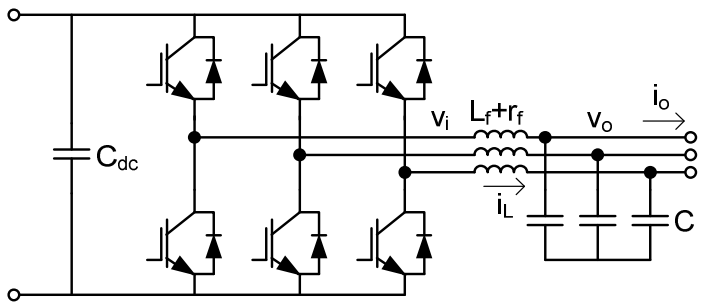

Fig. 5: Circuit diagram of three-phase, three-wire, voltage-source inverter.

$$\begin{bmatrix} v_{oa} \\ v_{ob} \\ v_{oc} \end{bmatrix} = -\begin{bmatrix} r_f & 0 & 0 \\ 0 & r_f & 0 \\ 0 & 0 & r_f \end{bmatrix}\begin{bmatrix} i_{La} \\ i_{Lb} \\ i_{Lc} \end{bmatrix} - \begin{bmatrix} L_f & 0 & 0 \\ 0 & L_f & 0 \\ 0 & 0 & L_f \end{bmatrix}\begin{bmatrix} d/dt(i_{La}) \\ d/dt(i_{Lb}) \\ d/dt(i_{Lc}) \end{bmatrix} + \begin{bmatrix} v_{ia} \\ v_{ib} \\ v_{ic} \end{bmatrix}. \tag{9}$$

$$\begin{bmatrix} i_{oa} \\ i_{ob} \\ i_{oc} \end{bmatrix} = -\begin{bmatrix} i_{La} \\ i_{Lb} \\ i_{Lc} \end{bmatrix} + \begin{bmatrix} C & 0 & 0 \\ 0 & C & 0 \\ 0 & 0 & C \end{bmatrix}\begin{bmatrix} d/dt(v_{oa}) \\ d/dt(v_{ob}) \\ d/dt(v_{oc}) \end{bmatrix}. \tag{10}$$

The inverter pole voltage, v_i, is synthesized using pulse-width modulation, and the LC filter acts as a low-pass filter to filter out the switching harmonics. Space-vector modulation is used to calculate the switch duty cycles [24]. The space-vector algorithm in [25] has been used in this work. Since the space-vector PWM algorithm accounts for the dc bus voltage in the duty cycle calculation, and it is assumed that the inverter has appropriately sized energy storage, dc bus dynamics are neglected in this work.

2.2.4. **DQ Transformation**

In the natural reference frame, or the abc frame, the phase quantities are sinusoidal, and thus most of the traditional control methods designed for regulating dc quantities cannot be used directly. However, if the reference frame is rotated at the synchronous frequency, as shown in Fig. 6, positive sequence phase quantities become constant. This technique was first proposed by R. H. Park in the late 1920's for analysis of synchronous machines, and has since been expanded to generic ac machines and ac

systems [26]. The dq transformation which transforms natural reference frame quantities f_a, f_b, f_c into dq frame quantities f_d, f_q, f_0 is given by (11), and the inverse transformation is given by (12). Note that this research only considers three-wire inverters, and since there is no path for zero sequence current, f_0 can be neglected.

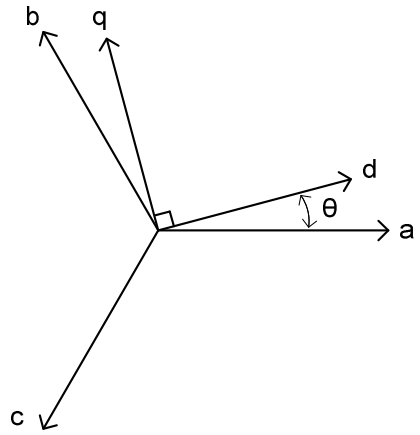

Fig. 6: Dq reference frame transformation.

$$\begin{bmatrix} f_d \\ f_q \\ f_0 \end{bmatrix} = \frac{2}{3}\begin{bmatrix} \cos(\theta) & \cos(\theta-2\pi/3) & \cos(\theta+2\pi/3) \\ -\sin(\theta) & -\sin(\theta-2\pi/3) & -\sin(\theta+2\pi/3) \\ 1/2 & 1/2 & 1/2 \end{bmatrix}\begin{bmatrix} f_a \\ f_b \\ f_c \end{bmatrix}. \tag{11}$$

$$\begin{bmatrix} f_a \\ f_b \\ f_c \end{bmatrix} = \begin{bmatrix} \cos(\theta) & \sin(\theta) & 1 \\ \cos(\theta-2\pi/3) & -\sin(\theta-2\pi/3) & 1 \\ \cos(\theta+2\pi/3) & -\sin(\theta+2\pi/3) & 1 \end{bmatrix}\begin{bmatrix} f_d \\ f_q \\ f_0 \end{bmatrix}. \tag{12}$$

Applying the dq transformation to (9) and (10) gives (13) and (14).

$$\begin{bmatrix} v_{od} \\ v_{oq} \end{bmatrix} = -\begin{bmatrix} r_f & 0 \\ 0 & r_f \end{bmatrix}\begin{bmatrix} i_{Ld} \\ i_{Lq} \end{bmatrix} - \begin{bmatrix} L_f & 0 \\ 0 & L_f \end{bmatrix}\begin{bmatrix} d/dt(i_{Ld}) \\ d/dt(i_{Lq}) \end{bmatrix} + \begin{bmatrix} 0 & -\omega \\ \omega & 0 \end{bmatrix}\begin{bmatrix} i_{Ld} \\ i_{Lq} \end{bmatrix} + \begin{bmatrix} v_{id} \\ v_{iq} \end{bmatrix}. \tag{13}$$

$$\begin{bmatrix} i_{od} \\ i_{oq} \end{bmatrix} = -\begin{bmatrix} i_{Ld} \\ i_{Lq} \end{bmatrix} + \begin{bmatrix} C & 0 \\ 0 & C \end{bmatrix}\begin{bmatrix} d/dt(v_{od}) \\ d/dt(v_{oq}) \end{bmatrix} + \begin{bmatrix} 0 & -\omega \\ \omega & 0 \end{bmatrix}\begin{bmatrix} v_{od} \\ v_{oq} \end{bmatrix}. \tag{14}$$

In the synchronous rotating reference frame, $\theta = \omega t$, where ω is the synchronous frequency. If $\omega = 0$, then $[f_d \ \ f_q \ \ f_0]^T = [f_\alpha \ \ f_\beta \ \ f_0]^T$, and it is called the stationary, or αβ, reference frame.

In this work, the inverter quantities per-unitized with base voltage $v_b=V_{ph}\sqrt{2}$, and base current $i_b=I_{ph}\sqrt{2}$, where V_{ph} is the rated line-neutral phase voltage, and I_{ph} is the rated line current. Base power is then expressed as $S_b=3/2v_bi_b$. Based on instantaneous power theory [27], instantaneous real power $\tilde{p}$ and reactive power $\tilde{q}$ can be expressed as

$$\tilde{p}=3/2(v_d i_d+v_q i_q), \tag{15}$$

$$\tilde{q}=3/2(v_d i_q-v_q i_d). \tag{16}$$

In dq, the instantaneous three-phase voltage magnitude $\tilde{v}$ can be expressed as

$$\tilde{v}=\sqrt{v_d^2+v_q^2}. \tag{17}$$

Either αβ or dq quantities can be used in (15)-(17).

In the synchronous dq frame, positive sequence fundamental components become constant, but other quantities such as negative sequence and harmonics are not constant. Negative sequence fundamental components rotate at –ω, and thus when transformed into the synchronous dq frame, which rotates at +ω, the negative sequence fundamental components rotate at 2ω, or 120 Hz. In the synchronous dq frame, positive sequence harmonics (n = 7, 13, etc.) rotate at (n-1)ω, negative sequence harmonics (n = 5, 11, etc.) rotate at (n+1)ω, and zero sequence harmonics (n = 3, 9, etc.) rotate at nω.

2.2.5. **Voltage and Current Control**

Voltage and current regulators are used in voltage-source inverters to control the output current and/or voltage. There are many types of regulators, and different types of regulators are applied in different reference frames. The most common are synchronous frame proportional-integral (PI) controllers, and αβ or abc frame proportional-resonant (PR) controllers. Various non-linear regulators have been developed such as predictive deadbeat, hysteresis, and sliding mode [13, 28, 29]. Since this thesis focuses on balanced operating conditions, only synchronous frame PI control has been implemented.

2.2.5.1. Synchronous Frame PI Control

A PI controller consists of a proportional and integral term, and is capable of eliminating steady state error at dc. The transfer function for a PI controller, $G_c(s)$, is given in (18).

$$G_c(s) = \left(k_p + k_i / s\right). \tag{18}$$

PI controllers have been applied for voltage and current regulation in the natural abc frame or stationary αβ frame, but are generally considered unsatisfactory because of the significant steady state error due to the PI controller's finite gain at non-zero frequencies [30].

As stated previously, balanced sinusoidal phase quantities are transformed into dc in the synchronous dq reference frame. PI regulators have infinite gain at dc, and thus can be used to track reference sinusoids with zero steady state error in the synchronous dq frame. However, components which are not rotating at the synchronous frequency, such as negative sequence or harmonics, are not dc in the synchronous frame. Since PI regulators have significant steady state error at non-zero frequencies, modifications are necessary if negative sequence or harmonic components need to be controlled. This can be done by having multiple dq transformations rotating at the frequencies of interest, i.e., (n-1)ω for positive sequence harmonics, (n+1)ω for negative sequence harmonics, 2ω for negative sequence fundamental, and nω for zero sequence harmonics. Alternatively, proportional-integral-resonant controllers may be used.

2.2.5.2. Stationary Frame PR Control

The proportional-resonant controller in the αβ or abc frame is mathematically similar to a synchronous PI controller transformed into the stationary frame [30]. The transfer function for a PR regulator is given in (19).

$$G_c(s) = k_p + k_i \frac{s}{s^2 + \omega_0^2}. \tag{19}$$

The PR controller has infinite gain at the controller resonant frequency, ω_0, and thus can be used to track a reference sinusoid in the stationary frame with zero steady state error [13, 28, 30]. In practical applications, the infinite gain at the resonant frequency can lead to numerical stability problems, and so a damped version of the resonant controller can be used that has a large, finite gain at the resonant frequency [30]. This controller has attracted significant attention in recent years due to its implementation in the stationary frame, straight-forward extension to compensation of multiple low-order harmonics, inherent ability to regulate negative sequence components, and lack of coupling terms [13]. Ability to regulate negative sequence is a significant advantage over synchronous dq regulators, which typically require separate positive and negative sequence regulators, or addition of a 120 Hz resonant controller.

2.2.5.3. DQ Current Control

DQ PI control is commonly used for current control in inverters. A typical implementation of dq current control is shown in Fig. 7, which includes optional output voltage feed-forward and decoupling terms [13, 28]. The control in Fig. 7 is grid-feeding control, where the dq transformation angle is given by a conventional dq phase-locked-loop (PLL) [31]. The dq PLL aligns the q-axis with the grid voltage by converting the grid voltage to dq, driving the d-axis voltage to zero with a PI controller, and feeding the integral of the PI output back as the dq transformation angle.

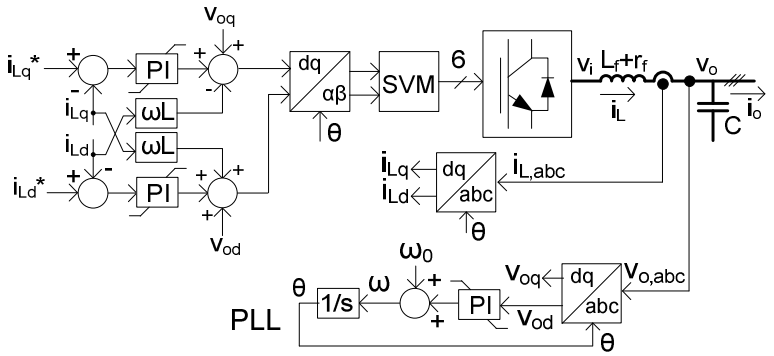

Fig. 7: DQ current control.

The inductor current transfer functions in dq can be written as:

$$i_{Ld} = \frac{1}{sL_f + r_f}\left(v_{id} - v_{od} + \omega L_f i_{Lq}\right), \tag{20}$$

$$i_{Lq} = \frac{1}{sL_f + r_f}\left(v_{iq} - v_{oq} - \omega L_f i_{Ld}\right). \tag{21}$$

By feeding-forward the output voltage and the inductor voltage drop coupling term, the current controller can be made into a single-input-single-output transfer function, neglecting the PWM delay associated with v_{id} and v_{iq}. Equations (20)-(21) are the motivation for the output voltage feed-forward and decoupling terms commonly used in dq current control.

2.2.5.4. DQ Voltage Control

DQ PI control is also commonly used for voltage control of inverters. A typical implementation of dq voltage control is shown in Fig. 8, which includes capacitor current feed-forward and output current feed-forward [32-34]. The control in Fig. 8 is composed of an outer voltage loop and an inner current loop, and is referred to as multi-loop voltage control. The voltage control also includes virtual impedance, where the voltage drop across a virtual impedance is subtracted from the voltage reference. Virtual impedance is discussed in more detail in Section 2.2.5.6.

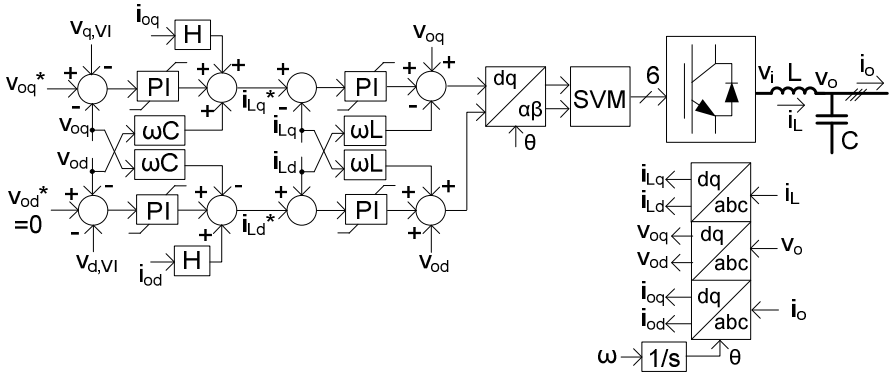

Fig. 8: Multi-loop dq voltage control.

The dq capacitor voltage transfer functions in dq can be written as:

$$v_{od} = \frac{1}{sC}\left(i_{Ld} - i_{od} + \omega C v_{oq}\right), \tag{22}$$

$$v_{oq} = \frac{1}{sC}\left(i_{Lq} - i_{oq} - \omega C v_{od}\right). \tag{23}$$

The capacitor current feed-forward terms $\omega C v_{od}$ and $\omega C v_{oq}$, and the output current feed-forward terms Hi_{od} and Hi_{oq} in Fig. 8, are intended to eliminate those terms from the closed-loop transfer function and improve the dynamics of the voltage control loop.

The dq transformation angle is obtained by integrating the frequency reference. The frequency reference may be a constant, as in grid-forming control, or given by droop, as in grid-supporting-grid-forming control.

2.2.5.5. Single-loop vs. Multi-loop Voltage Control

There are two main variations of voltage control: multi-loop and single-loop, shown in Fig. 9.

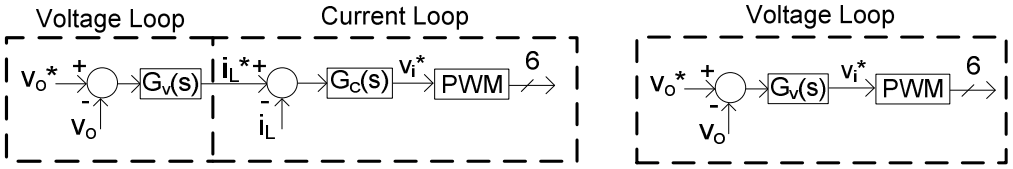

Fig. 9: Multi-loop (left) and single-loop (right) voltage control.

Single-loop control is based on having a single regulator that adjusts inverter voltage based on measured output voltage. Multi-loop control uses cascaded voltage and current loops, where the outer loop voltage regulator provides the reference to an inner loop current regulator.

Multi-loop control is typically preferred for its superior disturbance rejection performance and current limiting capability [35]. However, single-loop control is also used, most notably in the inverter control used by the Consortium for Electric Reliability Technology Solutions (CERTS) [36, 37], which is currently the most advanced microgrid research program in the United States in terms of testing and pilot installations.

2.2.5.6. Virtual Impedance

Virtual output impedance is a fast control loop that subtracts the voltage drop across a virtual output impedance from the voltage reference [13, 14, 17-23, 38], as illustrated by Fig. 10.

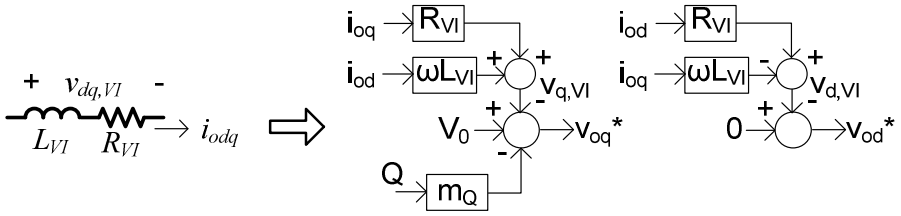

Fig. 10: Virtual impedance.

Virtual impedance is frequently used for controlling the output impedance to improve stability, and for current limiting [13, 19, 20, 38, 39]. In inverter-based microgrids, impedance has a significant impact on stability, and virtual impedance has been used to provide stable operation [13].

In the dq frame, the voltage drop across a virtual impedance, $Z_{VI} = R_{VI}+j\omega L_{VI}$, is given by:

$$v_{d,VI} = R_{VI} i_{od} - \omega L_{VI} i_{oq}, \tag{24}$$

$$v_{q,VI} = R_{VI} i_{oq} + \omega L_{VI} i_{od}. \tag{25}$$

2.3. Control of Synchronous Generators in Microgrids

This research is focused on relatively small synchronous generators in the range of tens of kW to a few MW used in backup and distributed generation applications. The focus is therefore on modern electronic governor and automatic voltage regulator (AVR) control systems used for internal combustion engine driven generators. The basic control diagram for a synchronous generator is shown in Fig. 11.

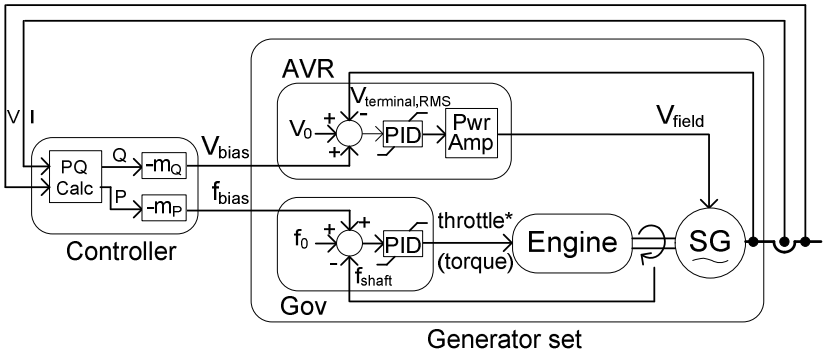

Fig. 11: Generator control where droop terms bias AVR and governor references.

The synchronous generator excitation system block diagram is shown in Fig. 12. It is composed of an AVR and brushless exciter, and its function is to regulate the terminal voltage. In modern digital AVRs a PID regulator is commonly used, the output of which goes to a power amplifier that supplies the exciter [40, 41]. The AVR typically has an analog bias input that can be used for a power system stabilizer, or an external generator controller, which in this case is used to apply reactive droop. The AVR may include extra functions such as a V/Hz function, where the voltage reference is decreased in proportion to the measured frequency to assist recovery from load steps by reducing the electrical output power. Brushless exciters are common in small to medium size synchronous generators, and in this system the dc excitation voltage is provided through another set of windings that produces ac on the shaft. This is rectified by shaft mounted diodes, the output of which goes to the field winding [42]. The excitation system in Fig. 12 is similar to the IEEE AC5A simplified brushless exciter model [43], except for using a PID regulator. In Fig. 12, k_p, k_i, k_d, T_d, T_A, T_E, K_E, and S_E are the proportional gain, integral gain, derivative gain, derivative time constant, voltage regulator time constant, exciter time constant, exciter gain, and exciter saturation functions, respectively.

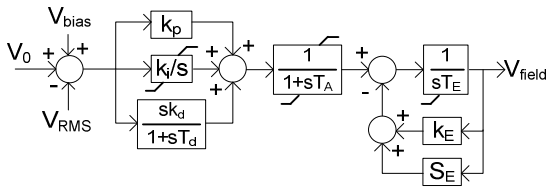

Fig. 12: Model of AVR and brushless exciter.

The governor measures the shaft speed and adjusts the engine throttle position to regulate the speed to the desired set point. A basic model for the diesel engine and governor is shown in Fig. 13, where the governor uses PID control, and the diesel engine is modeled as an actuator time constant and time delay [44, 45]. In Fig. 13, k_p, k_i, k_d, T_d, T_1, T_2, B, H, T_m, T_L, and ω_m are the proportional gain, integral gain, derivative gain, derivative time constant, actuator time constant, delay time, friction constant, pu inertia constant of the engine and generator, mechanical torque, load torque, and mechanical speed, respectively. Therefore the output of the PID controller sets the torque command. The time delay represents the inherent time delay between cylinder firings. The governor typically also has a bias input that may come from an automatic generation control (AGC) system, or an external generator controller for implementing droop or isochronous control.

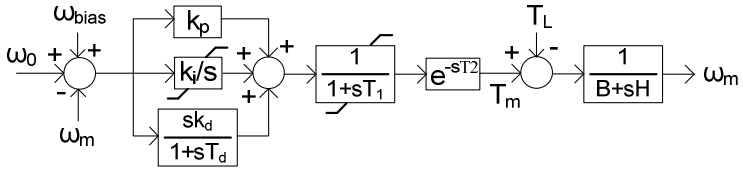

Fig. 13: Model of governor and diesel engine.

2.4. Microgrids with Inverters and Synchronous Generators

Most of the existing microgrid research focuses on inverter controls for inverter-based microgrids. However, synchronous generators are most common type of DER [1], and are reliable and cost effective. Therefore it is important to consider the interactions of inverters and synchronous generators in microgrids. Hybrid systems with renewables and generators are popular for ability to reduce fuel consumption, particularly in remote areas where fuel cost is high [44]. Unlike grid-feeding inverters, grid-supporting inverters have the capability to assist with voltage and frequency regulation and to operate when the generator is unavailable or intentionally turned off. Grid-supporting inverter controls are

the focus of this research, and this section gives an overview of the existing research on grid-supporting inverters and synchronous generators in microgrids.

2.4.1.1. Grid-Supporting-Grid-Feeding Inverter Control

Grid-supporting-grid-feeding inverter control has been proposed for operation in microgrids, and has demonstrated the real and reactive power sharing without communications provided by droop. Most of the literature on grid-supporting-grid-feeding control with synchronous generators focuses on basic operation, and analyzes system damping and stability. A diagram showing a typical configuration of grid-supporting-grid-feeding inverter is shown in Fig. 14 [46-48]. The current reference is obtained from the power references, which are derived from ω-P and V-Q droop, i.e.:

$$P^* = \frac{1}{m_P}(\omega_0 - \omega), \tag{26}$$

$$Q^* = \frac{1}{m_Q}(V_0 - V). \tag{27}$$

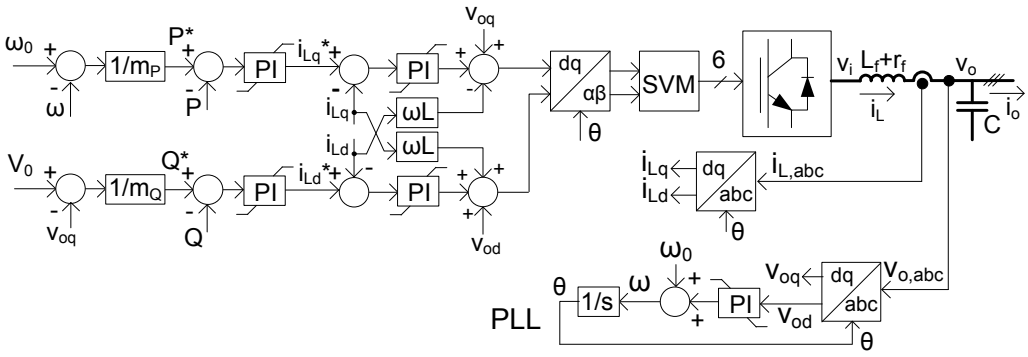

Fig. 14: Grid-supporting-grid-feeding inverter control.

References [46, 47] use small-signal analysis to study the stability of an islanded microgrid with multiple grid-supporting-grid-feeding inverters and a synchronous generator. In [47], the small-signal analysis concluded that the eigenvalues corresponding to the generator's mechanical oscillations were dominant, and that when the inverters supply more of the load the system damping is increased. In [46] it is also concluded that

the eigenvalues corresponding to the generator's mechanical oscillations are dominant, and that the generator droop slope has a significant impact on stability.

2.4.1.2. Grid-Supporting-Grid-Forming Inverter Control

Grid-supporting-grid-forming inverter control is commonly proposed for microgrid operation [5, 6, 49, 50], [4, 20, 23, 32], and is more common than grid-supporting-grid-feeding control [14]. The literature on generators and grid-supporting-grid-forming inverters mostly focuses on showing basic functionality. In [51, 52], a synchronous generator with voltage and frequency droop is combined with the CERTS single loop grid-supporting-grid-forming inverter control. The basic features of droop are demonstrated between the inverter and synchronous generator, such as stable real and reactive power sharing and transition between grid-connected and islanded modes. In [53] the transient load sharing characteristics of synchronous generators and grid-supporting-grid-forming inverters are investigated, and grid-supporting-grid-feeding control methods are proposed to improve the load sharing. In [54] the addition of a synchronous generator to a multi-loop grid-supporting-grid-forming inverter control is considered, but that uses P-V, Q-ω droop based on the assumption of highly resistive line impedance. Since generators naturally droop their frequency in response to real power changes, they are not directly compatible with the P-V, Q-ω droop scheme, so modifications are made to the generator control to make it compatible.

The problem of transient load sharing between inverters and generators has been identified in the literature, but the fundamental cause has not been investigated thoroughly.

2.5. Chapter Conclusion

Synchronous generators will play an important role in microgrids, because they are trusted and cost effective in backup power applications. Inverters enable functions such as seamless islanding, which provides added value for end users. Inverters operating

in grid-supporting-grid-forming mode are able to operate in any mode – grid-connected or islanded, and with or without other grid-forming sources. Elimination of control mode transitions is beneficial, as experience suggests that most problems occur during mode transitions. There is a need to investigate the performance of microgrids with synchronous generators and inverters, but this area has not been investigated thoroughly in the literature. Specifically, the transient interactions between inverters and synchronous generators need to be explored in greater detail.

Before exploring generator-inverter interactions, a study of microgrid value propositions is made. This study analyzes an important topic that is largely missing from the microgrid literature: how to distinguish between what is technically feasible and how to derive economic value.

CHAPTER 3: DESIGN CONSIDERATIONS FOR POWER QUALITY MICROGRIDS

3.1. Common Assumptions in Microgrids

A survey of the 20 most frequently cited microgrid papers [2, 4-9, 12, 17, 18, 20, 23, 32, 38, 47, 49, 50, 55-57] from the last 10 years has been conducted to analyze the motivations for microgrid development and common assumptions. Note that this search was limited to papers specifically referring to microgrids to avoid subjectivity in deciding what qualifies as a microgrid paper, and citation counts from Google Scholar as of July 2012 were used. Some of the important assumptions made in these papers are listed below, along with how many of the 20 papers made the assumption:

- Seamless islanding is desired to improve power quality (13/20)
- Primarily inverter based sources will be used in microgrids (13/20)
- Energy storage is required for transients and load steps, i.e. fully dispatchable inverters (16/20)
- Peak shaving, integration of renewables, combined heat and power (CHP), etc. are primary objectives, i.e. energy arbitrage (17/20)

These assumptions about microgrids are important for many reasons. Seamless islanding impacts inverter ratings, energy storage requirement, interconnection switch type, cost, etc. The choice of inverter vs. synchronous generator based sources impacts the ratings of sources due to differences in overload capacity, and it also impacts energy storage requirements due to lack of inertia in most inverter based sources. The requirement for energy storage significantly impacts cost. Energy arbitrage is important as it is seen as the main value proposition of distributed energy resources (DER) and microgrids. The term energy arbitrage is used in this thesis to describe anything intended to provide economic value in grid connected operation, such as peak shaving, integration of renewables, CHP, ancillary services, etc. While only 13 of the 20 references assumed

seamless islanding, only one assumed non-seamless islanding and the others did not specify whether or not islanding should be seamless. The assumption of using primarily inverter based sources is common, but not universal, as seen by the seven references that assumed synchronous generators are used. Often when synchronous generators are used, it is assumed that storage is not necessary, as in the case of the four references that did not assume fully dispatchable inverters. This survey shows that these four listed assumptions are very prevalent in the microgrid literature. The impact of these assumptions on microgrid designs, costs, and feasibility is the main focus of this chapter.

One of the main underlying assumptions upon which much of the existing microgrid research is based is that customers need better power quality than what the power grid offers. However, improved power quality, i.e. uninterruptible power supply (UPS) functionality, is only necessary for loads that are sensitive to momentary disturbances and have a demonstrably high cost of downtime. Sensitivity to momentary disturbances is an important factor that distinguishes loads that need UPS functionality from loads that only need backup. While there is a large market for improved power quality, most notably in datacenters and sensitive manufacturing processes, this market is well developed. The examination of existing power quality solutions in Section 3.2.1 shows that microgrids with seamless islanding will face significant barriers in competing in the power quality market because of cost and customer perception against exposing critical loads to any disturbances. Note that in this chapter improved power quality refers primarily to compensation of short duration voltage sags, i.e. UPS functionality. In this chapter improved reliability refers to traditional power system reliability indices (system-average-interruption-duration index (SAIDI), system-average-interruption-frequency index (SAIFI), etc.), which consider only outages. Other power quality problems must be dealt with when designing microgrids, but this chapter focuses on voltage sags because of the impact on energy storage requirements, system architectures, and cost.

If microgrids can provide seamless islanding at low or zero marginal cost, then seamless islanding may receive widespread adoption. However, islanded operation brings up many challenges and costs not encountered with grid connected operation [58], and thus providing seamless islanding at low or zero marginal cost is unlikely. In [59] the marginal cost of islanding functionality over purely grid connected DER (i.e. microgrid vs. virtual power plant) is evaluated. It is concluded that any interconnection switch more expensive than a thyristor based static switch (e.g. IGBT based switch or back-to-back inverter) is not economical. That conclusion is based on the optimistic assumption that the only additional cost for a microgrid with islanding functionality over purely grid connected operation is the interconnection switch. It has been pointed out that microgrids with multi-cycle response times would be satisfactory in many applications [3], but it is questionable whether the customers in those applications could justify paying extra for that feature.

The focus on microgrids with seamless islanding inherently assumes that providing improved power quality for large sections of the load is desirable. However, the critical loads for which there is a demonstrable return on investment (ROI) for improved power quality is normally a small fraction of the total load [60]. Providing improved power quality for more loads than necessary is expensive. Additionally, attempting to provide improved power quality for a large group of loads reduces the power quality/reliability compared to providing compensation at the point of load, due to the increased probability of faults within the protected zone [61]. This chapter shows some of the primary ways that providing improved power quality in microgrids significantly increases cost over providing non-seamless backup and energy arbitrage, specifically how high inrush loads and realistic grid disturbances impact inverter and energy storage ratings.

In the microgrid space, there is a need to distinguish between what is technically feasible and how to derive economic value. A "one-size fits all" approach of microgrid design where every microgrid has energy storage, the ability to seamlessly island, solely inverter-based sources, active filtering, etc. is not appropriate and will drive up costs. This thesis identifies three main value propositions for microgrids and defines three types of microgrids focused on each value proposition:

- Reliability: Improve reliability by providing backup during outages.
- Energy arbitrage: Provide revenue in grid connected operation through peak shaving, CHP, renewables, demand response, ancillary services, etc.
- Power quality: Improve power quality by rapidly islanding during utility disturbances, i.e. UPS functionality.

By focusing on the main functions provided by microgrids, architectures can be identified to provide those functions in the most cost effective manner.

3.2. Challenges for Power-Quality Microgrids

A summary of existing power-quality solutions provides insight into the competition power-quality microgrids will face. Competing with existing power-quality solutions is necessary because experience suggests that most customers cannot justify paying extra for improved power quality, and those who can justify it have strong perceptions against exposing their mission-critical loads to disturbances. Providing 1/4 cycle response is important for providing a similar level of performance as existing power-quality solutions, but force commutating the static switch in distributed line-interactive microgrids is difficult.

3.2.1. Existing Power-quality Solutions

For critical loads a short power-quality event can result in long process shutdowns, loss of critical data, etc. Much research has been performed to understand

power-quality events and their impact on sensitive loads, to gather statistics on their types, frequency, and severity, and to develop products to mitigate their impact [62-64].

Two main approaches are used to protect sensitive loads: series-connected devices like the dynamic voltage restorer (DVR) or dynamic sag corrector (DySC) that restore the voltage to the load by injecting the missing voltage, or shunt-connected devices like the uninterruptible power supply (UPS) that rapidly isolate the load from grid disturbances and supply it from stored energy [64]. Three main types of existing power-quality solutions of particular relevance to power-quality microgrids are shown in Fig. 15. Power-quality solutions vary in their depth of compensation, ride through duration, energy-storage requirement, and cost. Depth of compensation and ride through are important parameters, as they determine what percentage of power-quality events will be protected against.

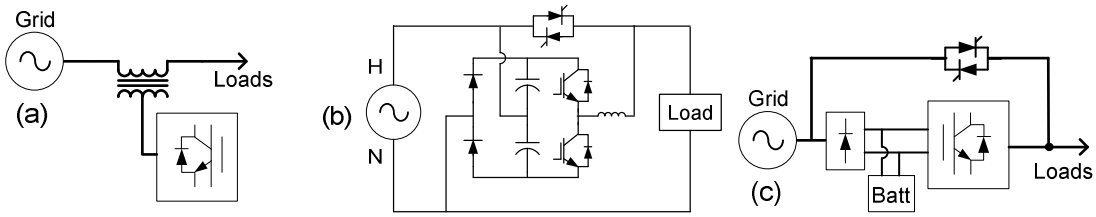

Fig. 15: Existing power-quality solutions, (a) dynamic voltage restorer, (b) dynamic sag corrector [63], (c) double-conversion UPS.

3.2.1.1. Competition with Industrial Sag Correctors

Industrial sag correctors such as the DVR and DySC are designed to protect against 80 % – 96 % of power-quality events by riding through short duration disturbances (< 2 s) with minimal energy storage [63, 64]. Industrial sag correctors are normally only applied to a small fraction of the total load [60], and the facilities where they are applied are often connected to high reliability utility feeds where long duration disturbances (> 2 s) and outages are rare. Therefore, the marginal cost of protecting against the remaining few percent of disturbances by providing backup and energy storage for most or all of the loads, i.e. UPS plus backup, is prohibitively high. Power-

quality microgrids take a similar approach to UPS plus backup solutions, and are therefore expected to face significant cost barriers in competing with industrial sag correctors. Only if power-quality microgrids can drastically reduce the total cost of ownership by integrating energy arbitrage might they be competitive with industrial sag correctors. However, if energy arbitrage is desired, it may still be cheaper to use sag correctors for critical loads, and simply add the desired amount of grid-connected energy-arbitrage sources.

3.2.1.2. Competition with UPSs

A look at the UPS market indicates that the distributed line-interactive microgrid architecture will face significant barriers competing with UPSs in the power-quality market due to customer perception against exposing critical loads to grid disturbances. IEC 62040-3 classifies UPSs into three main categories: passive-standby, double-conversion, and line-interactive [65]. The double-conversion UPS topology, shown in Fig. 15(c), dominates the market for medium and high power UPSs, with 80 % - 97 % market share in UPSs 5-200 kVA, and 99 % in UPSs over 200 kVA, according to a 2005 study on U.S. datacenters [66]. The double-conversion topology is preferred primarily because it provides complete isolation from grid disturbances. The passive-standby and line-interactive topologies are typically not used in large UPSs because of slow response time and the lack of isolation from grid disturbances. Delta-conversion UPSs are a special type of line-interactive UPS that are gaining market share in higher power applications due to higher efficiency and nearly complete isolation from grid disturbances through a series converter. Some double-conversion UPSs offer a high efficiency “eco” mode, where the UPS normally operates in bypass mode with the static switch closed. Various forms of “eco” mode have been available for many years, but have rarely been used primarily because of customers’ concern over exposing critical loads to disturbances [67].

However, the speed of detection and transfer has improved, and modern "eco" modes are gaining acceptance because of increased focus on energy efficiency.

Customer perception against exposing critical loads to utility disturbances will be a significant obstacle for power-quality microgrids to compete with UPSs for mission-critical applications. This is because a microgrid is typically a line-interactive architecture, where the sources are always online and the loads are exposed to utility disturbances. Double-conversion UPSs with "eco mode" have made inroads despite the possibility of exposing loads to utility disturbances, in part because of the fact that the transfer to double conversion mode can typically be made in 2 ms [67]. Line-interactive microgrids, however, have difficulty offering 1/4 cycle or faster response time because of the challenge of force commutating the static switch.

3.2.2. **Static Switch Forced Commutation and Response Time in Line-Interactive Microgrids**

Systems that use an inverter with a static bypass switch, such as line-interactive UPSs, double conversion UPSs in bypass mode, and DySCs all use forced commutation of the static switch to achieve rapid isolation from utility disturbances [63]. This is the only way to guarantee 1/4 cycle or faster response time with a line-interactive architecture.

To force commutate the static switch, the static switch gating should be disabled and the current driven to zero. After the static switch gating is disabled, the static switch will naturally commutate at the next current zero crossing unless the inverter voltage is used to force the current to zero. Shunt connected devices rely on applying a differential voltage across the grid impedance to drive the current to zero, as seen in the equivalent circuit in Fig. 16. During a voltage sag, if the inverter voltage magnitude is larger than the grid voltage magnitude, then the voltage across the grid impedance will drive the grid

current to zero. If exporting power, then the inverter voltage magnitude should be less than the grid voltage magnitude to drive the current to zero [68].

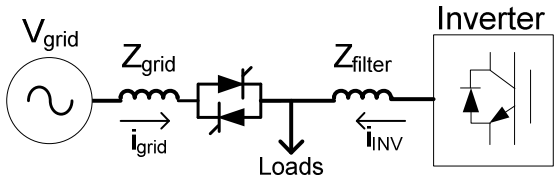

Fig. 16. Equivalent circuit for commutation of static switch.

Fig. 17 shows a simulation of the system in Fig. 18, using the control in Fig. 19. Prior to the voltage sag, the inverter is connected but not switching, and the phase is synchronized with the output. Once the sag is detected, the static switch gating is disabled and 1 ms later the inverter is turned on, driving the static switch current to zero. The total response time is dependent on the detection time and the time required to turn on the inverter, and the nominal voltage can be restored in less than 1/4 cycle.

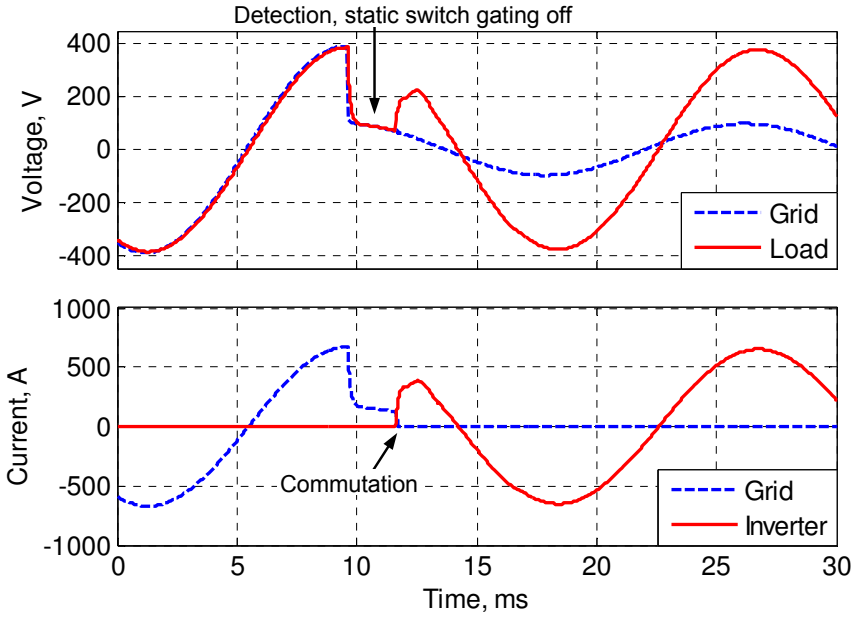

Fig. 17. Simulation demonstrating use of the inverter to provide forced commutation of static switch.

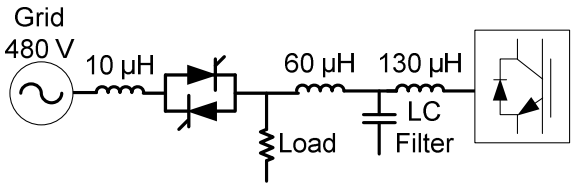

Fig. 18. Network for forced static switch commutation simulations.

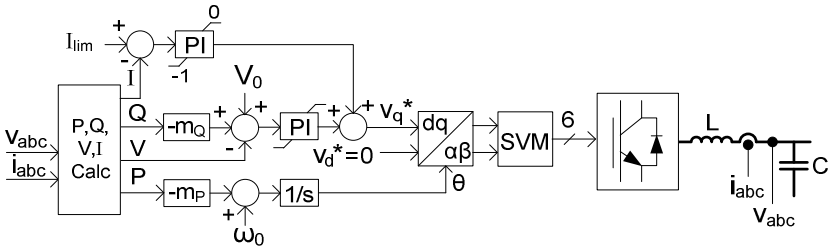

Fig. 19. Inverter voltage and frequency droop control.

The voltage across the grid and filter impedance determines the time required to drive the current to zero. The voltage across the combined grid and inverter inductance is

$$v_L = L\frac{di_L}{dt}. \tag{28}$$

The time required for the grid current to reduce to zero [68] is

$$\Delta t = L\frac{\Delta i_L}{v_L}. \tag{29}$$

The simulated Δt is 0.13 ms, and using (29) with L = 70 µH (neglecting the L in the LC filter due to the presence of the filter capacitor) and v_L = 0.75*277*1.414, gives Δt = 0.16 ms, which is close to the calculated value.

In the simulation the load is resistive, and the inverter uses the voltage and frequency droop control shown in Fig. 19. The control is single-loop voltage control with the control parameters given in Section 4.3, except with the addition of a current limiting PI controller [69] using gains k_p = 1, k_i = 10, and I_{lim} = 1.5. When the instantaneous dq current magnitude exceeds a threshold, the output voltage is decreased to limit the current, similar to virtual impedance current limiting [19, 20].

In the case of a distributed line-interactive microgrid, the inverter is typically always on, and operates in voltage control mode, i.e. grid-supporting-grid-forming

control. During a voltage sag the inverter will try to restore the voltage and will feed fault current into the grid, up to its current limit. Other loads such as motors will also feed fault current into the grid. By feeding fault current into the grid, the inverter will reverse the static switch current before the static switch is disabled.

A simulation of the network in Fig. 18, with the control in Fig. 19 is shown in Fig. 20. Unlike the previous simulation, the inverter is online and regulating the voltage, but the droop settings are chosen such that the inverter output current is zero. When the voltage sag occurs, the static switch current decreases rapidly like in the previous simulation, except that here the static switch gating has not yet been disabled. Because the static switch gating has not yet been disabled, the static switch current reverses and does not commutate until the next natural zero crossing. The response time cannot be guaranteed to be less than 1/2 cycle.

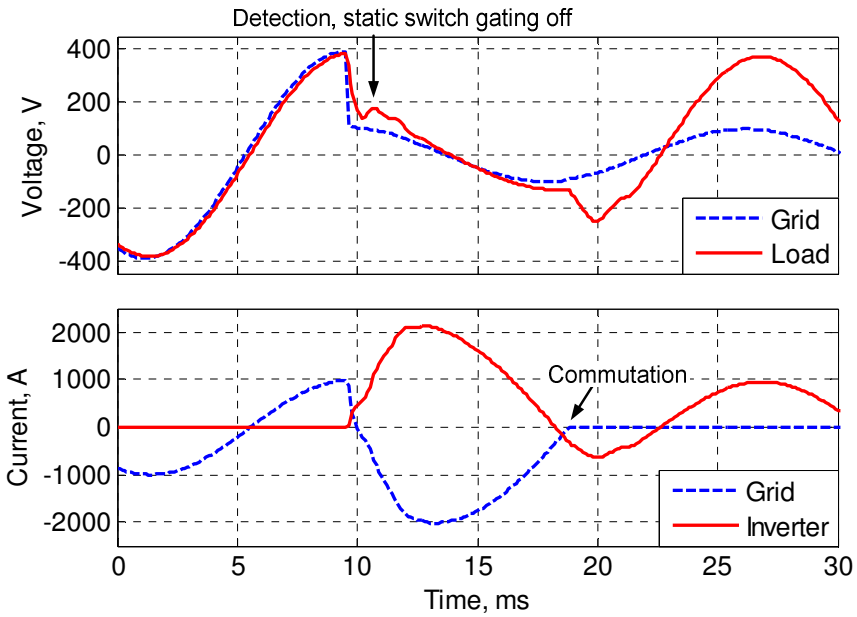

Fig. 20. Simulation of unsuccessful forced static switch commutation in line-interactive topology, where the inverter reverses the static switch current before gating is disabled.

The problem of line-interactive inverters interfering with static switch commutation is significant for *distributed* line-interactive architectures, because the inverters use only locally measured information and do not have access to the static

switch current to know that they are feeding fault current to the grid. If the inverter is co-located with the static switch, or has high speed communications with the static switch, as in Fig. 17, then it may be able to avoid feeding fault current. However, having a distributed plug & play architecture is a typically stated as a primary goal of microgrids [5, 6]. A distributed plug & play architecture should not rely on high speed communication for control, and thus should not rely on communication or coordination between the inverter and static switch. Changes in configuration, as generators switch in and out also represent challenges for coordinating with the static switch. The difficulty in performing forced static switch commutation is a significant problem for the distributed, decentralized, line-interactive microgrid's ability to compete with existing power quality solutions.

3.2.3. **Methods for Providing 1/4 Cycle Response**

For microgrids to compete with existing power quality solutions, it is important to provide similar response time to existing products. Possible methods to provide similar response time include fully rated back-to-back or series- parallel converters, self-commutating switches, and finding a way to use the inverters to provide static switch forced commutation. Back-to-back or series-parallel converters have been proposed for microgrids [59, 70]. These methods eliminate the need for rapid static switch commutation by using a converter to isolate the load from the utility, and may resemble conventional UPS solutions. If the ability to force commutate the static switch is the main barrier to a competitive power quality microgrid, it is possible to simply use a self-commutating switch. An IGBT based switch [59] or a static switch with an external commutation circuit would add cost, but would allow 1/4 cycle or faster isolation from utility disturbances. Methods for using microgrid inverters to force commutate the static switch have been proposed where the inverter switches from current control mode to voltage control mode upon detection of a grid disturbance [68, 71]. However, this method

has been demonstrated only in centralized solutions, where the static switch is co-located with at least one inverter. Thus it is not a plug & play solution, and so it may be desirable to develop methods to provide forced static switch commutation in a distributed line-interactive system.

3.3. Characteristics of Different Types of Microgrids and Example Case

Microgrid designs should look significantly different depending on the customer requirements. This section describes characteristics of microgrids designed for each of the three main microgrid value propositions: reliability, energy arbitrage, and power quality. Sample designs for each type of microgrid are provided and then compared.

3.3.1. Example Case Description

An industrial facility is considered with 600 kW of load that requires backup and 200 kW of non-critical load that does not require backup, all fed by a 1 MVA transformer. Feeder 1 contains 200 kW of line-start induction motors, Feeder 2 contains 200 kW of lighting and electronic loads, and Feeder 3 contains 200 kW of sensitive electronics and motor drives. For the reliability and energy-arbitrage microgrids, it is assumed that none of the loads require seamless islanding. For energy-arbitrage purposes, it is assumed that this facility is suitable for CHP. For the power-quality microgrid, it is assumed that only Feeder 3 has loads sensitive enough to merit paying for improved power quality, since critical loads usually make up a small fraction of the total load [60]. It is assumed that the feeders can be sequenced to prevent all loads from starting simultaneously. Simplified radial architectures are shown since this analysis is primarily intended to show the types and ratings of sources used.

3.3.2. Reliability Microgrids

A reliability microgrid is intended for customers who only need to improve the reliability of their electrical supply by providing backup during outages. A reliability

microgrid is essentially a standby power system, and thus the objective is to provide reliable backup at the lowest cost. The sources are only operated in islanded mode, and islanded mode is normally only initiated after an outage is detected. Standby diesel generators are used because of their low cost and ability to handle block load steps.

A power reliability microgrid applied to the example industrial facility is shown in Fig. 21. Commercial generator sizing software [72] was used to estimate the appropriate standby generator rating for the loads described in the example case. According to the software, the peak power demand in the example microgrid is 720 kW, and the peak kVA demand is 1,630 kVA, if the motors on Feeder 1 start intermittently. Therefore 750 kW of standby diesel generation is required.

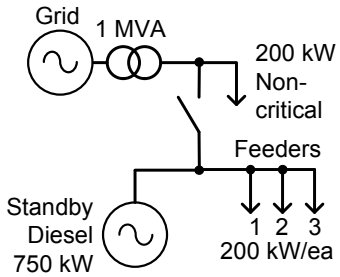

Fig. 21: Power reliability microgrid applied to the example industrial facility.

3.3.3. Energy-Arbitrage Microgrids

If the customer's main objective is to earn revenue through peak shaving, CHP, renewables, demand response, ancillary services, etc., then an energy-arbitrage microgrid is appropriate. When a microgrid is designed for energy arbitrage, the focus is on grid-connected mode, and islanded mode is an emergency mode used only during outages. The grid power quality is assumed to be sufficient, and seamless islanding is not required. In many cases islanded mode is not even needed, and the DER should only be designed for grid-connected mode. However, in this example it is assumed that backup is desired, because microgrids include the ability to operate in islanded mode by definition [58]. Various sources may be considered, including microturbines, fuel cells, PV, wind, natural-gas generators and natural-gas turbines. Inverter-based DER require energy

storage for load following, and have reduced load inrush and fault clearing capabilities compared to synchronous generators. Non-dispatchable sources such as PV and wind may also be desirable, although they must be combined with dispatchable source(s) to allow islanded operation. However, islanded operation with a high penetration of non-dispatchable renewables causes issues because of increased variability and the possibility of running the dispatchable sources at excessively low loading.

Two possible configurations of energy-arbitrage microgrids are shown in Fig. 22. The first configuration is shown in Fig. 22(a), where a microturbine with CHP is used for energy arbitrage and backup operation. Because of the slow response of the microturbine energy source, energy storage must be used [73], and the inverter front end should be over-rated for dynamic loads, as described in Section 3.3.4.3. If PV is desired for additional energy arbitrage it can be added either inside or outside the point of common coupling (PCC), since the microturbine is already required to have a battery sized for the entire load. However, a high penetration of PV may impact the required battery kWh rating.

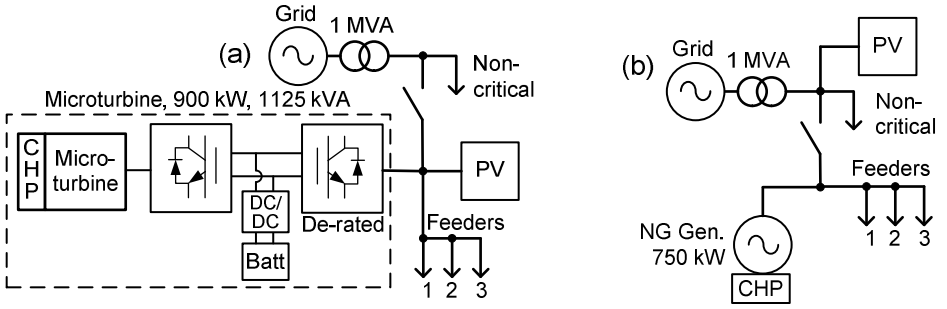

Fig. 22: Two possible configurations for an energy-arbitrage microgrid: (a) PV and microturbine with dc bus storage and de-rated front end, (b) PV and natural-gas generator with CHP.

An alternative energy-arbitrage microgrid is shown in Fig. 22(b) that uses a natural-gas (NG) generator with CHP instead of inverter-based source(s). The natural-gas generator provides the same backup and energy-arbitrage functions, but at a lower cost than a microturbine [11]. The trend of falling natural gas prices in the United States

makes the natural-gas generator powered microgrid a preferred alternative. Falling PV prices make natural gas plus PV an attractive choice. The natural-gas generator is sized to support the entire load, along with any oversizing required to support load inrush. Although the generator sizing software does not give estimates for sizing natural-gas generators, the maximum load step is 320 kW and should be easily handled by a 750 kW natural-gas generator. If a high penetration of PV is used, it may be necessary to place the PV outside the PCC to avoid running the generators at excessively low loading. Placing the PV inside the PCC would create minimal cost savings in terms of reduced fuel consumption during islanded mode, since islanded mode is typically only used during outages, which are rare.

3.3.4. **Power-Quality Microgrids**

A power-quality microgrid is appropriate when there are loads that are sensitive to momentary disturbances with a demonstrably high cost of downtime, and sufficient ROI can be demonstrated. For islanded operation of both inverter-based energy-arbitrage microgrids and inverter-based power-quality microgrids energy storage is required for load following, and the inverters must be rated to handle any high inrush or high crest factor loads present.

In Fig. 23 a power-quality microgrid is shown where a microturbine with CHP and energy storage provides seamless islanding for all loads that require backup. This inverter based power-quality microgrid is almost the same as the inverter-based energy-arbitrage microgrid in Fig. 22(a), except that the inverter must remain online at all times to be ready for an islanding transient, and a static switch is used instead of a mechanical switch.

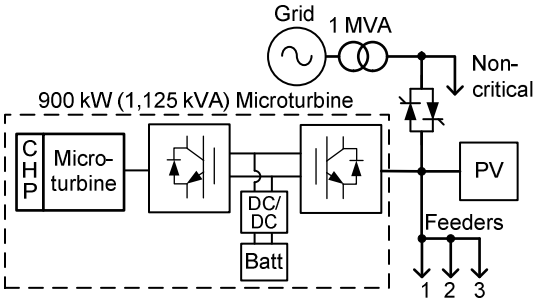

Fig. 23: Power-quality microgrid where seamless islanding is provided for all loads that require backup.

The microgrid in Fig. 23 is representative of the typical microgrid proposed in the literature, although the number and type of inverter based DER varies in the literature. The key similarities are: all inverter based sources, energy storage, and isolation from grid disturbances at the point of common coupling through a static switch. Because the inverter must be rated for the entire load, this architecture is similar in terms of inverter ratings and energy storage requirements to sizing a UPS for the entire microgrid load. However, unless proper precautions are taken, this centralized power-quality microgrid will suffer from the static switch forced commutation problem described in Section 3.2.2, and will only be able to guarantee 1/2 cycle response times to grid disturbances and outages.

3.3.4.1. Preferred Architecture

In most applications, critical loads make up a small portion of the total load [60]. Instead of providing UPS functionality for every load in the microgrid, a more economical solution may be to provide UPSs for each critical load, and to provide non-seamless backup for the rest of the loads that require backup. A microgrid similar to the natural-gas generator based energy-arbitrage microgrid of Fig. 22(b) is shown in Fig. 24, with the addition of individual UPSs for each critical load.

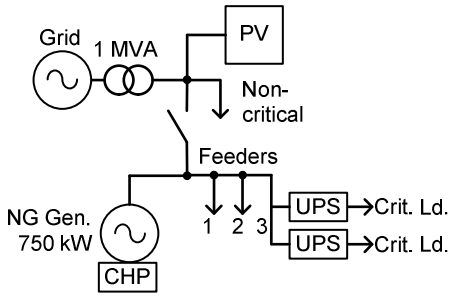

Fig. 24: Power-quality microgrid where each critical load has its own UPS, and non-critical loads receive non-seamless backup.

Providing a UPS for each critical load gives better power quality and reliability for critical loads because critical loads are not affected by faults elsewhere in the microgrid. A UPS at the point of load provides isolation from grid disturbances and disturbances inside the microgrid. Double-conversion UPSs can also provide complete isolation from grid disturbances, as opposed to the line-interactive microgrids which have difficulty providing better than 1/2 cycle response to grid disturbances. The required inverter ratings may be lower if only critical loads have UPSs, which could result in lower overall cost.

Overall this is expected to be the most viable architecture, as it provides all three value propositions to the degree needed by the customer without adding unnecessary cost. Backup is provided, but the additional costs associated with seamless islanding are avoided. The backup source can also be used for energy arbitrage, and natural gas plus PV are expected to be a cost effective combination. If a load is truly critical, it is supplied by a UPS, which provides better power quality than a line-interactive power-quality microgrid.

3.3.4.2. Impact of Internal Faults on Reliability of Critical Loads

In a centralized architecture such as the power-quality microgrid in Fig. 23, the reliability for critical loads is limited by the reliability of downstream loads, because any faults within the microgrid will interrupt critical loads. Therefore, an architecture where power-quality devices are applied at the point of load, such as the decentralized power-

quality microgrid of Fig. 24, provides better reliability than providing a single compensation device further upstream [61]. In the centralized power-quality microgrid of Fig. 23, seamless islanding is provided for all the loads that require backup. If a fault occurs inside the microgrid, the voltage will be reduced within the entire microgrid, and any critical loads inside the microgrid will be interrupted by the severely reduced voltage, even if the fault is cleared within a few cycles.

The decentralized power-quality microgrid of Fig. 24 uses separate UPSs for each critical load, and is not impacted by faults on adjacent feeders. The one-line diagram in Fig. 25 depicts a fault on Feeder 1 for the decentralized power-quality microgrid. Fig. 26 shows the simulated voltage at Feeder 2 (non-critical load bus) and at one of the critical loads (supplied by a UPS) for a three-phase fault on Feeder 1. The fault is cleared by opening the Breaker 1 after 3 cycles. Any sensitive loads that are not supplied by a UPS would be interrupted, which is the case for all microgrid loads in the centralized power-quality microgrid. The critical loads that are supplied by a UPS are unaffected by the fault inside the microgrid.

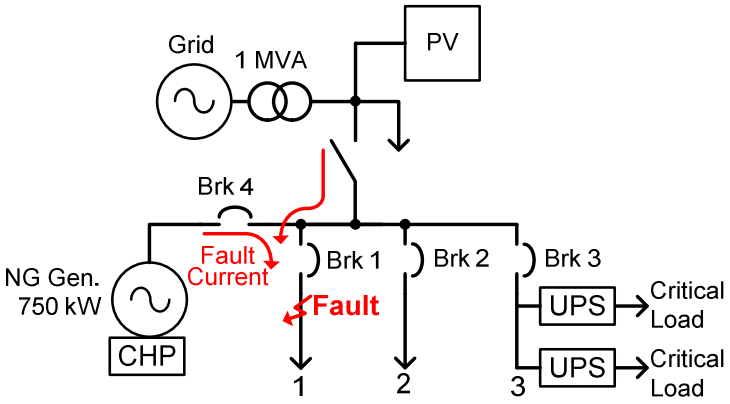

Fig. 25: Fault inside the decentralized power-quality microgrid, which causes interruption to non-critical loads but does not impact critical loads.

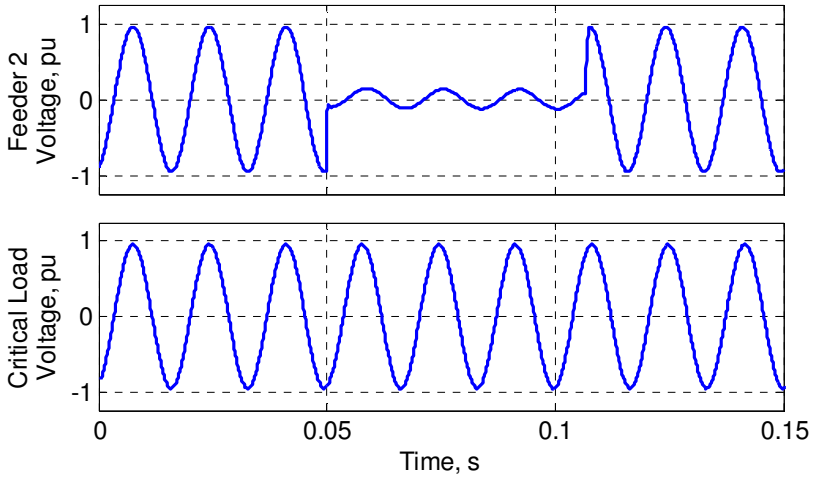

Fig. 26: Simulation of voltages at Feeder 2 (adjacent to faulted feeder) and at a critical load (supplied by a UPS) caused by a fault within the microgrid, resulting in interruption of loads not supplied by a UPS.

Because of the increased probability of critical loads being interrupted by local faults, it would be impractical to attempt to provide improved power quality throughout a microgrid that covers a large geographical area. For customers with mission-critical loads, attempting to provide improved power quality for a large portion of the network may actually decrease reliability compared to providing protection at the point of load.

3.3.4.3. Impact of Dynamic Loads on Component Ratings

High inrush and high crest factor loads require over-rating of inverters, which increases the cost of inverter-based microgrids. This may be problematic especially if microgrids target industrial or commercial facilities, where there is a high penetration of dynamic loads. The purpose of this section is to extract the required inverter and energy-storage rating from a simulation of starting a high inrush motor load.

A simulation of the network in Fig. 22(a) or Fig. 23 is shown in Fig. 27, where the inverter operates in islanded mode and Feeder 1 starts up with Feeders 2 and 3 already online. Because of the high-inrush motor loads, the current reaches 1,700 A_{RMS}, and the power peaks at 950 kW. If the feeders were not sequenced, the inrush would be worse. The peak power draw is higher than in the synchronous generator case because the inverter allows a smaller voltage sag, and thus the motor develops higher starting torque.

The high-inrush loads result in a peak battery rating of 950 kW, and a peak inverter rating of 1,410 kVA ($1{,}700 * 480 * \sqrt{3}$). If separate de-rating of the inverter front-end from the turbine and battery are available, this could be satisfied by a 950 kVA inverter, 650 kW battery, and 600 kW turbine, assuming 150 % overload capability for up to 10 seconds. However, for this example it is assumed that the manufacturer does not de-rate the inverter front-end separately, and the necessary inverter rating is calculated as

$$P_{rated,INV} = 1{,}410 \text{ kVA} * 0.8 \text{ PF} / (125\ \%) = 902 \text{ kW} \quad (30)$$

where the inverter's rated power factor (PF) is 0.8, and motor starting is limited to 125 % of rated current [74]. Therefore in this example the entire microturbine must be over-rated by 50 % because of high inrush loads, even though motors only represent 33 % of the total load.

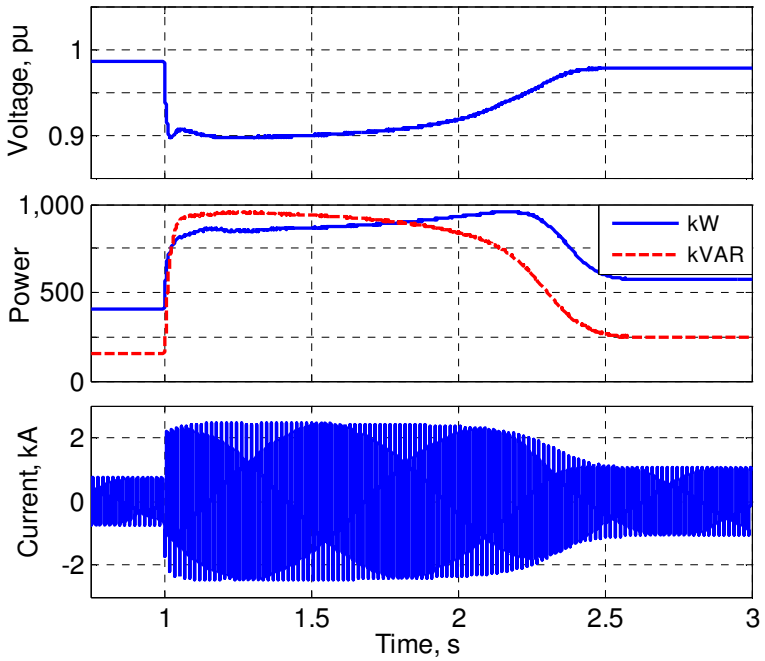

Fig. 27: Simulation of inverter starting high-inrush motor loads showing that inverter must be over-rated by 50 % to support dynamic loads when islanded.

3.3.5. **Design Comparison**

The reliability, energy-arbitrage, and power-quality microgrids are summarized and compared in Table 1. The ratings of the sources and the type of interconnection switch are compared, with the assumption that ratings are proportional to cost.

Table 1: Comparison of component ratings and reliability.

Microgrid Type	**Reliability Fig. 21**	**Energy Arbitrage Fig. 22(a)**	**Energy Arbitrage Fig. 22(b)**	**Power Quality Fig. 23**	**Power Quality w/ UPS Fig. 24**
Standby Diesel Gen.	750 kW	–	–	–	–
NG Gen. w/ CHP	–	750 kW	–	–	750 kW
Microturbine w/ CHP	–	–	900 kW	900 kW	–
Inverter	–	–	1,125 kVA	1,125 kVA	250 kVA
Battery	–	–	900 kW	900 kW	200 kW
Interconnection Switch Type	Mechanical	Mechanical	Mechanical	Static Switch	Mechanical
Reliability for Critical Loads	–	–	–	Medium/ High	High

The standby diesel generator in the reliability microgrid and the natural-gas generators in the energy-arbitrage and power-quality microgrids all require 25 % over-rating because of dynamic loads. Additional sequencing of motor loads may reduce or eliminate the over-rating requirement of the generators. The inverter-based power-quality microgrid of Fig. 23 requires 50 % over-rating of the battery and inverter, assuming the manufacturer does not offer separate de-rating of the inverter front, as described in Section 3.3.4.3. This represents a relatively conservative estimate and does not account for any desired redundancy. The inverter-based power-quality microgrid also requires a static switch, whereas the others use a mechanical switch. The inverter-based power-quality microgrid offers reduced reliability compared to the power-quality microgrid that provides separate UPSs for each critical load, because of faults on non-critical loads interrupting critical loads.

The need to over-rate inverters to a greater degree than synchronous generators is an important consideration that may impact the choice of inverter vs. synchronous generator based DER in microgrids. Many of the prominent types of inverter based DER are more expensive than synchronous generators, as shown by the capital cost comparison in Table 2, further impacting the cost of inverter vs. synchronous generator based DER. The inverter based power quality microgrid also requires a static switch, whereas the others use a mechanical switch. Finally, the inverter based power quality microgrid offers reduced reliability compared to the power quality microgrid that provides separate UPSs for each critical load, due faults on non-critical loads interrupting critical loads.

Table 2: Comparison of Capital Costs.

Component	Capital Cost	O&M Cost
NG Gen. w/ CHP [11]	$1,100-$2,200/kW	$0.009-$0.022/kWh
Microturbine w/ CHP [11]	$2,400-$3,000/kW[a]	$0.012-$0.025/kWh[a]
Fuel Cell w/ CHP [11]	$5,000-$6,500/kW[a]	$0.032-$0.038/kWh[a]
Energy Storage Inverter [75]	$450/kW[b]	$10/kW-yr

a. May not include the added cost of off-grid functionality [76] over purely grid-connected operation (battery + DC/DC converter).

b. $400/kW for power conversion system plus 15 min battery at $330/kWh. May only represent equipment cost, and not total project cost.

3.3.6. **Role of Energy Storage**

Many papers assume that energy storage is a necessary and integral part of microgrids, e.g. [2, 9, 50]. However, energy storage is only required for inverter based power quality microgrids, and is optional for other types of microgrids. This point needs to be emphasized in the microgrid literature because of its impact on microgrid cost. Synchronous generator based DER can perform the same load following and voltage and frequency regulation functions as inverters with energy storage. Synchronous generators can also perform the two microgrid functions for which there is more often a solid business case – backup and energy arbitrage. While inverters may be able to provide better power quality than generators, it should be recognized that providing improved

power quality is expensive, and most customers cannot justify the cost. Energy storage should be used in microgrids only if some combination of energy arbitrage, backup, and/or power quality make it economical to do so.

3.4. Chapter Conclusion

In the literature and in practice, it has been assumed that power quality is a primary objective of microgrids. This chapter has identified fundamental drawbacks to power quality microgrids: the need to compete with existing power quality solutions, providing similar level of reliability and response time to existing solutions, and not providing more power quality than needed due to the traditional difficulty of demonstrating sufficient ROI on power quality investments. A distributed power quality microgrid has been identified as the preferred architecture, which provides UPSs for critical loads and non-seamless backup and energy arbitrage for the rest of the microgrid. Design considerations for sample microgrids designed for reliability and energy arbitrage have also been discussed.

The issues described in this chapter have not been aired in the literature. In general, important issues with microgrids such as cost and ratings have been glossed over. This work defines for the first time the design considerations and tradeoffs associated with realizing the different types of microgrids. By identifying the main value propositions, economical solutions can be identified that provide the desired functionality without adding unnecessary cost.

CHAPTER 4: POWER SHARING BETWEEN INVERTERS AND SYNCHRONOUS GENERATORS

Energy-storage inverters and synchronous generators may be used together in energy-arbitrage microgrids, or power-quality microgrids that do not require 1/4 cycle response. Inverters with energy storage enable seamless islanding transitions, and may be used in the case of high penetrations of renewable energy generation to buffer sudden load or renewable output changes, and to avoid operation of generators at excessively low loading. This is particularly the case for microgrids designed for extended islanded operation with a high penetration of renewables, which may use a combination of renewables, battery energy-storage inverters, and synchronous generators for backup.

The interactions between synchronous generators and inverters are an important topic in microgrids. Internal combustion engine driven synchronous generators are the most common distributed generation source with a combined installed capacity exceeding 100,000 MW [1], and thus are expected to play a significant role in microgrids.

Inverters operated with grid-supporting-grid-forming control exhibit poor transient load sharing with synchronous generators when operated in islanded mode, where the inverter initially picks up the majority of any load step. The lack of transient power sharing with inverters in grid-supporting-grid-forming control can be observed in [51, 52], but is not addressed. Reference [53] studies this topic in simulation, and states that the reason for lack of transient power sharing is that the generator is slow compared to the inverter. This explanation is common in the literature, but is an oversimplification. However, the next section describes how the poor transient power sharing is caused by significant differences in how the two sources regulate voltage and frequency. In [53] an angle-droop control is proposed to improve the transient power sharing. However, this is a grid-supporting-grid-feeding control and requires a generator to be online.

The basic transient power sharing characteristics between voltage controlled inverters and generators are investigated, and an equivalent circuit is proposed to describe the initial power sharing. The effects of increased inverter droop slope and increased governor integral gain on the power sharing are also investigated. It is shown that any method that improves transient power sharing with generators does so at the expense of increased voltage and frequency transients.

4.1. Frequency Regulation Characteristics

The lack of transient power sharing between generators and inverters in voltage control mode can be understood by considering the differences between the generator's and the inverter's voltage and frequency control loops. The control diagram for an inverter operating with voltage and frequency droop is shown in Fig. 28, where the voltage and frequency references are obtained from droop, and the resulting voltage is directly synthesized. The control in Fig. 28 is essentially the same as CERTS inverter control [36, 37].

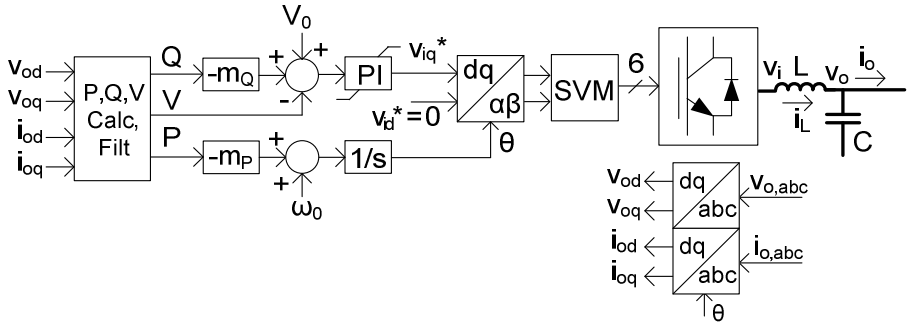

Fig. 28: Inverter control where voltage droop biases voltage controller reference, but frequency droop directly biases frequency output.

The filtered real power, reactive power, and voltage magnitude are calculated as in (31). The instantaneous real and reactive power $\tilde{p}$ and $\tilde{q}$ and voltage magnitude $\tilde{v}$ are calculated using instantaneous dq calculations given by (15)-(17). The fundamental real and reactive power, P and Q, and voltage, V, are given by filtering the instantaneous values with a single order low-pass filter with cutoff frequency ω_c.

$$P = \tilde{p} \cdot \omega_c /(s+\omega_c), \quad Q = \tilde{q} \cdot \omega_c /(s+\omega_c), \quad V = \tilde{v} \cdot \omega_c /(s+\omega_c) \tag{31}$$

The inverter frequency, ω^*, and phase, θ, are given by (32) and (33), and the inverter voltage commands, v_{id}^* and v_{iq}^*, are given by (34) and (35), where m_P and m_Q are the frequency and voltage droop slopes, respectively, and k_{pV} and k_{iV} are the voltage controller proportional and integral gains, respectively.

$$\omega^* = \omega_0 - m_P P \tag{32}$$

$$\theta = \omega^* / s \tag{33}$$

$$V^* = V_0 - m_Q Q \tag{34}$$

$$v_{iq}^* = (k_{pV} + k_{iV}/s)\cdot(V^* - V), \; v_{id}^* = 0 \tag{35}$$

The control diagram of a synchronous generator operating in droop is shown in Fig. 29, where droop is implemented by biasing the automatic voltage regulator (AVR) voltage reference and governor frequency reference in proportion to measured real and reactive power, respectively.

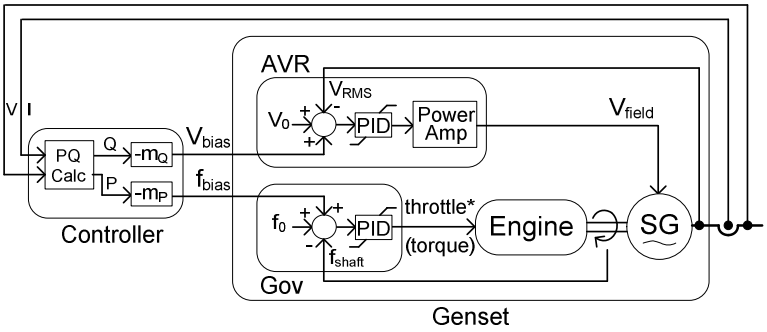

Fig. 29: Generator control where droop terms bias AVR and governor references.

The synchronous generator regulates frequency by controlling the engine's mechanical torque, T_m, in order to regulate the mechanical speed, ω_m. This is shown by (36) and (37), where T_e is the electrical torque, B is the friction constant, and H is the inertia constant. Note that (36) neglects the diesel engine dynamics. In (36), ω^* is given by (32), and $k_{p\omega}$ and $k_{i\omega}$ are the speed controller proportional and integral gains, respectively.

$$T_m = (\omega^* - \omega_m) \cdot (k_{p\omega} + k_{i\omega} / s) \tag{36}$$

$$\omega_m = \frac{1}{s}\left(\frac{T_m - T_e - B \cdot \omega_m}{H}\right) \tag{37}$$

The inverter and generator regulate frequency in fundamentally different ways. The generator adjusts torque based on speed error to regulate frequency, and adjusts its speed reference in proportion to measured power. The inverter, however, directly outputs a frequency proportional to the measured power. Therefore, the inverter operates on a dynamic frequency droop, while the generator operates in frequency droop only in steady state, once the speed error term is driven to zero by the governor's integral action. The inverter and generator have similar methods for voltage regulation, but the inverter's voltage regulator is much faster than the generator's AVR. So again, the inverter operates on a dynamic voltage droop, while the generator only operates in voltage droop once the voltage reference error has been driven to zero by the AVR integral action. These significant differences between methods of voltage and frequency regulation are the main cause of unequal transient load sharing.

4.2. Experimental Setup

The experimental setup shown in Fig. 30 was constructed for this thesis, and is used to demonstrate the transient power sharing between an inverter and a generator. The generator is a 12.5 kW Marathon Electric Magnaplus 282PSL1704 with a DVR2000E digital voltage regulator and permanent magnet excitation. The generator is coupled to a 25 hp induction motor (IM) powered by a 20 hp variable frequency drive. The drive runs closed loop speed control to emulate a diesel engine. The induction motor and variable speed drive were chosen to allow flexibility in emulating various types of prime movers, and because of the difficulties of installing a diesel engine in a lab environment. The inverter's rated current is 31 A, or 11.1 kVA at 208 $V_{L\text{-}L}$. The inverter is composed of a diode rectifier input, a dc brake chopper, and a standard three-phase IGBT bridge.

Inverter control and data acquisition have been implemented in a National Instruments CompactRIO field programmable gate array (FPGA) and real-time controller. A picture showing the main components of the experimental setup is provided in Fig. 31.

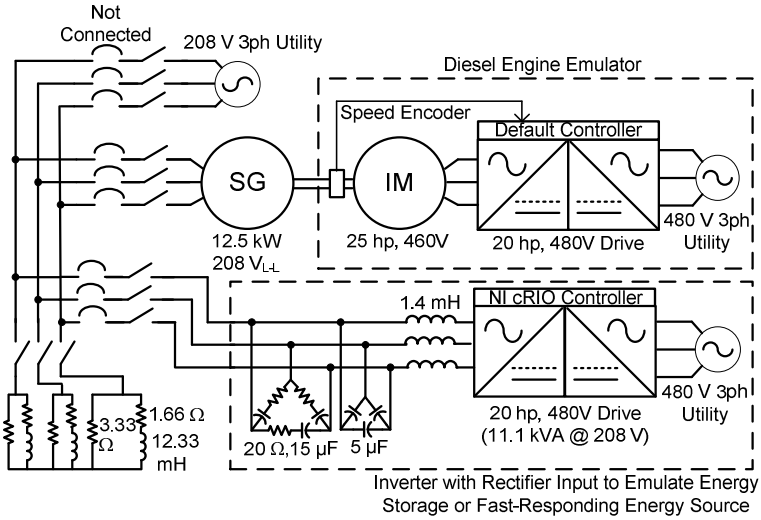

Fig. 30: Experimental microgrid setup with inverter and synchronous generator.

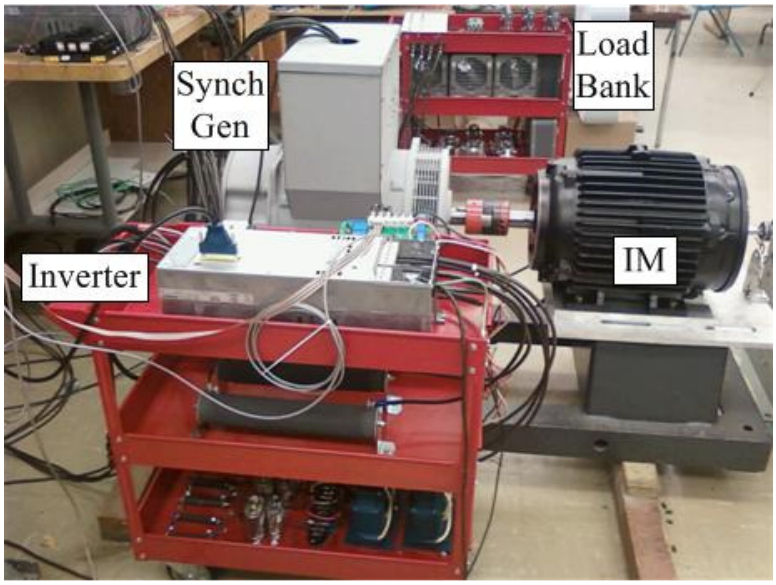

Fig. 31: Picture of experimental microgrid setup.

The resistive-inductive load is composed of two load banks, each controlled by a contactor. A partial diagram of one load bank is shown in Fig. 32. Each load bank has two fixed 10 Ω resistive loads per phase, and one resistive load switchable between 10 Ω and 20 Ω. Each load bank also has two fixed inductive branches per phase with a 5 Ω

resistor in series with a 37 mH single-phase reactor, and one branch switchable between 5 Ω + 37 mH and ~1 Ω + 74 mH. The series 5 Ω resistors are used because without the extra resistance, the 37 mH inductors saturate due to the dc offset at turn-on. Resistive loads are thus adjustable from 0 to 25.5 kW, and inductive loads are adjustable from 0 to 6 kW + j16.5 kVAR (0.34 power factor).

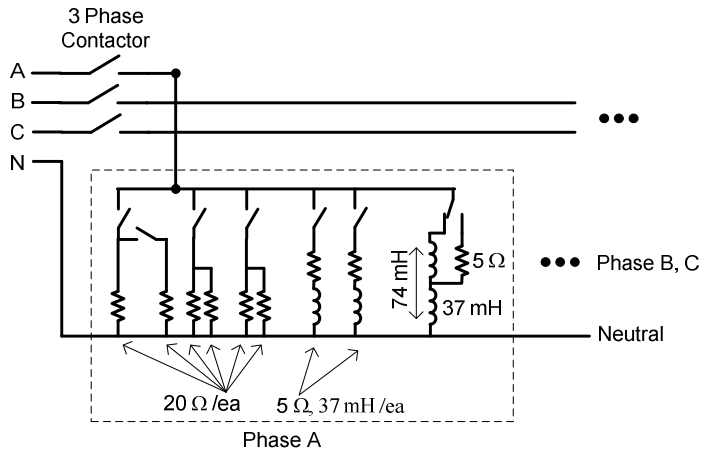

Fig. 32: Resistive-inductive load bank schematic.

4.3. Simulation Results

The system in Fig. 30 is simulated with the generator and inverter operating with the controls in Fig. 29 and Fig. 28. The inverter and generator control parameters used are shown in Table 3, where the subscript pu denotes per-unit. The generator parameters are based on the experimental setup. The simulation of application and rejection of a 100 % (21.4 kW, 16 kVAR) linear load is shown in Fig. 33. The inverter initially picks up almost the entire load step, and the generator increases power slowly until they reach steady state in which they share load relative to their droop settings. In this case the droop settings are such that they share load proportional to their ratings. When the load is removed, the inverter absorbs most of the load step, and the power reaches -0.75 pu. This simulation demonstrates how an inverter may need to be over-sized to handle more than its share of the load during large load steps, possibly having a negative impact on battery life in battery storage inverters. The lack of power sharing may be especially problematic

for negative load steps, where a battery inverter that is charging prior to a negative load step would likely trip because of excessive reverse power.

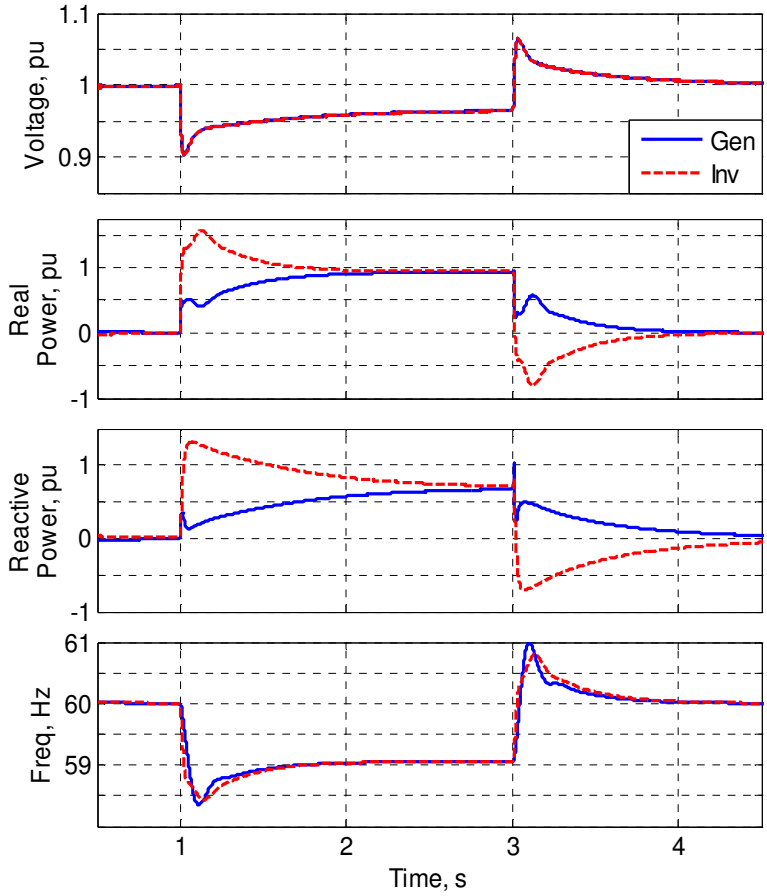

Fig. 33: Simulation of generator and inverter response to 100 % load step, showing poor transient load sharing resulting in inverter overload.

Table 3: Controller Parameters.

Parameter	Value
P, Q, V calculation filter cutoff frequency, ω_c	2π*10 rad/s
Frequency droop gain, m_P	2π*1 (rad/s)/P_{pu}
Voltage droop gain, m_Q	0.05 V_{pu}/Q_{pu}
AVR k_p	1.62 V_{pu}/V_{pu}
AVR k_i	10.4 (V_{pu}/V_{pu})/s
AVR k_d	0.05 (V_{pu}/V_{pu})-s
AVR T_d	0.1 (V_{pu}/V_{pu})/s
AVR T_E	0.01(V_{pu}/V_{pu})/s
AVR K_E	1 V_{pu}/V_{pu}
AVR S_E	0 V_{pu}/V_{pu}
Governor k_p	7 T_{pu}/ω_{pu}
Governor k_i	57 (T_{pu}/ω_{pu})/s
Governor k_d	0 (T_{pu}/ω_{pu})-s
Governor T_d	0 (T_{pu}/ω_{pu})/s
Engine T_1	0 s
Engine T_2	0 s
Engine B	0.04 T_{pu}
Engine + Generator, H	0.34 s
Voltage controller k_p (Fig. 28)	0.5 V_{pu}/V_{pu}
Voltage controller k_i (Fig. 28)	44 (V_{pu}/V_{pu})/s

4.4. Experimental Results

The generator and inverter are operating with the droop control shown in Fig. 29 and Fig. 28, respectively. The same settings are used as in the simulation, except for slight differences in tuning of the simulated vs. actual governor and AVR. The experimental results for application and rejection of a three-phase 16 kW, 8 kVAR linear load (3.33 Ω and 1.66 Ω + 12.33 mH) are shown in Fig. 34 and Fig. 35. The experimental results closely match the simulation results. From Fig. 35 it can be seen that the current reverses when the load is turned off, and the inverter absorbs power from the generator. In the experimental setup, the energy is dissipated in the dynamic brake resistor. The generator real and reactive power plots are per-unitized with base power S_b = 12.5 kVA, which is the real power base, and the inverter plots with S_b = 0.8*11.1 kVA. The inverter frequency shown is the internal output frequency, and the generator frequency is the motor speed from the variable frequency drive. All measured power, voltage, and

frequency traces are filtered through a first-order Butterworth low-pass filter with a 60 Hz cutoff to facilitate visual comparison, unless otherwise stated.

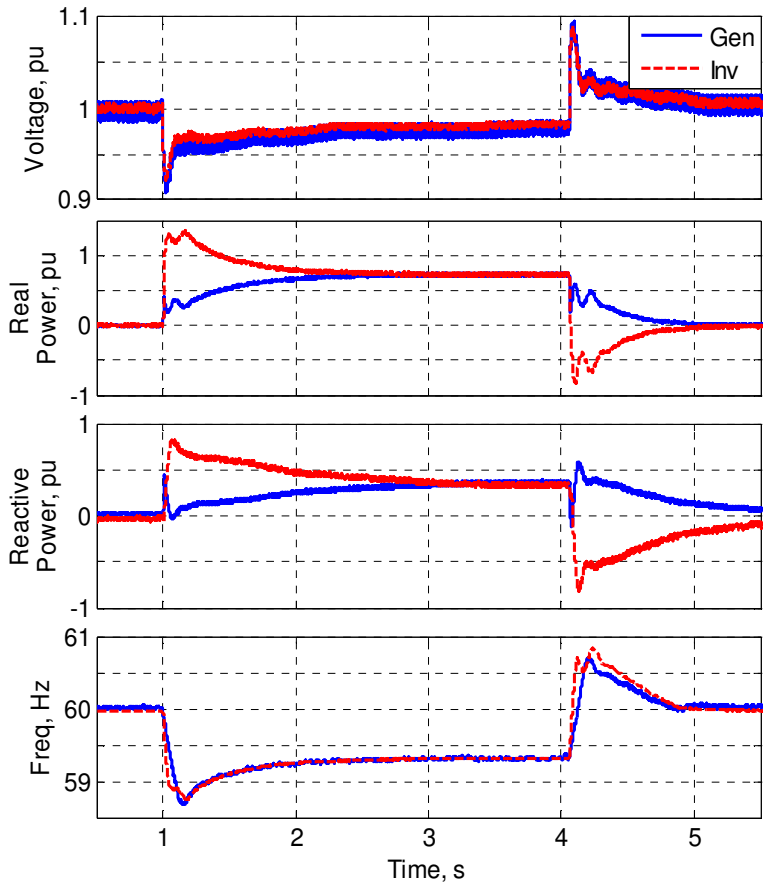

Fig. 34: Experimental results for load step with inverter in voltage control mode.

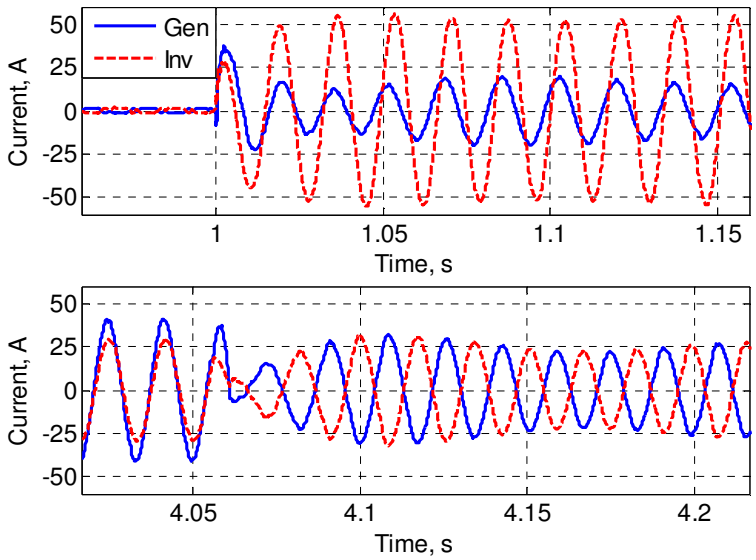

Fig. 35: Measured current with inverter in voltage control mode during load step changes shown in Fig. 34.

4.5. Impact of Generator Governor on Settling Time

The governor integral action primarily determines the rate at which steady state is reached. As described previously, the generator operates in droop only when the speed error is driven to zero by the governor integral action. Once the speed error is zero, the generator operates along its droop curve, and the inverter and generator share power according to their relative droop settings. Therefore the rate at which the power sharing reaches steady state depends on the governor time constant. In Fig. 36 the measured real power from Fig. 34 is compared with a second experiment where the generator governor integral gain is doubled. When the integral gain is doubled, the system reaches steady state in roughly half the time, indicating that the settling time is dominated by the governor's integral gain.

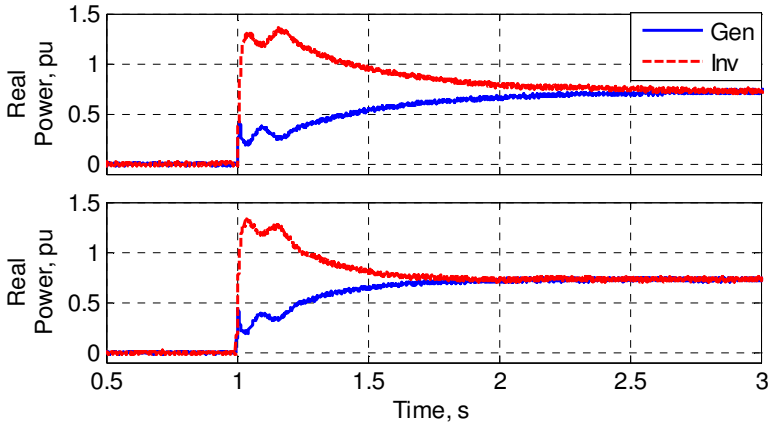

Fig. 36: Impact of governor integral gain on settling time, (top) default, (bottom) doubled.

The lack of transient power sharing becomes a more serious issue in a larger system with slower generator prime movers. For a generator with a slow prime mover, such as a large turbo-charged engine, the generator will pick up the load more slowly, and the inverter will be overloaded for a longer time.

The lack of transient load sharing is serious for multi-MW microgrids, where the inverter may be significantly smaller than the generator(s) [77]. The cost of large, multi-MW inverters begins to be prohibitive for multi-MW microgrids, and thus designers may choose inverters significantly smaller than the synchronous generators. Therefore transient power sharing with grid-supporting-grid-forming inverters could be especially problematic in large microgrids.

4.6. Equivalent Circuit for Initial Power Sharing

While most of the transient load sharing characteristics are dominated by the differences between the inverter and generator frequency regulation controls, the initial few power cycles after the transient are dominated by the output impedance characteristics of each source. In the inverter control, the voltage and frequency references are drooped in proportion to the filtered power measurement. Therefore the inverter control inputs do not change significantly during the first half cycle or more, depending on the filtering time constants. With the generator, the AVR and governor have almost no impact during the first few power cycles. To obtain an estimate of the

initial power sharing, the generator can be modeled as a simple voltage behind transient reactance and the inverter as a voltage behind filter reactance. This is shown in Fig. 37, where E_q' is the generator voltage behind transient reactance, X_d' is the generator d-axis transient reactance, E_{INV} is the inverter voltage, and X_{filt} is the inverter filter reactance. The voltage behind transient reactance model is the simplest model of an generator, and is commonly used for transient stability studies [42].

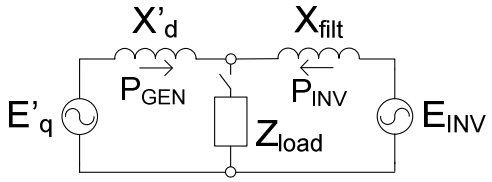

Fig. 37: Equivalent circuit to describe initial power sharing.

The ratio of inverter to generator power, or the relative load sharing, in the circuit of Fig. 37 is given by a ratio of output impedances. Applying Kirchhoff's current law (KCL) gives (38), where the bar superscript denotes a complex phasor. Note that this analysis is not in per-unit, since the inverter and generator have different base powers.

$$\frac{\overline{E}_{INV}-\overline{V}_L}{jX_{filt}}+\frac{\overline{E}_q^{'}-\overline{V}_L}{jX_d^{'}}=\frac{\overline{V}_L}{\overline{Z}_{load}} \tag{38}$$

The complex power for the inverter and generator can be written as

$$\overline{S}_{INV}=\overline{V}_L\left(\frac{\overline{E}_{INV}-\overline{V}_L}{jX_{filt}}\right)^*, \quad \overline{S}_{GEN}=\overline{V}_L\left(\frac{\overline{E}_q^{'}-\overline{V}_L}{jX_d^{'}}\right)^*, \tag{39}$$

where the superscript * denotes a complex conjugate. Solving (38) for $\overline{V}_L$ and combining with (39), the ratio of inverter power to generator power can be written as

$$\frac{P_{INV}}{P_{INV}+P_{GEN}}=\frac{\mathrm{Re}(\overline{S}_{INV})}{\mathrm{Re}(\overline{S}_{INV})+\mathrm{Re}(\overline{S}_{GEN})}=\frac{\overline{E}_{INV}X_d^{'}}{\overline{E}_{INV}X_d^{'}+\overline{E}_{GEN}X_{filt}}, \tag{40}$$

where $\mathrm{Re}(\overline{S}_{INV})$ is the real component of $\overline{S}_{INV}$. Assuming both sources are initially at no load, then $\overline{E}_{INV}=\overline{E}_q^{'}$, and the ratio of inverter to generator power is

$$\frac{P_{INV}}{P_{INV}+P_{GEN}}=\frac{X_d^{'}}{X_d^{'}+X_{filt}}. \tag{41}$$

The same method can be followed to obtain the ratio of inverter reactive power to generator reactive power, resulting in

$$\frac{Q_{INV}}{Q_{INV}+Q_{GEN}} = \frac{X_d^{'}}{X_d^{'}+X_{filt}}. \tag{42}$$

From (41) and (42) it is apparent that the relative output impedances govern the initial power sharing, which is intuitive based on the equivalent circuit. A few important points can be seen from (41) and (42). First, for a given inverter rating, a smaller filter reactance leads to the inverter producing a larger percentage of a load step. Second, as the ratio of inverter to generator rating decreases, the inverter overloading will become more severe. Finally, for a generator with a smaller $X_d^{'}$, the inverter overloading is decreased.

Using the initial power values from Fig. 33, except with power in kW and kVAR instead of per-unit, (43) – (45) compare the expected (43) vs. simulated (44), (45) power sharing to show that the equivalent circuit is useful for estimating the initial power sharing ratio.

$$X_d'/(X_d'+X_{filt}) = 0.807/(0.807+0.528) = 0.604 \tag{43}$$

$$P_{INV}/(P_{INV}+P_{GEN}) = 12.8/(12.8+7.6) = 0.627 \tag{44}$$

$$Q_{INV}/(Q_{INV}+Q_{GEN}) = 8.7/(8.7+6.7) = 0.565 \tag{45}$$

4.7. Impact of Increased Inverter Droop Slope

Based on the description of the generator and inverter frequency regulation characteristics, it is expected that an increased inverter frequency droop slope will cause the generator to pick up load more quickly by allowing the governor to see a larger speed error. However, the droop slope is not expected to have any impact on the initial power sharing. Experimental results for the impact of doubling and quadrupling the inverter's frequency droop slope, m_P, are shown in Fig. 38. The power traces are the unfiltered, instantaneous power calculation given by (15), and it can be observed that the power output during the first approximately one cycle is independent of the inverter droop slope.

This supports the conclusion that the initial power sharing is given by the output impedance characteristics of the inverter. Note that if an increased droop slope is used, it should be a transient droop to avoid changing the steady state power sharing.

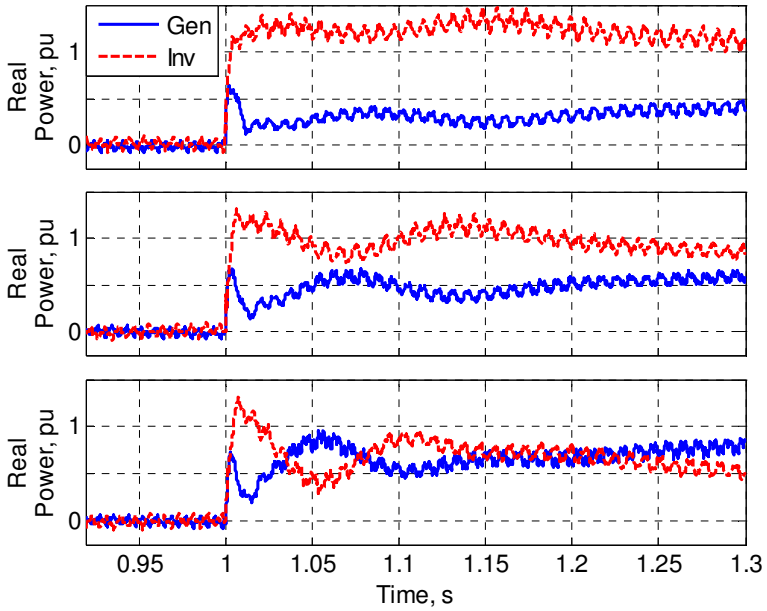

Fig. 38: Impact of varied inverter frequency droop slope on transient power sharing, (top) 1x, (middle) 2x, (bottom) 4x.

4.8. Inverter-Generator Power Sharing with Grid-Supporting-Grid-Feeding Control

Poor transient load sharing is also problematic for grid-supporting-grid-feeding inverter controls. Although the generator initially picks up the load, for large load steps, the inverter ends up supporting most of the load during the transient. With grid-supporting-grid-feeding control the inverter begins injecting power once the voltage and frequency begin to sag. During a load step the voltage and frequency sag because of the generator transient response to picking up load. Therefore, for a small load step the generator will initially pick up the load step and then the inverters will pick up their share of the load. However, for a large load step, where the generator frequency would otherwise transiently drop below the rated droop frequency, the inverter will end up picking up the majority of the load step in order to maintain the frequency. For example,

if the generator frequency would sag to 57 Hz without the help of the inverter, but the inverter operates on a 1 Hz frequency droop, the inverter will inject 1 pu power once the frequency drops to 59 Hz, thereby partially unloading the generator. Once the inverter is carrying more than its per-unit share, the generator will see a speed reference error and will increase its output power similar to the grid-supporting-grid-forming inverter case. Therefore the problem of overloading is still present, although the beginning portion of the transient occurs differently.

The transient load sharing between a generator and grid-supporting-grid-feeding inverter is simulated with the inverter control shown in Fig. 14, and the network in Fig. 30. The simulation results are shown in Fig. 41, where the generator initially picks up the load step, then the inverter picks up most of the load as the frequency sags, and finally the generator increases its output power until the system reaches steady state. In the simulation the current controller, power controller, and PLL [31], bandwidths are set at 260 Hz, 17 Hz, and 5 Hz, respectively, with the gains in Table 4. The voltage and frequency feedback are filtered with the same low-pass filter as in (31). This simulation shows that the tradeoff between power sharing and voltage and frequency regulation is also present with the grid-supporting-grid-feeding control. With this method the inverter could be made to respond more slowly such that it does not immediately take up the load from the generator, but this would be at the expense of allowing a larger voltage and frequency transient.

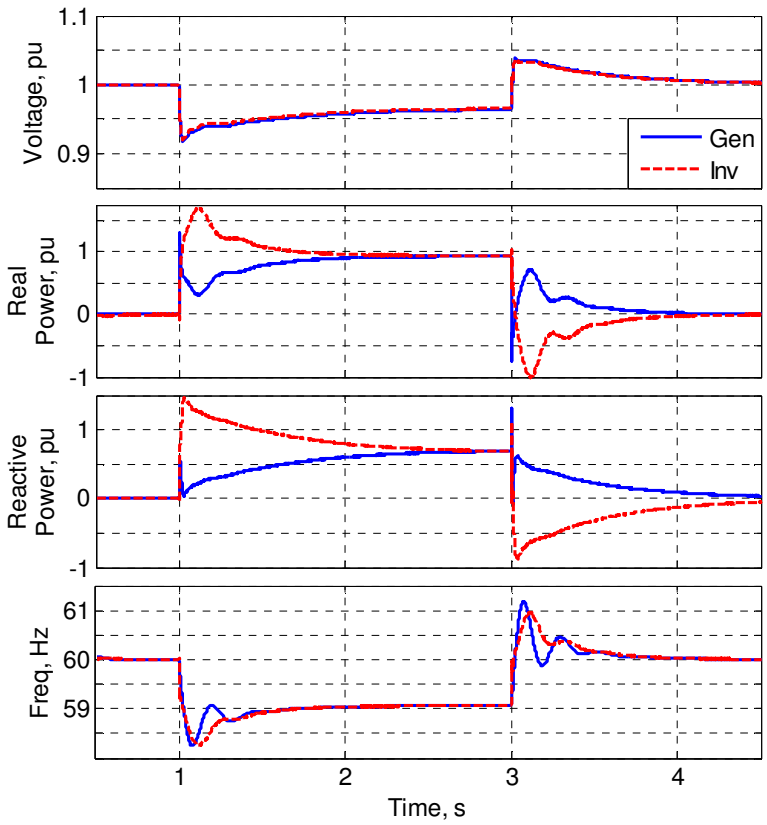

Fig. 39: Simulation of 100 % load step showing the same poor transient load sharing resulting in overload of the inverter with grid-supporting-grid-feeding control mode.

Table 4: Grid-supporting-grid-feeding Control Parameters

Parameter	**Value**
P,Q control k_p	0.5 I_{pu}/P_{pu}
P,Q control k_i	50 (I_{pu}/P_{pu})/s
Current Control k_p	0.5 V_{pu}/I_{pu}
Current Control k_i	150 (V_{pu}/I_{pu})/s
PLL k_p	22.2 ω_{pu}/V_{pu}
PLL k_i	246.7 (ω_{pu}/V_{pu})/s

4.9. Chapter Conclusion

The impact of increased inverter droop slope shows an important tradeoff between improved transient load sharing and increased voltage and frequency transients. By increasing the inverter's droop slope, the generator picks up load more quickly by allowing a larger frequency deviation. This is intuitive for real power output: the generator only increases its mechanical torque in response to an error between its

measured speed and speed reference, and if the inverter tightly regulates the frequency, the governor will see a small speed error and will increase its output power slowly. Thus any control that improves transient load sharing between inverters and generators will do so by allowing larger voltage and frequency deviations.

The inverter effectively acts as a stiff source that controls the generator behavior. It is only by making the inverter less than ideal, and therefore allowing for smaller inverter ratings, that a cost effective relationship can be realized. While inverters are capable of regulating the voltage and frequency more tightly than synchronous generators, this is not always necessary in islanded operation.

Superior power quality is often not the highest priority in backup operation. Existing backup generator systems use synchronous generators, and thus tend to have large voltage and frequency transients during load steps. In those systems, the main power-quality restriction is simply to ensure that loads do not drop out. Large voltage and frequency transients may be tolerated (large in comparison to what is achievable with inverter based sources) because islanded operation is an emergency mode, and because the cost of providing perfect power quality is high. In situations where specific power quality requirements must be met, load steps may be limited and generators oversized.

In designing microgrids it is important to recognize the tradeoffs between cost and power quality. While intuitively it seems obvious that customers will want better power quality, they traditionally have not been willing to pay more for it, as it is difficult to demonstrate sufficient return on investment. Inverter cost is primarily driven by peak ratings, and if sacrificing some of the inverter's fast voltage and frequency regulation capabilities for improved transient load sharing results in reduced inverter ratings and improved battery life, it may be a justified tradeoff.

CHAPTER 5: EMULATING SYNCHRONOUS GENERATOR

Over-rating of inverters and reduced battery life are two of the main consequences of poor transient load sharing between inverters and generators, and these consequences could have significant impact on microgrid cost. While it may often be desirable for the inverter to improve power quality by supplying transient loads, cost constraints may prevent sizing the inverter to supply the largest possible load step. One method to alleviate the over-rating and reduced battery life is to ensure equal transient power sharing. A method to guarantee equal transient power sharing is to emulate a generator via a power hardware-in-the-loop (HIL) approach. Using inverters to emulate machines has been done before in various power HIL applications including testing of motor drives [78, 79] and this method is expanded on here to demonstrate equal transient power sharing.

5.1. Control Strategy

An inverter can be made to exactly emulate a generator by simulating the equations governing a generator inside the inverter's controller, and using the simulated stator currents as a current reference for the inverter operating in current control, as seen in Fig. 40. References [80-82] describe designing inverters to emulate generators, but [80, 81] only approximate the machine dynamics and [82] does not close the loop by simulating a governor and AVR. This work fully emulates a generator, including the governor and AVR, to demonstrate equal transient power sharing between an inverter and a generator.

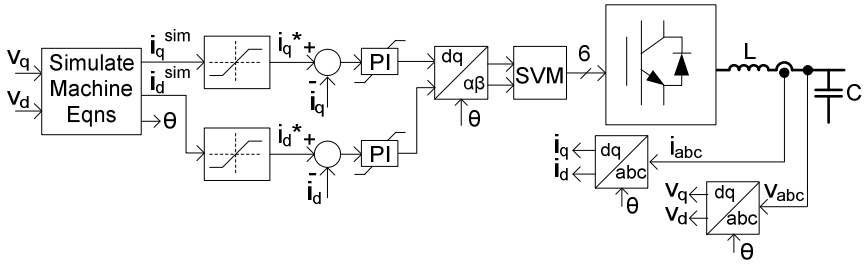

Fig. 40: Inverter control for emulation of a generator.

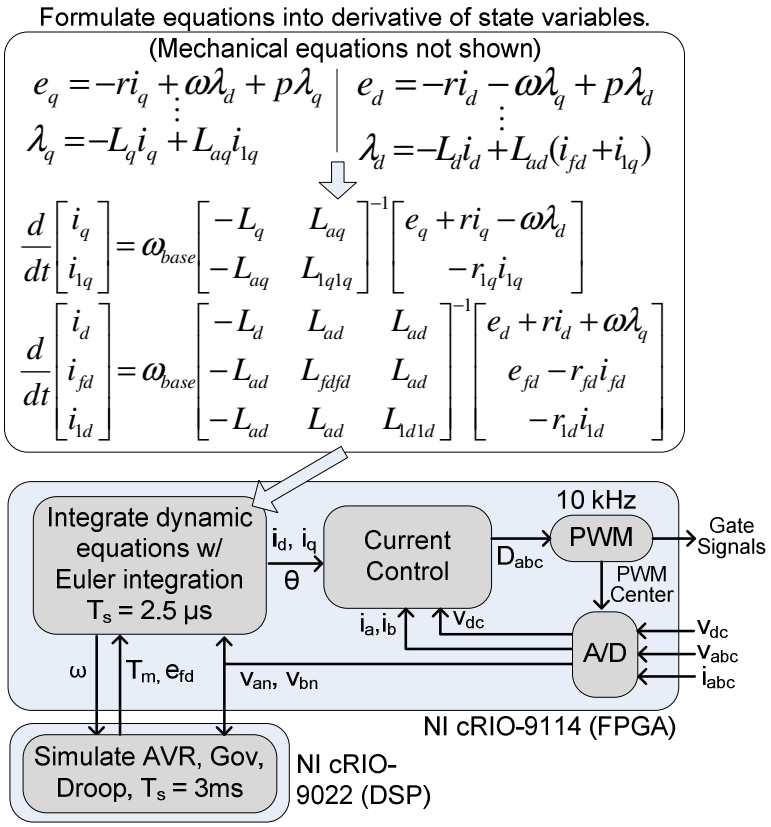

Fig. 41: Structure of generator emulation algorithm.

The math and control structure for emulating a generator are shown in Fig. 41. The electrical and mechanical dynamic equations [42] are formulated into the derivatives of the state variables [83], and the state variables are integrated in real-time on the FPGA, as shown in Fig. 41. The stator and rotor voltage equations are given by:

$$
\begin{aligned}
e_d &= -ri_d - \omega\lambda_q + p\lambda_d \,, \\
e_{fd} &= r_{fd} i_{fd} + p\lambda_{fd} \,, \\
e_{1d} &= 0 = r_{1d} i_{1d} + p\lambda_{1d} \,, \\
e_q &= -ri_q + \omega\lambda_d + p\lambda_q \,, \\
e_{1q} &= 0 = r_{1q} i_{1q} + p\lambda_{1q} \,,
\end{aligned}
\tag{46}
$$

and the flux-linkage equations are given by:

$$
\begin{aligned}
\lambda_d &= -L_d i_d + L_{ad}(i_{fd} + i_{1d}) \,, \\
\lambda_{fd} &= L_{ad}(-i_d + i_{1d}) + L_{fdfd} i_{fd} \,, \\
\lambda_{1d} &= L_{ad}(-i_d + i_{fd}) + L_{1d1d} i_{1d} \,, \\
\lambda_q &= -L_q i_q + L_{aq} i_{1q} \,, \\
\lambda_{1q} &= -L_{aq} i_q + L_{1q1q} i_{1q} \,,
\end{aligned}
\tag{47}
$$

The electrical torque equation is given by:

$$
T_e = \lambda_d i_q - \lambda_q i_d \,. \tag{48}
$$

Equation (49) gives the relationship between the non-scaled field voltage E_{fd} (the output from the AVR) and the per-unit field voltage e_{fd}.

$$
e_{fd} = E_{fd} r_{fd} / L_{ad} \text{ (Note: } E_{fd} = 1 \text{ pu gives rated voltage at no load)} \tag{49}
$$

The electrical and mechanical dynamic equations are formulated into the derivatives of the state variables in (50)-(52).

$$
\frac{d}{dt}\begin{bmatrix} i_d \\ i_{fd} \\ i_{1d} \end{bmatrix} = \omega_{base} \begin{bmatrix} -L_d & L_{ad} & L_{ad} \\ -L_{ad} & L_{fdfd} & L_{ad} \\ -L_{ad} & L_{ad} & L_{1d1d} \end{bmatrix}^{-1} \begin{bmatrix} e_d + ri_d + \omega\lambda_q \\ e_{fd} - r_{fd} i_{fd} \\ -r_{1d} i_{1d} \end{bmatrix} \tag{50}
$$

$$
\frac{d}{dt}\begin{bmatrix} i_q \\ i_{1q} \end{bmatrix} = \omega_{base} \begin{bmatrix} -L_q & L_{aq} \\ -L_{aq} & L_{1q1q} \end{bmatrix}^{-1} \begin{bmatrix} e_q + ri_q - \omega\lambda_d \\ -r_{1q} i_{1q} \end{bmatrix} \tag{51}
$$

$$
\frac{d}{dt}\begin{bmatrix} \omega \\ \theta \end{bmatrix} = \omega_{base} \begin{bmatrix} \dfrac{1}{2H\omega_{base}}(T_m - T_e - B\omega) \\ \omega \end{bmatrix} \tag{52}
$$

Note that when integrating the state variables in real-time, the derivatives are with respect to time in seconds as opposed to time in per-unit, thus all derivatives should be multiplied by ω_{base}. The simulated stator currents and rotor angle are used as the current reference and dq transformation angle in the inverter current control, as seen in Fig. 40. The

algorithm has been implemented in fixed point on a National Instruments CompactRIO FPGA and real-time processor.

5.2. Experimental Results

In this set of experimental results, the inverter is controlled to emulate a generator by using the control shown in Fig. 40 and Fig. 41, and is programmed with the datasheet parameters of the 12.5 kW generator. The current control gains are the same as in Table 4. The current control gains were chosen heuristically and provide a closed loop current control bandwidth of 260 Hz. This is a relatively low bandwidth, but provides sufficient performance for emulating a generator in standalone mode or in parallel with an actual generator.

The experimental results with the same 16 kW and 8 kVAR load step are shown in Fig. 42 and Fig. 43. The inverter and generator share power proportionally, both transiently and in steady state. There are some minor differences in the output power due to small error in the datasheet parameters, which impacts the first few cycles after the transient and slight differences between the tuning of the simulated and actual AVR and governor. The errors in real power sharing are similar during load application and rejection, although the reactive power sharing error is significantly larger during turn-off. However, some error is not surprising, and would be present even in two identical generators due to manufacturing and tuning variations. These experimental results show that emulating a generator is effective for providing transient power sharing between inverters and generators.

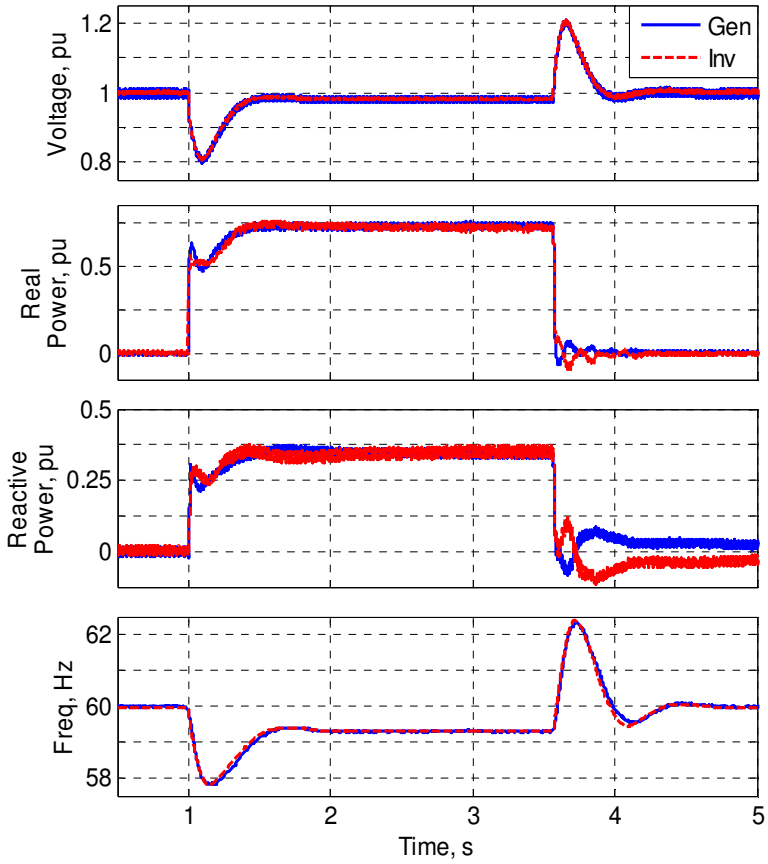

Fig. 42: Experimental results for load step with inverter emulating generator.

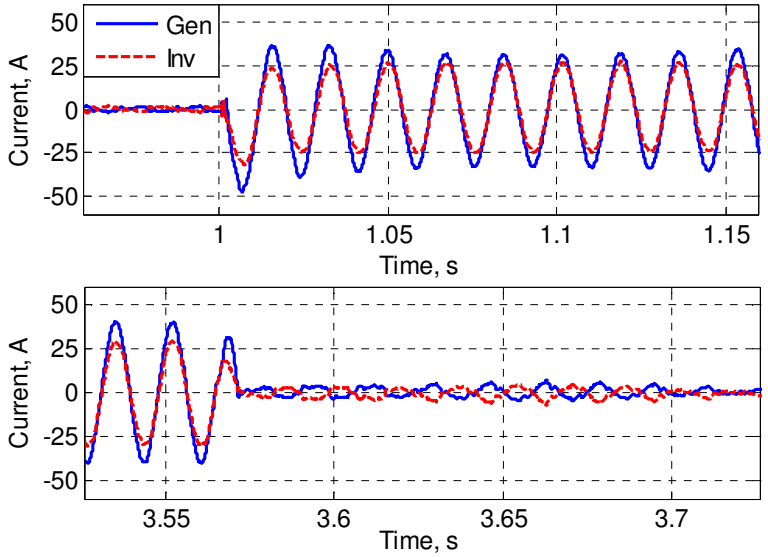

Fig. 43: Measured current with inverter emulating generator during load step changes shown in Fig. 42.

5.2.1. **Impact of Inaccurate Datasheet Parameters**

With the inverter emulating a generator, any discrepancies between the actual generator and the generator's datasheet parameters, i.e. L_{ad}, L_{aq}, etc. in Fig. 41, impact the initial power sharing. If the inverter is programmed with different datasheet parameters than those of the generator, then it is as though two different generators are being paralleled, and thus the transient power sharing will not be equal. When testing this method with the original factory datasheet parameters, the initial power sharing was significantly off as seen in Fig. 44. The datasheet parameters for the generator were experimentally extracted for validation, and were used to obtain the accurate transient power sharing in Fig. 42. The procedure used to experimentally validate the generator parameters is described in Appendix A. The only difference between Fig. 42 and Fig. 44 is the original vs. validated datasheet parameters, indicating that incorrect datasheet parameters have a significant impact, particularly on the reactive power sharing.

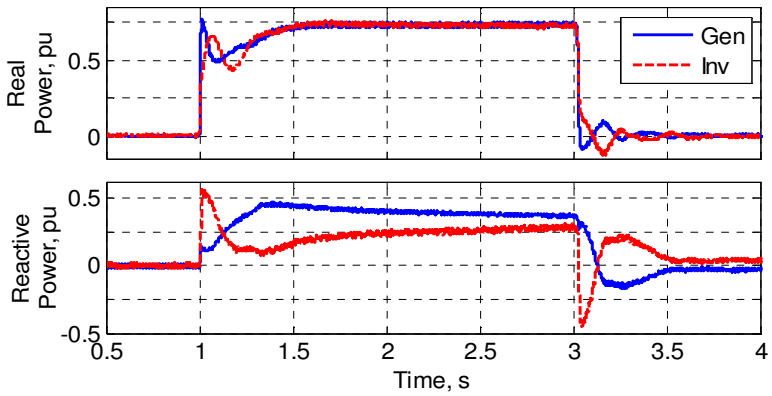

Fig. 44: Measured power sharing with original datasheet parameters showing impact of inaccurate datasheet parameters.

5.2.2. **Settling Time of Generator Emulation vs. Grid-Supporting-Grid-Forming Control**

It is interesting to note that the generator emulation method reaches steady state more quickly than the grid-supporting-grid-forming control, as seen in Fig. 42 vs. Fig. 34, respectively. The main reason for the faster settling time is that a power sharing error creates a relatively small reference error for the generator AVR and governor, and thus

the generator responds slowly to a power sharing error. For the generator emulation method, the power sharing error stays close to zero, and the system reaches steady state quickly. Fig. 45 shows the power sharing error ($P_{INV,pu}$ - $P_{GEN,pu}$) and generator frequency reference error (f - f_{ref}) from the grid-supporting-grid-forming control and generator emulation control experimental results in Fig. 34 and Fig. 42, respectively. In the grid-supporting-grid-forming case, the generator frequency reference error decreases slowly and roughly in proportion to the power sharing error. Another factor causing the emulation method to settle more quickly is that a larger voltage and frequency dip causes the AVR and governor to make larger control actions. However, if a power sharing error were present in the emulation case, it would also take longer to settle.

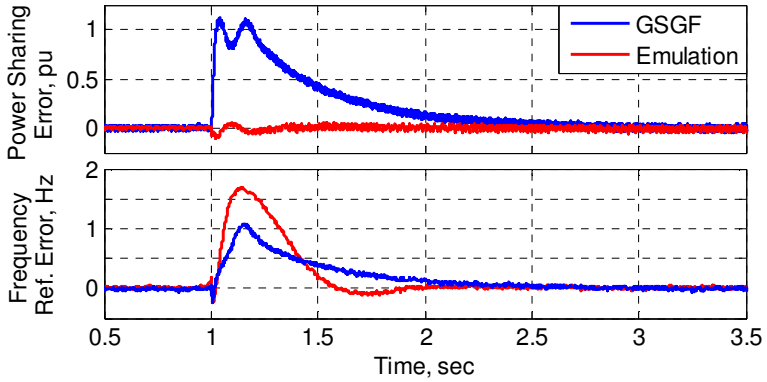

Fig. 45: Power sharing error and generator frequency reference error for grid-supporting-grid-forming (GSGF) and generator emulation controls.

While using the inverter to emulate a generator provides equal transient power sharing with generators, there are drawbacks. The generator emulation method is sensitive to measurement channel DC offsets and unbalance that cause dc and negative sequence currents, respectively, in the simulated stator currents. For emulating large generators, it is necessary to properly model the governor and prime mover dynamics, and extensive modeling efforts would be required to emulate large, turbo-charged engines. As noted in [81], the emulated generator model breaks down during severe transients and faults, when the inverter cannot supply the same peak currents as a generator due to the inverter's limited overcurrent capabilities.

5.3. Tradeoff between Transient Power Sharing and Voltage and Frequency Regulation

One of the main contributions of the generator emulation method is to highlight the inherent tradeoff between improved transient power sharing and fast voltage and frequency regulation. As described previously, the only way for the generator to contribute more during a transient, and thus improve the transient power sharing, is by allowing the voltage and frequency to dip. If the inverter regulates the voltage and frequency tightly, it will do so at the expense of supporting most of the load step, resulting in significant oversizing of the inverter.

The grid-supporting-grid-forming control and generator-emulation control give the endpoints of the spectrum of power sharing error vs. voltage & frequency dip. In Table 5 the power sharing error and voltage and frequency dip are compared for the experimental results, showing maximum real and reactive power sharing error ($P_{INV,pu}$ - $P_{GEN,pu}$, $Q_{INV,pu}$ - $Q_{GEN,pu}$), and the minimum voltage (V_{min}) and frequency dip (f_{min}) during the load application transient. When the inverter acts as a stiff, grid-forming source, the inverter will supply almost the entire load step and the voltage & frequency dip will be given by the transient response characteristics of the inverter. With the generator emulation method, the load sharing is equal, and the voltage & frequency dip are given by the transient response characteristics of the generator.

Table 5: Power Sharing Error vs. Voltage & Frequency Dip

Control Method	$\mathbf{P_{err}}$	$\mathbf{Q_{err}}$	$\mathbf{V_{min}}$	$\mathbf{f_{min}}$
GSGF (Fig. 34)	1.1 pu	0.86 pu	0.92 pu	58.7 Hz
Gen. emulation (Fig. 42)	0.1 pu	0.05 pu	0.81 pu	57.8 Hz

5.4. Chapter Conclusion

While inverters are capable of regulating the voltage and frequency more tightly than synchronous generators, this is not always necessary in islanded mode. Superior

power quality is often not required in islanded mode. Traditional backup generator systems use synchronous generators, and thus have large voltage and frequency transients during load steps. In designing microgrids it is important to recognize the tradeoffs between cost and power quality, and the impact of poor-transient load sharing on inverter rating requirements. Sacrificing some of the inverter's fast voltage and frequency regulation capabilities for improved transient load sharing may be justified if it has a significant impact on microgrid cost. Note that the exploitation of this tradeoff may be limited by specific power quality requirements in some applications, e.g. hospitals and Department of Defense (DOD) applications. Cost constraints may also restrict the inverter rating, forcing a reduction in voltage and frequency regulation.

CHAPTER 6: VIRTUAL IMPEDANCE AND TRANSIENT DROOP

The analysis of inverter-generator power sharing in the previous chapters established that the initial power sharing ratio between an inverter and synchronous generator is a function of the output impedances, and that a larger inverter frequency droop slope helps the generator to pick up load more quickly. This leads to the idea of using a virtual output impedance in the inverter control to cause the initial power sharing to be equal, and using a transient droop to match the characteristics of the governor and prime mover.

For the remainder of the work in this thesis, the modified experimental setup in Fig. 46 is used. This is the same experimental setup as in Fig. 30, except for the addition of a delta-wye transformer on the inverter output. The delta-wye transformer allows the three-wire inverter to supply single-phase loads. The inverter's rated power is left at 11.1 kVA to maintain the same relative rating between the inverter and generator.

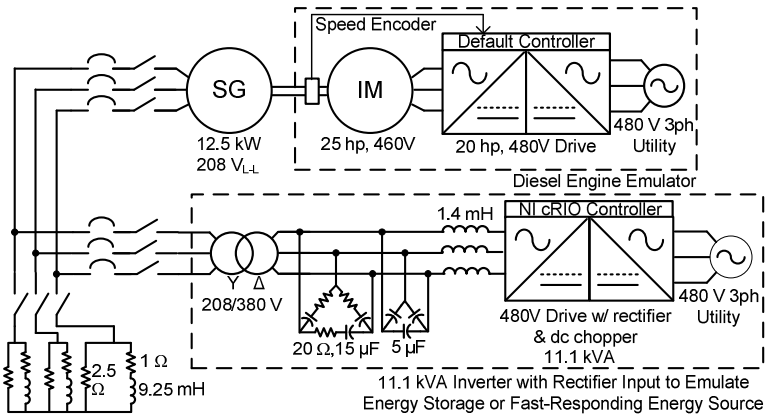

Fig. 46: Diagram of modified experimental microgrid setup with delta-wye transformer added to inverter output.

6.1. Virtual Impedance

Virtual impedance can be added to the single loop voltage control to add additional output impedance, which will impact the initial power sharing ratio. Transient voltage and frequency droop terms can be used to allow the voltage and frequency to transiently dip further to allow the generator to pick up more of the load. The control

diagram in Fig. 47 shows the single-loop inverter control from Fig. 28, but with virtual output resistance R_{VI} and inductance L_{VI}, and transient voltage droop $G_v(s)$ and transient frequency droop $G_f(s)$. The virtual impedance voltage drops $v_{d,VI}$ and $v_{q,VI}$ are given by (24)-(25).

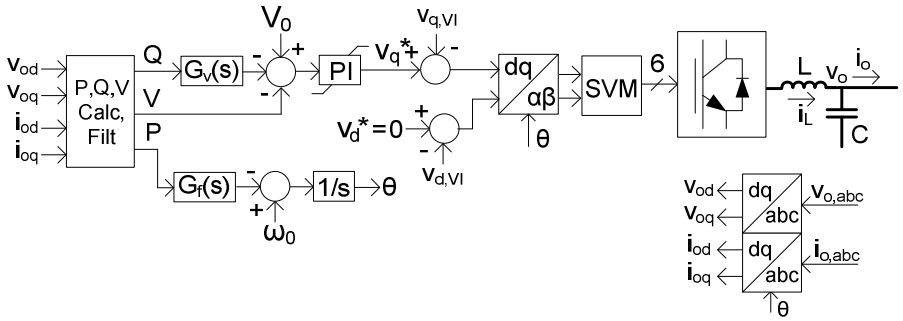

Fig. 47: Single-loop inverter control with virtual impedance and transient droop.

The impact of virtual impedance on the initial power sharing ratio is investigated here. Various magnitudes and X/R ratios of the virtual impedance have been simulated. Note that in this thesis, the virtual impedance is typically be given by its magnitude, $|Z_{VI}|=\sqrt{R_{VI}^{\ 2}+(\omega L_{VI})^2}$, and X/R ratio, X_{VI}/R_{VI}, where $X_{VI}=\omega L_{VI.}$ Fig. 48 shows the impact of increasing the virtual impedance magnitude on the initial power sharing. As $|Z_{VI}|$ increases, the generator takes more of the initial load step. With a virtual impedance magnitude of 0.15 pu, the initial real power sharing is approximately equal. The inverter's reactive power output decreases more quickly than its real power output with increasing virtual impedance magnitude.

After approximately the first cycle, the power sharing changes significantly. The change in power sharing after the first cycle is due to two main factors. The short transient and sub-transient time constants in the small generator in the lab setup cause the generator output to decay quickly. Also, the remainder of the transient is dominated by the voltage and frequency regulation characteristics of the inverter and generator, not the output impedance.

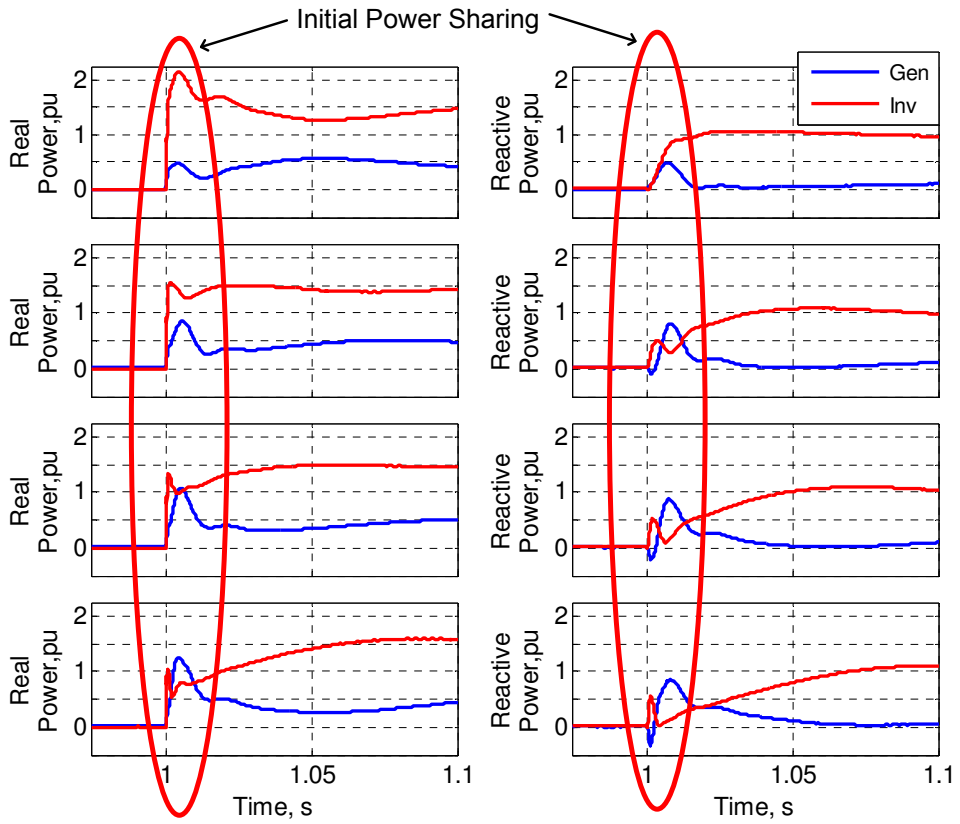

Fig. 48: Simulated initial power sharing with varied virtual impedance magnitude (top to bottom - $|Z_{VI}|$ = 0 pu, 0.075 pu, 0.15 pu, and 0.3 pu, with X_{VI}/R_{VI} = 3).

Fig. 49 shows the initial real and reactive power with virtual impedance X/R ratios of 1/0 (purely inductive), 3, and 1. It can be seen that the virtual resistance improves damping of oscillations present immediately after the load step. More analysis of damping is provided in the small-signal analysis in Section 6.3.3.

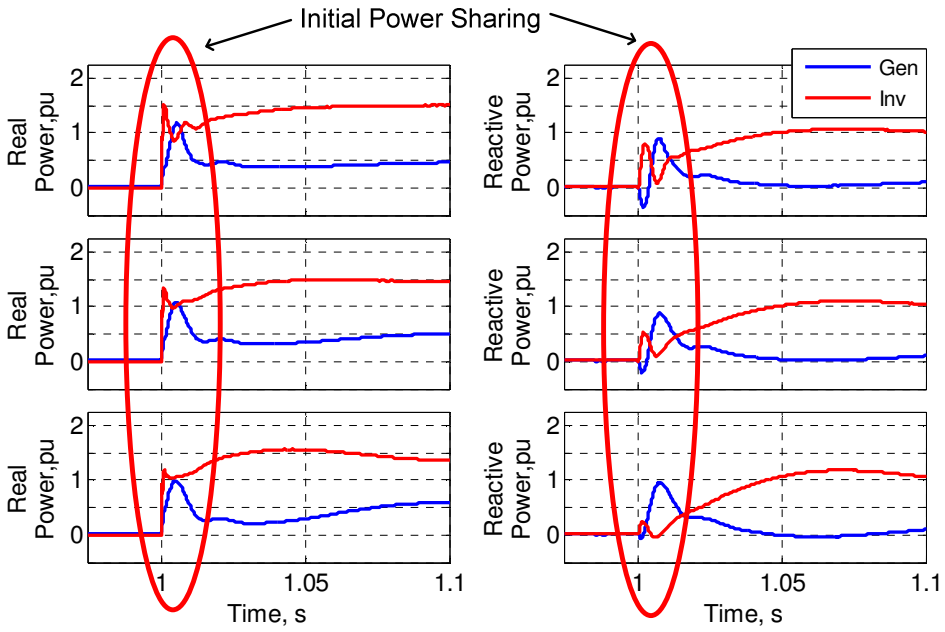

Fig. 49: Initial power sharing with varied X_{VI}/R_{VI} (top to bottom - X_{VI}/R_{VI} = 1/0, 3, and 1, with $|Z_{VI}|$ = 0.15).

In summary, simulations show that virtual impedance magnitude can be used to change the initial power sharing ratio, and that virtual impedance X/R ratio impacts damping of oscillations more than it impacts the initial power sharing ratio.

6.2. Transient Droop

In Section 4.7, it was shown that increased frequency droop slope caused the generator to pick up load more quickly. However, if the inverter uses a larger droop slope, the steady state power sharing will be changed. A transient droop term that decays to zero in steady state would allow the inverter frequency to have a larger droop during transients without impacting the steady state power sharing.

6.2.1. Transient Droop Transfer Function

Transient droop terms have been proposed before in order to control the transient behavior of inverter based microgrids. The primary transient droop method reported in the literature is proportional + derivative (PD) droop [22, 23, 33, 38], as given by (53) and (54), and variations thereof.

$$G_v(s)=m_Q+m_{Q2}\cdot s \tag{53}$$

$$G_f(s)=m_P+m_{P2}\cdot s \tag{54}$$

In the literature, the introduction of a derivative term is motivated by unsatisfactory transient response yielded by normal droop control. The droop gain has a significant impact on small-signal dynamics, but the choice of droop gain is constrained by steady state voltage and frequency limits. The derivative term is introduced to control the transient response without impacting steady state operation.

For the purpose of improving transient load sharing with synchronous generators, the inverter should allow its voltage and frequency to droop transiently, and to restore the voltage to the nominal droop set points (proportional droop) with a time constant similar to the generator's natural governor and AVR response characteristics. A derivative droop term has a large initial value, when *dP*/*dt* is high (although limited, since P is low-pass filtered), but decays quickly with the power calculation filter time constant. A high-pass filtered transient droop, given by (55) and (56), would allow for the decay rate of the transient term to be controlled independently.

$$G_v(s)=m_Q+m_{Q2}\frac{s}{s+\omega_{c3}} \tag{55}$$

$$G_f(s)=m_P+m_{P2}\frac{s}{s+\omega_{c2}} \tag{56}$$

A comparison of derivative and high-pass filtered transient droop to the generator's transient response is given in Fig. 50. The inverter traces show the inverter's response to a 100 % load step (by itself, not in parallel with the generator) with the droop given by (53)-(54), and (55)-(56), and with $\omega_{c2} = \omega_{c3} = 1*2\pi$ rad/s. The generator traces show the generator's voltage and frequency in response to a 100 % load step (also by itself). It can be seen that the derivative droop decays much more quickly than the generator's natural transient response, but the high-pass filtered droop's decay rate is closer to the generator's transient response.

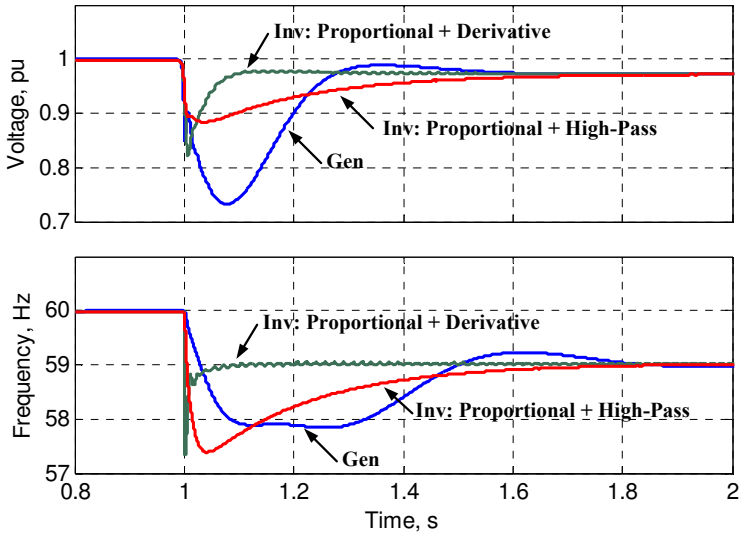

Fig. 50: Inverter voltage and frequency with derivative and high-pass filtered transient droop compared to generator transient response.

The high-pass filtered transient droop term is used in this work. The overall voltage and frequency references are given by (57) and (58), where m_P and m_Q are the frequency and voltage droop gains, m_{P2} and m_{Q2} are the transient frequency and voltage droop gains, ω_{c2} and ω_{c3} are the transient frequency and voltage droop high pass filter cutoff frequencies, and P and Q are the low-pass filtered power measurements given by (31).

$$V^* = V_0 - Q\left(m_Q + m_{Q2}\frac{s}{s+\omega_{c3}}\right) \tag{57}$$

$$f = f_0 - P\left(m_P + m_{P2}\frac{s}{s+\omega_{c2}}\right) \tag{58}$$

6.2.2. Transient Droop Time Constant

The transient droop term consists of a single-order high-pass filter, and thus the transient droop will decay with the filter's time constant. If the transient droop term decays quickly, the inverter frequency and voltage reference will increase quickly, causing the inverter to still transiently pick up the majority of the load step. If the transient droop time constant is too long, the inverter will allow it's voltage and frequency to sag longer than necessary, and the generator will transiently pick up more of

the load step than the inverter. Therefore the transient droop time constants should be primarily based on the response time of the synchronous generator's governor and AVR. Simulations of the real and reactive power sharing error ($\tilde{p}_{inv}$ - $\tilde{p}_{gen}$, and $\tilde{q}_{inv}$ - $\tilde{q}_{gen}$, where $\tilde{p}$ and $\tilde{q}$ are the instantaneous power calculations given by (15)-(16)) for various values of the frequency and voltage transient droop cutoff frequency, ω_{c2} and ω_{c3}, are overlaid in Fig. 51. As ω_{c2} and ω_{c3} are increased (i.e. the time constants $1/\omega_{c2}$ and $1/\omega_{c3}$ are decreased), the generator takes less of the load step. For real power sharing with the given system, ω_{c2} = 1 Hz causes minimal overshoot of real power sharing error. In the remainder of this work, ω_{c2} = ω_{c3} = 1 Hz is used, unless stated otherwise. Note that reactive power sharing error is non-zero in steady state due to different coupling impedances between the generator and inverter, primarily the inverter's output transformer. Methods exist to correct this error, such as adaptive droop or tertiary control [19, 23]. However, since a steady state reactive power sharing error isn't deemed critical, it has not been corrected in this work.

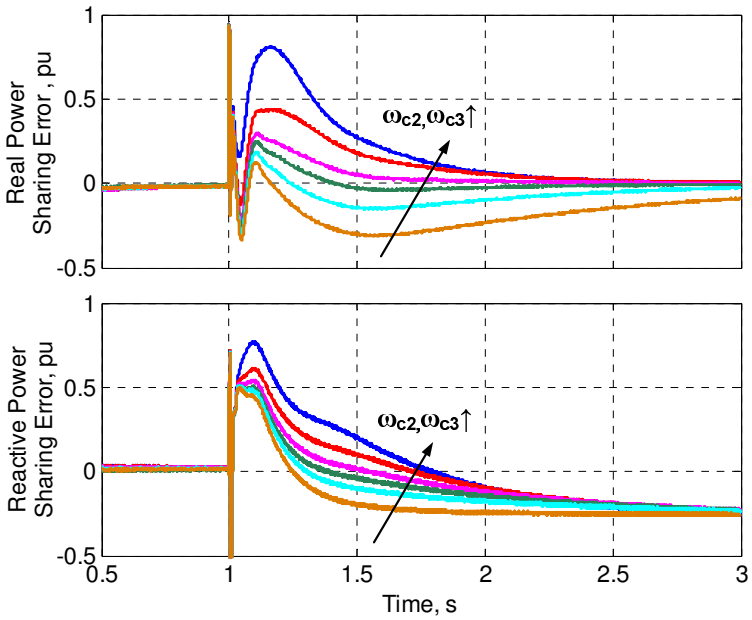

Fig. 51: Real and reactive power sharing error for varied transient droop time constant (ω_{c2}= ω_{c3}= 5 Hz, 2 Hz, 1.25 Hz, 1 Hz, 0.75 Hz, and 0.5 Hz – top to bottom, with m_{P2} = 3 Hz and m_{Q2} = 0.3 pu).

6.2.3. **Mean Squared Error as Metric for Degree of Power Sharing**

Virtual impedance and transient droop are used to allow control over the tradeoff between power sharing and voltage and frequency transients. Mean squared error (MSE) of the difference between the inverter and generator power has been chosen to evaluate the relative degree of transient power sharing error. The choice of MSE as a metric is somewhat arbitrary, but has been chosen because it is useful as a quantitative comparison of the degree of power sharing between different values of transient droop gain. The real power sharing MSE_P and reactive power sharing MSE_Q are given by (59) and (60), where $\tilde{p}$, and $\tilde{q}$ are the instantaneous real and reactive power given by (15)-(16). The integrals in (59)-(60) are evaluated from the beginning of the load step, t_0, to steady state, t_{ss}. In this system, t_{ss} is typically around 3 seconds, but the integrals account for steady state error, such that MSE is not affected by t_{ss} being longer than necessary.

$$MSE_P = \int_{t_{ss}}^{t_0} \left(\tilde{p}_{INV} - \tilde{p}_{GEN}\right)^2 dt \,. \tag{59}$$

$$MSE_Q = \int_{t_{ss}}^{t_0} \left(\tilde{q}_{INV} - \tilde{q}_{GEN} - \left(\tilde{q}_{INV}(t_{ss}) - \tilde{q}_{GEN}(t_{ss})\right)\right)^2 dt \,. \tag{60}$$

MSE_Q is the integral of the square of power sharing error minus the steady state power sharing error, since the steady state reactive power sharing error is often nonzero. A small value of MSE indicates nearly equal transient power sharing, and a large value indicates poor transient load sharing. To compare the degree of voltage and frequency dip, the mean squared error between the voltage and frequency and the steady state voltage and frequency are calculated by (61) and (62), where $\tilde{v}$ is the instantaneous voltage magnitude given by (17). Maximum voltage and frequency dip will be tabulated as well to compare the maximum depth of the voltage and frequency sag.

$$MSE_V = \int_{t_{ss}}^{t_0} \left(\tilde{v}_{INV} - \tilde{v}_{INV}(t_{ss})\right)^2 dt \,. \tag{61}$$

$$MSE_f = \int_{t_{ss}}^{t_0} \left(f_{INV} - f_{INV}(t_{ss})\right)^2 dt \tag{62}$$

6.2.4. **Simulations**

Increasing the transient droop slope will allow the voltage and frequency to sag further, causing the generator to pick up more of the load. The impact of transient frequency droop gain on real and reactive power sharing error is shown in Fig. 52. As the transient frequency droop gain is increased, the generator picks up more of the load, and the real power sharing error decreases. If the transient droop gain is increased too much, the generator picks up more of the load than the inverter, as seen in the bottom plot of Fig. 52. Increasing the transient frequency droop gain tends to increase the reactive power sharing error, absent of the transient voltage droop.

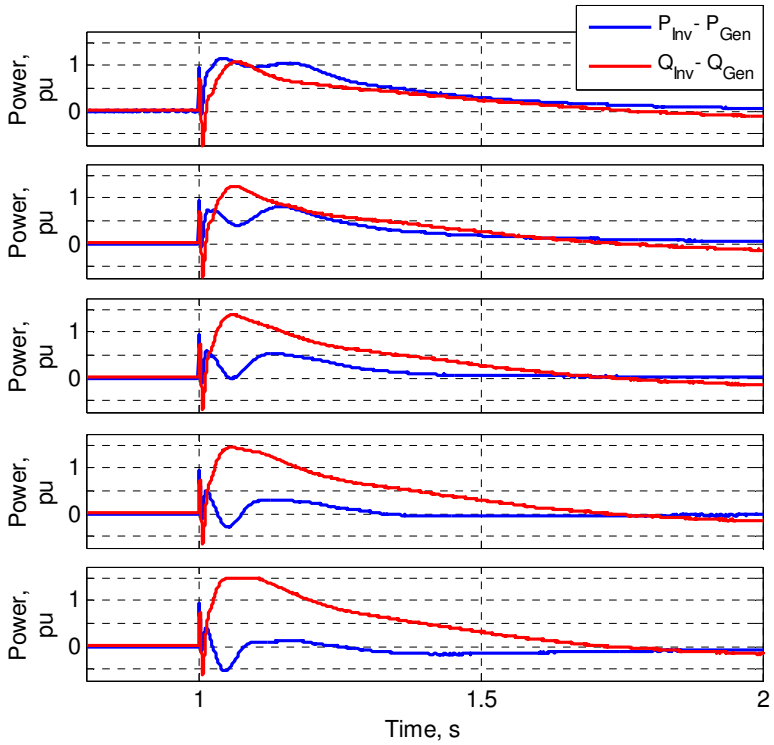

Fig. 52: Real and Reactive power sharing error for varied m_{P2} (m_{P2} = 0 Hz, 1 Hz, 2 Hz, 3 Hz, 4 Hz – top to bottom, with m_{Q2} = 0 pu).

The impact of varying the transient voltage droop gain is shown in Fig. 53. As the transient voltage droop gain is increased, the transient reactive power sharing is improved. Note that in steady state Q_{INV}-Q_{GEN} = -0.24 pu due to unequal coupling impedances, composed primarily of the inverter's output transformer.

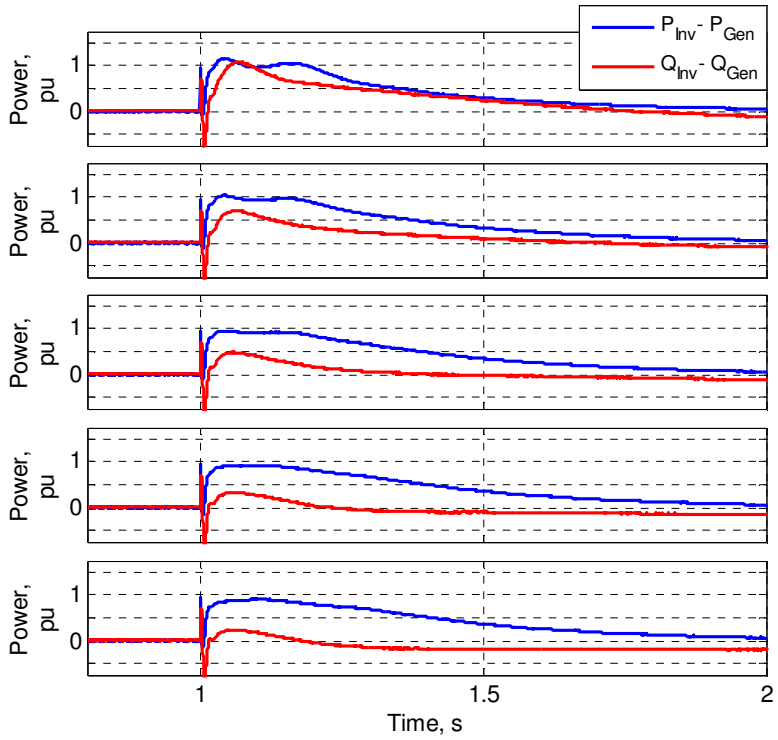

Fig. 53: Real and Reactive power sharing error for varied m_{Q2} (m_{Q2} = 0 pu, 0.1 pu, 0.2 pu, 0.3 pu, 0.4 pu – top to bottom, with m_{P2} = 0).

The combination of transient voltage and frequency droop result in improved real and reactive power sharing, as seen in Fig. 54. The results of the simulations in Fig. 54 are tabulated in Table 6, showing the real and reactive power sharing MSE, the voltage and frequency MSE, and the minimum voltage and frequency values. The arrows on Table 6 show the trend of each parameter, in the increasing direction. As the transient voltage and frequency droop gains increase, MSE_P and MSE_Q decrease, maximum voltage and frequency dip increase, and MSE_V and MSE_f increase. The rows corresponding to no virtual impedance or transient droop (base case), and maximum transient droop are bold. The base case gives the best power quality (i.e. highest V_{min} and f_{min}), and the maximum transient droop case gives the best transient load sharing. With the generator emulation method described in Section 5.1, the power sharing error is nearly zero, but with a slightly larger voltage and frequency dip.

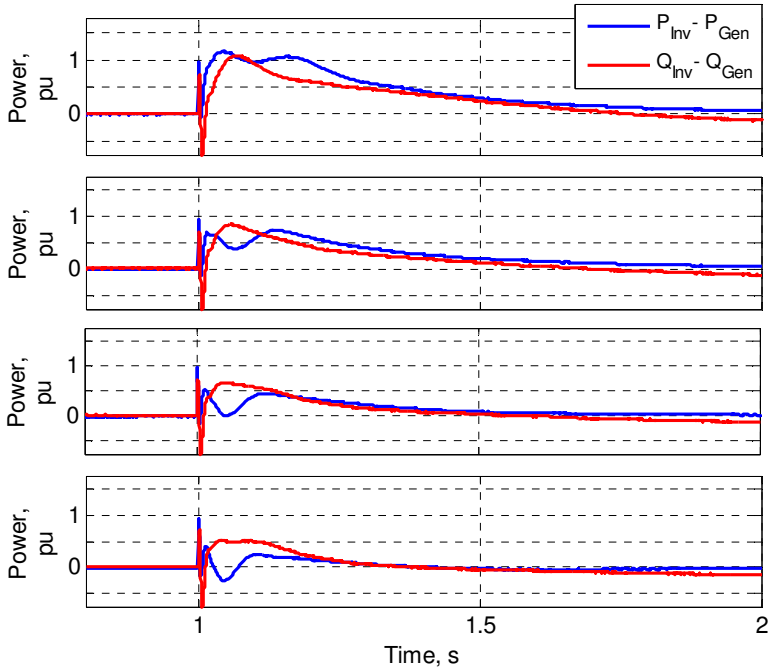

Fig. 54: Real and Reactive power sharing error for varied m_{P2} and m_{Q2} (0 Hz, 0 pu; 1 Hz, 0.1 pu; 2 Hz, 0.2 pu; 3 Hz, 0.3 pu – top to bottom).

Table 6: Power sharing MSE vs. transient droop.

Z_{VI}	m_{P2} (Hz)	m_{Q2} (pu)	MSE_P	MSE_Q	MSE_V (x10^{-3})	MSE_f	V_{min} (pu)	f_{min} (Hz)
$\|Z_{VI}\| = 0$	**0**	**0.0**	**0.311**	**0.384**	**0.357**	**0.080**	**0.918**	**58.40**
$\|Z_{VI}\| = 0.15$, $X_{VI}/R_{VI} = 3$	0	0.0	0.308	0.383	0.515	0.091	0.866	58.44
"	1	0.1	0.121	0.254	1.093	0.177	0.859	58.03
"	2	0.2	0.038	0.177	1.981	0.277	0.842	57.73
"	**3**	**0.3**	**0.011**	**0.123**	**2.932**	**0.374**	**0.813**	**57.38**
Generator Emulation (Fig. 42)			0.005	0.007	4.797	0.462	0.81	57.81

While the proposed transient voltage and frequency droop do not create perfect transient load sharing, they do improve the power sharing MSE significantly, and the degree of transient load sharing can be controlled. Finally, simulations of the base case and the case with both transient voltage and frequency droop are shown Fig. 55 and Fig. 56 to allow a visual comparison of the effectiveness of the transient droop terms. Note that $V_{INV}>V_{GEN}$ in Fig. 55-Fig. 56 because of the voltage drop across the inverter's transformer.

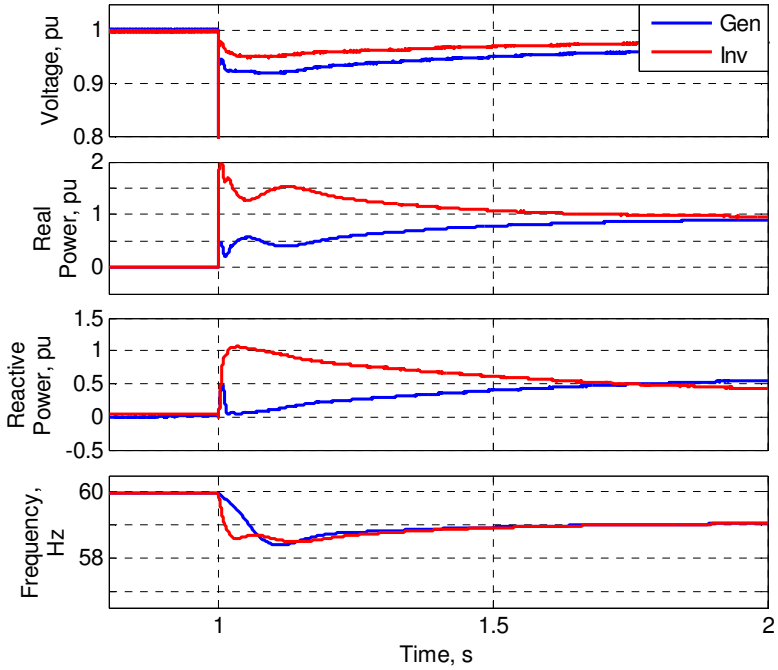

Fig. 55: Simulation of base case ($|Z_{VI}| = 0$, $m_{P2} = 0$ Hz, $m_{Q2} = 0$ pu).

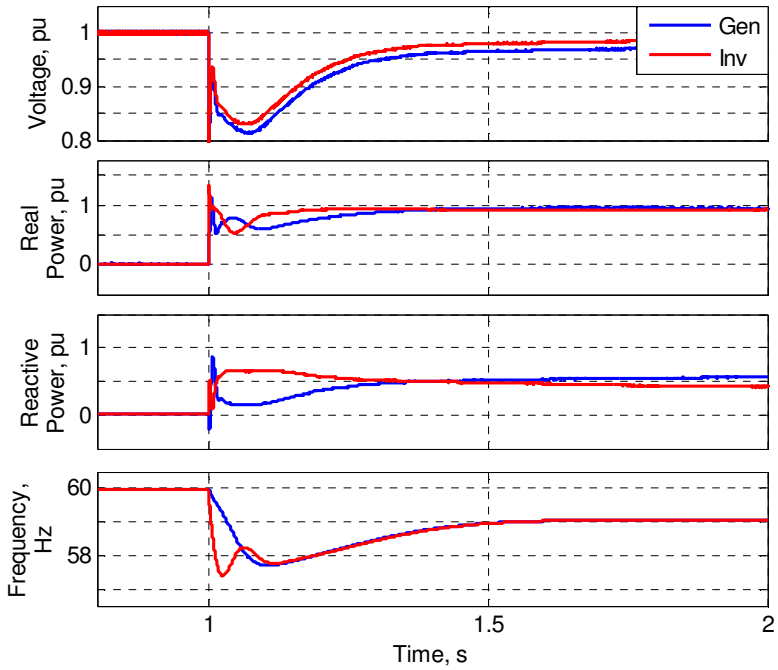

Fig. 56: Simulation of transient voltage and frequency droop ($|Z_{VI}| = 0.15$, $X_{VI}/R_{VI} = 3$, $m_{P2} = 3$ Hz, $m_{Q2} = 0.3$ pu).

6.3. Small-Signal Analysis

Small-signal modeling and sensitivity analysis [32, 33, 47, 51, 84-86] provide understanding of the impact of various system parameters and control parameters on system eigenvalues. A linearized small-signal model provides insight into the system's frequency components and damping associated with small disturbances around an operating point [32, 86]. Sensitivity analysis provides insight into the relationship between certain parameters, states, and eigenvalues. Specifically, participation factors [86] will be used to examine the relationships between specific eigenvalues and states. To see the impact of specific controller and system parameters and on system eigenvalues, parameters will be swept and the resulting eigenvalue trajectories (or root locus) will be observed.

6.3.1. Small-Signal Analysis Methodology

In [32], a method is presented for creating a small-signal model of an arbitrary microgrid. The full differential equations of the controllers, DER, connecting impedances, and RL loads, are written, linearized, and organized into a complete system state equation of the form $\Delta\dot{x}_{system}=A_{system}\Delta x_{system}$. From the A_{system} matrix, the closed-loop system eigenvalues can be calculated. Small-signal analysis for large power systems typically uses phasor analysis, where the dynamics of the stator and lines are neglected. The method in [32] includes the dynamics of the lines.

A modified version of the small-signal analysis method in [32] has been used in this work, outlined in Fig. 57. Instead of linearizing the equations by hand, the complete differential equations are written in MATLAB Simulink and simulated to obtain the steady state operating point. Then MATLAB's built-in linearization tools are used to extract the linearized model. As in [32], the differential equations for the inverter and generator are written in dq, and the local dq frames are connected to a global dq frame. The full differential equations for the synchronous machine are used, including the field,

damper, stator, and rotor dynamics, using the equations given in Section 5.1. Inclusion of the damper windings proves critical in this work, as the problematic modes (eigenvalues) disappear if the damper windings are eliminated from the linearization.

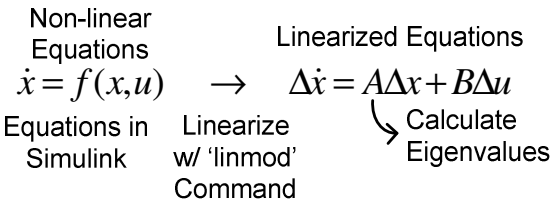

Fig. 57: Small-signal analysis overview.

6.3.2. **Applicability to Large-Signal Behavior**

Linearized small-signal models represent the system dynamics for small perturbations around an operating point [32, 86]. For non-linear systems, the small-signal behavior may be a poor representation of the large-signal behavior (e.g., large load steps, which is the focus of this work). To investigate the similarity or dissimilarity between small and large-signal behavior in the system under consideration, a comparison between simulations of the non-linear and linearized model has been made. The analysis shows that there are differences between the small-signal and large-signal dynamics, but that the small-signal model still gives useful insight into the dominant modes seen in large-signal behavior. The relatively close agreement of large and small-signal behavior indicates that the system under consideration does not exhibit a high degree of nonlinearity.

For small perturbations, the linearized small-signal model agrees well with the full non-linear equations, as expected. Fig. 58 shows simulations of the linearized model and the full non-linear model for a 10 % load step, showing close agreement.

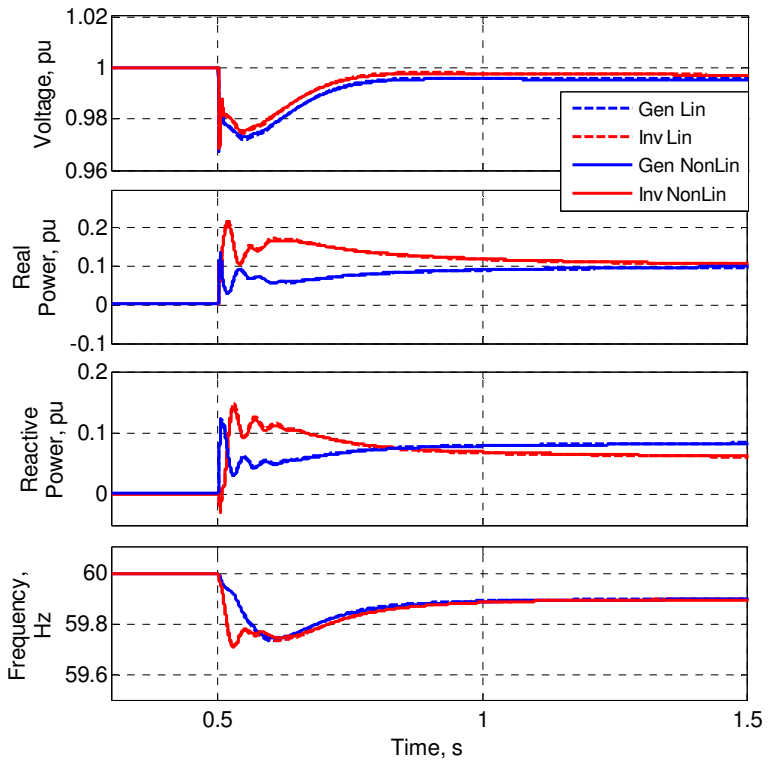

Fig. 58: Comparison of linearized model to non-linear for 10 % load step.

The linearized model is simulated by specifying linearization inputs and outputs in Simulink, using the MATLAB command 'linearize', simulating the linearized system with the MATLAB command 'step.' The operating point is added as an offset for plotting. The load step magnitude (for specifying the RL load) was chosen as the linearization input, and the power, voltage, and frequency as the linearization outputs.

Fig. 59 shows the linearized and non-linear simulations for a 100 % load step. The damping in the linearized model is significantly worse than the non-linear model. However, if the model is linearized around the full-load operating point, as shown in Fig. 60, (the linearized model in Fig. 59 is linearized around the no-load operating point), and then a load step is applied to the linearized model, the linearized model matches more closely. In Fig. 60, the offsets from the no-load operating point are added to the simulation of the model linearized around the full-load operating point, to allow the linearized and non-linear models to be plotted together. The lightly damped ~20 Hz

oscillations in particular are better represented by the linearization around full-load vs. no-load. In this system, the dominant eigenvalues are damped better at full-load than no-load.

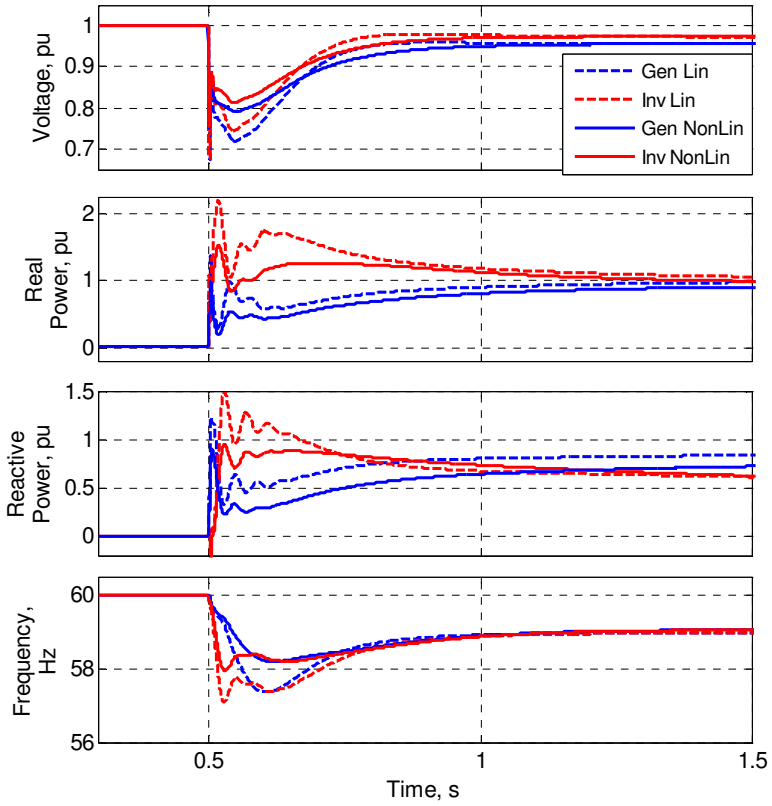

Fig. 59: Comparison of linearized model to non-linear for 100 % load step, with model linearized around no-load operating point.

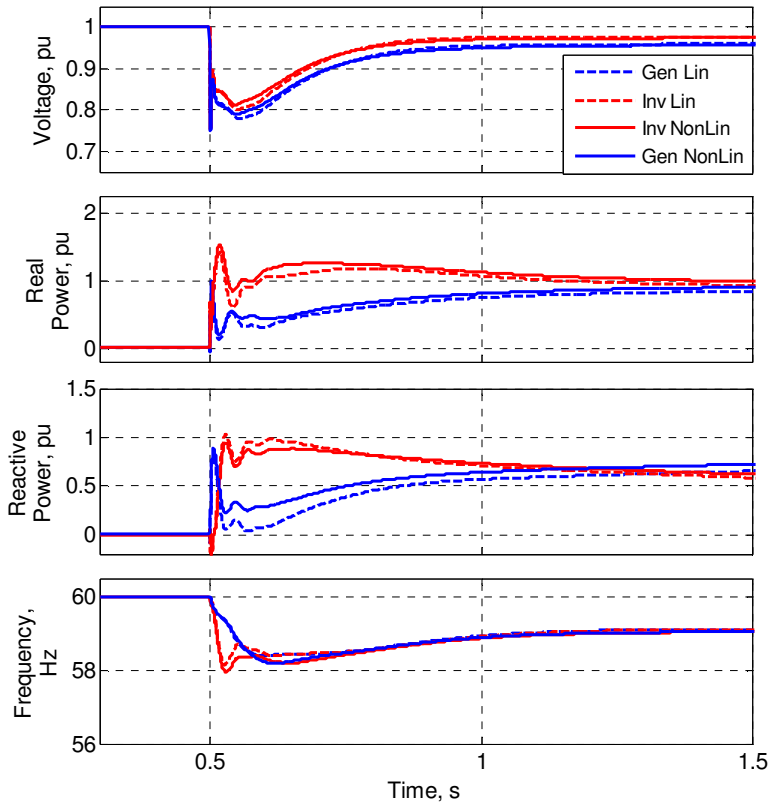

Fig. 60: Comparison of linearized model to non-linear for 100 % load step, with model linearized around full-load operating point.

For load rejection, the system is more oscillatory. A comparison between the linearized and non-linear models is shown in Fig. 61, for linearizations around no-load and full-load operating points. For load rejection, the linearization around no-load gives a better representation, and for load application, the linearization around full-load gives a better representation.

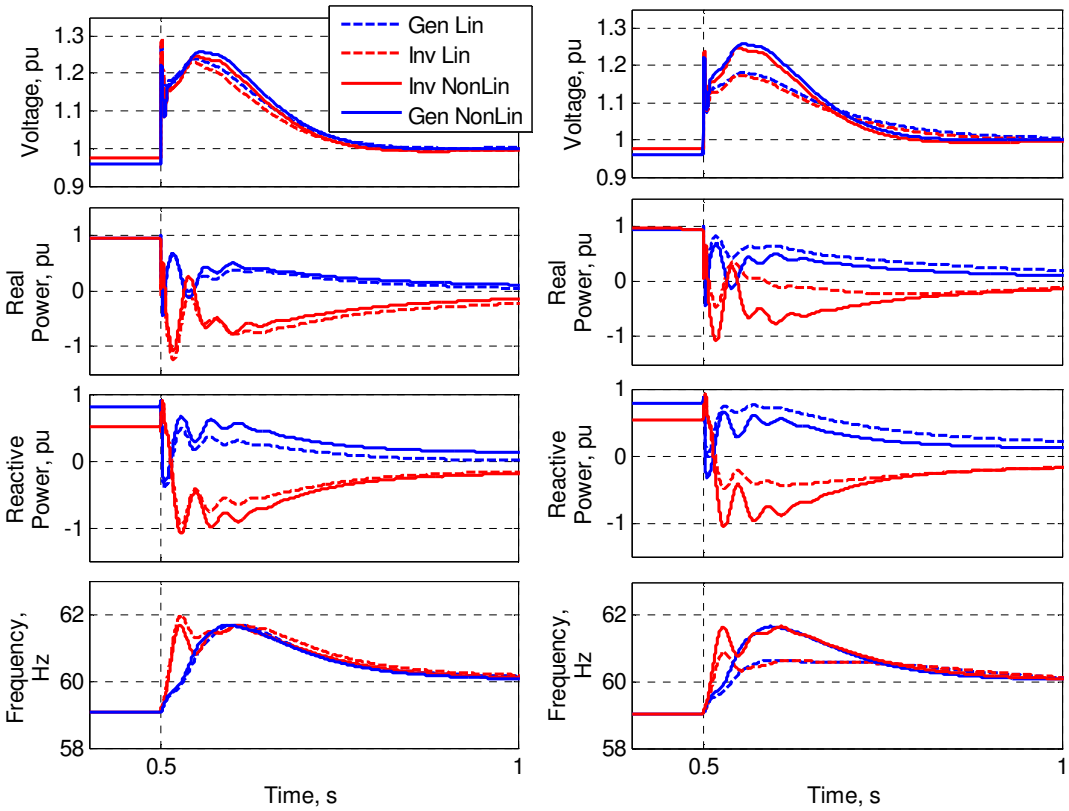

Fig. 61: Comparison of linearized and non-linear models for rejection of 100 % load, with linearization around no-load (left) and rated-load (right).

These comparisons have shown that, in this particular system, the linearized small-signal models give a reasonably accurate representation of the large-signal behavior. This justifies the use of linearized small-signal models to aid in the design of controls for improving transient power sharing. Note that for the comparisons in this section between the linearized and non-linear models, the following settings were used: Multi-loop control, m_{P2}=1 Hz, m_{Q2} = 0.1 pu, $|Z_{VI}|$=0.15 pu, X_{VI}/R_{VI} = 3. These settings were chosen because they yield a relatively low damping factor on the dominant eigenvalues, to show whether or not the linearized model accurately reflects dominant eigenvalues.

6.3.3. Impact of Virtual Impedance and Transient Droop on Small-Signal Stability

Virtual impedance has been proposed to improve the initial power sharing ratio, and transient droop to improve the remainder of the transient. The impact on small-signal

stability of the virtual impedance and transient droop terms is investigated here. The impact of virtual impedance magnitude, $|Z_{VI}|$, and X/R ratio are investigated in Fig. 62 and Fig. 63. There is one complex eigenvalue pair of primary interest, $\lambda_{17,18}$, which based on participation factor analysis [32, 86] is primarily associated with the generator electromechanical states. As $|Z_{VI}|$ is increased, damping of $\lambda_{17,18}$ decreases, as seen in Fig. 62. As the virtual impedance X/R ratio is decreased, damping of $\lambda_{17,18}$ also decreases, as seen in Fig. 63. Stability of the single-loop control is relatively insensitive to virtual impedance. In the eigenvalue plots in this thesis, a line showing damping factor $\zeta = 0.2$ is shown to give a visual reference of the damping factor of the eigenvalues.

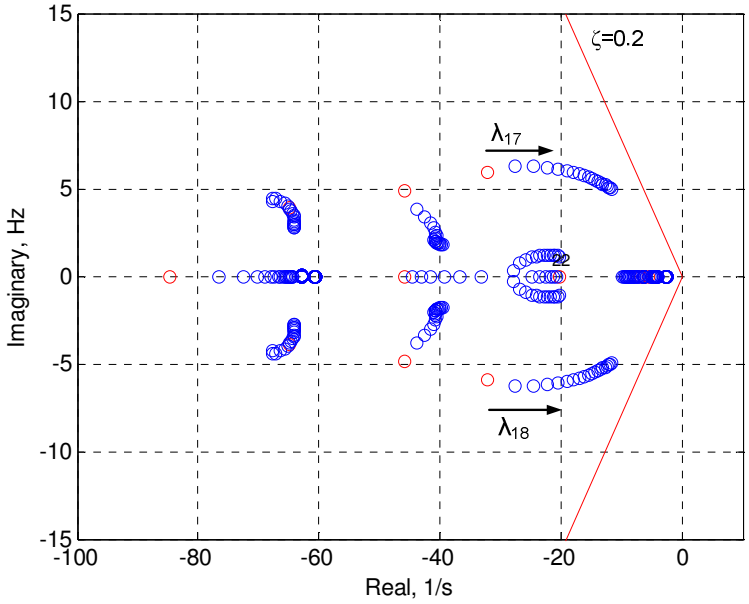

Fig. 62: Eigenvalue trajectories with single-loop control when sweeping $|Z_{VI}|$ from 0 pu to 0.4 pu (with $X_{VI}/R_{VI} = 3$).

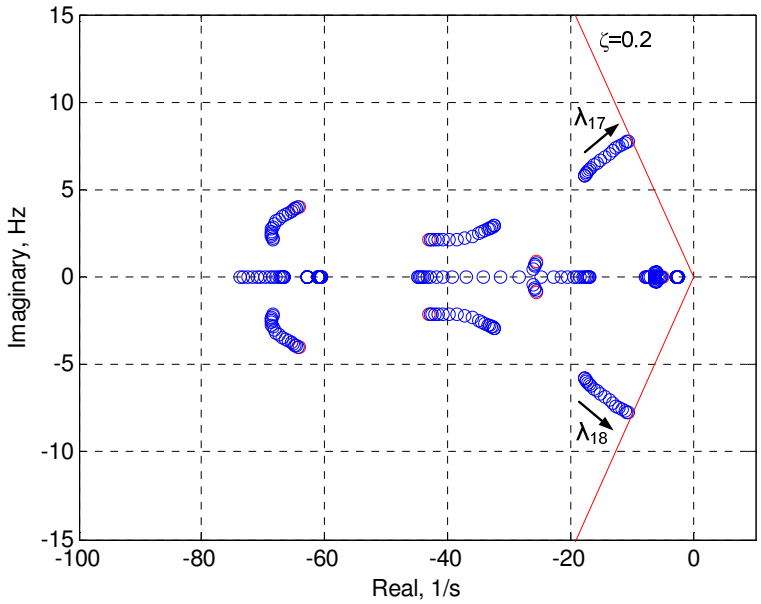

Fig. 63: Eigenvalue trajectories with single-loop control when sweeping X_{VI}/R_{VI} from 10 to 0.1 (with $|Z_{VI}| = 0.15$ pu).

As the transient frequency droop gain is increased, the frequency of the generator electromechanical mode $\lambda_{17,18}$ increases. When the transient voltage droop gain is changed by itself (not shown), it does not affect $\lambda_{17,18}$ significantly, but does increase the damping of two other eigenvalue pairs, $\lambda_{26,27}$ and $\lambda_{22,23}$. As the transient voltage and frequency droop gains are increased simultaneously, as seen in Fig. 64, the primary effect is to increase the frequency of $\lambda_{17,18}$.

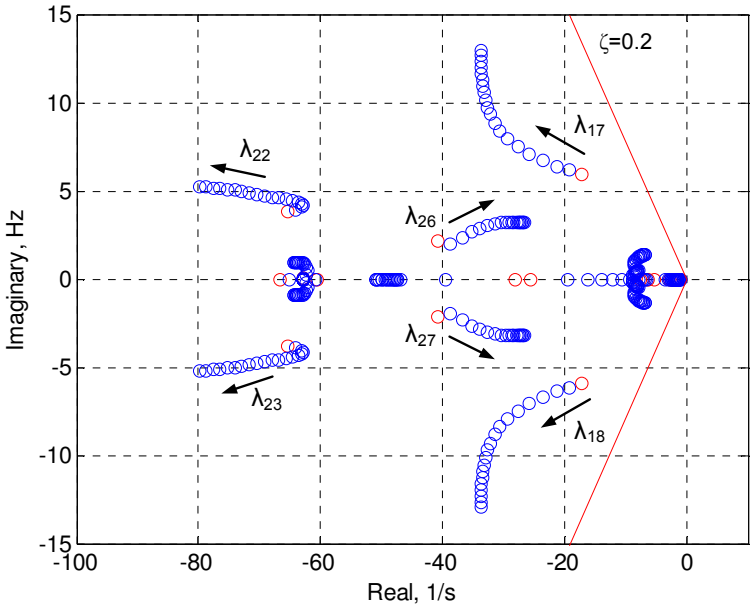

Fig. 64: Eigenvalue trajectories with single-loop control when sweeping from m_{P2} from 0 Hz to 3 Hz and m_{Q2} from 0 pu to 0.3 pu (with $|Z_{VI}| = 0.15$ pu and $X_{VI}/R_{VI} = 3$).

In Section 6.2.2 it was shown that the transient droop cutoff frequency, or high-pass filter time constant (i.e., $1/\omega_c$), should be selected similar to the natural transient response of the inverter to give the inverter similar transient response to the generator. If the transient droop time constant was too small, the inverter tries to restore the voltage and frequency quickly, and the transient power sharing is poor. If the transient droop time constant is too large, the generator ends up taking more of the load step than the generator. The impact of the transient frequency droop high-pass filter cutoff frequency ω_{c2} on small-signal stability is shown in Fig. 65. A larger transient droop time constant has the effect of increasing the settling time of the power sharing, i.e. increasing the real component of the over-damped modes related to the governor and AVR states. The eigenvalue plot for sweeping the transient voltage droop time constant is similar, and is not shown.

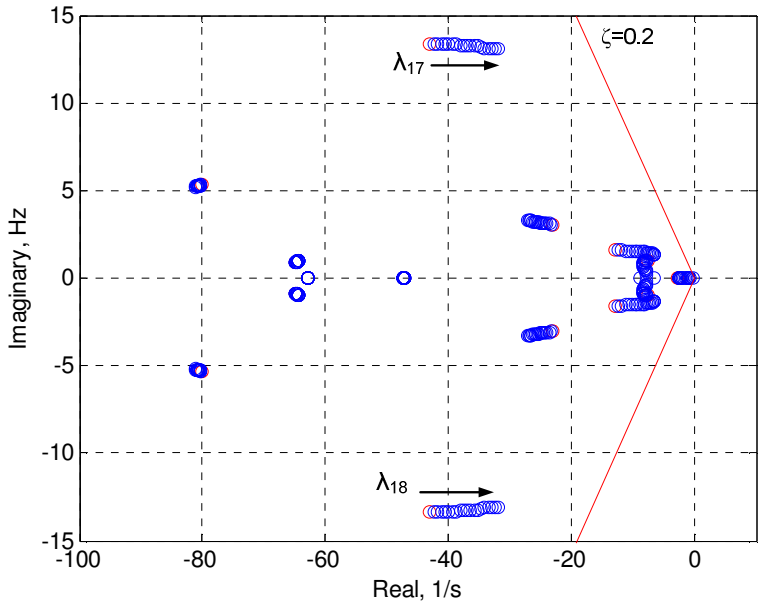

Fig. 65: Eigenvalue trajectories with single-loop control when sweeping from ω_{c2} from 5 Hz to 0.1 Hz (with m_{P2} = 3 Hz, m_{Q2} = 0.3 pu, $|Z_{VI}|$ = 0.15 pu and X_{VI}/R_{VI} = 3).

The small-signal analysis has shown that small-signal stability is not problematic for single-loop control with the chosen values of transient droop.

6.4. Virtual Impedance and Transient Droop in Multi-loop Control

6.4.1. Multi-Loop DQ Control

6.4.1.1. Description of Multi-Loop DQ Control

Multi-loop voltage control uses an outer voltage loop that provides the current reference to an inner current loop. In grid-supporting-grid-forming controls, the voltage reference and frequency are given by voltage and frequency droop [13]. The multi-loop dq voltage control used in this work is shown in Fig. 66. The voltage reference and frequency are given by conventional voltage and frequency droop. Virtual output impedance is added by subtracting the voltage drop across a virtual resistance, R_{VI}, and virtual inductance, L_{VI}, from the voltage reference. The outer voltage loop includes output current feed-forward (with gain H) [32-34]. Other feed-forward and compensation terms were investigated in this work (specifically voltage feed-forward and decoupling terms in the current controller, and filter capacitor current compensation in the voltage

controller [32-34]), but have been omitted because small-signal analysis indicated they had negligible impact on any of the important modes. Also, significant measurement noise was present in the experimental setup, and some of the compensation terms significantly degraded performance by feeding forward noise into the current and voltage commands.

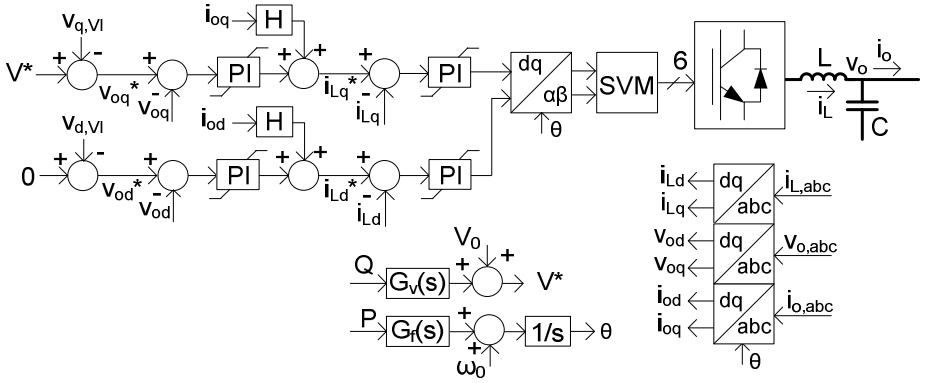

Fig. 66: Multi-loop dq grid-supporting-grid-forming control with virtual impedance and output current feed-forward.

6.4.1.2. Transient Virtual Impedance

Virtual output impedance degrades voltage regulation due to steady state voltage drop across the virtual impedance. It has been proposed to use a supervisory control (or tertiary control [13, 21]) to adjust each source's voltage reference to compensate for virtual impedance voltage drops. However, when operating in parallel with a synchronous generator, a steady state voltage drop causes significant reactive power sharing error, because the generator's automatic voltage regulator (AVR) does not include a steady state voltage drop. To avoid the need for a central controller to continuously modify all of the voltage references, a variation of the conventional virtual impedance is proposed.

This work proposes using a transient virtual impedance, wherein a high-pass filtered version of the dq output current is used for the virtual impedance, as given by:

$$v_{d,VI} = R_{VI}{}^{0}i_{od}\,s/(s+\omega_{c,hpf}) - \omega L_{VI}{}^{0}i_{oq}\,s/(s+\omega_{c,hpf}) \tag{63}$$

$$v_{q,VI}=R_{VI}^{0} i_{oq} s/(s+\omega_{c,hpf})+\omega L_{VI}^{0} i_{od} s/(s+\omega_{c,hpf}) \quad (64)$$

where $\omega_{c,hpf}$ is cutoff frequency of a single-order high-pass filter. The positive sequence fundamental component of the current is constant in the synchronous dq frame, and thus the positive sequence fundamental virtual impedance voltage drop will decay to zero in steady state. This allows the virtual impedance to impart the necessary stabilizing effects without the steady state voltage drop.

Note that the transient virtual impedance is denoted as the nominal virtual impedance $Z_{VI}^{0} = R_{VI}^{0}+j\omega L_{VI}^{0}$, and will typically be specified by its magnitude $|Z_{VI}^{0}|= \sqrt{(R_{VI}^{0})^2+(\omega L_{VI}^{0})^2}$ and X/R ratio X_{VI}^{0}/R_{VI}^{0}, where $X_{VI}^{0} = \omega L_{VI}^{0}$. It is called the nominal virtual impedance since it is constant, and because a variable virtual impedance term is proposed later for current limiting.

It should be noted that in this work the inverter uses an output transformer, and the voltage drop across the transformer is not currently being compensated. The extra output impedance from the transformer causes steady state reactive power sharing error. If it is desired to compensate for the voltage drop across the output transformer, a slower, extra outer voltage loop may be used to modify the primary voltage loop's reference to slowly restore the transformer output voltage to the droop set point. In the case of an extra outer voltage loop, transient virtual impedance is not necessary since the outer loop will compensate for the voltage drop across both the virtual output impedance and the transformer impedance.

6.4.1.3. Tuning of Controller Gains and Virtual Impedance

The stability of multi-loop dq control operating in parallel with other grid-forming sources is significantly more sensitive to virtual impedance and controller tuning than single-loop control. In this section the design of the multi-loop dq controller parameters is described. The controller gains were set with a combination of heuristic tuning and small-

signal analysis, subject to limitations caused by the influence of measurement noise in the experimental setup.

The design of the inverter controller parameters must consider the interaction with the rest of the microgrid, particularly with the synchronous generator. Typical methods for designing the current and voltage loops based on the bandwidth of closed-loop transfer functions neglect the rest of the system and treat the inverter output current as a disturbance input. If the inverter controller is designed using assumptions of the desired current and voltage loop bandwidth, and then is operated in parallel with the synchronous generator, it is very likely that unstable oscillations will emerge. For this reason, a combination of heuristic tuning and small-signal analysis has been used to tune the inverter controls. Small-signal analysis inherently accounts for all of the system closed-loop dynamics.

The impact of measurement noise in the experimental setup restricts the choice of controller gains, particularly for feed-forward terms. Significant measurement noise was present in the experimental setup due to poor design of the data acquisition system. The noise manifested itself as harmonics of 60 Hz and a dc offset, all of which varied with the operating condition, and could not be eliminated with a static offset correction. Efforts were undertaken to eliminate the measurement noise, but were unsuccessful, pending a complete redesign of the data acquisition circuits.

Feed-forward terms were found to degrade performance by adding noise into references. With dc offsets and harmonics in the voltage measurement, output voltage feed-forward in the current controller caused the inverter to inject actual dc voltages and harmonics into the PWM voltage command. This caused large dc and harmonic currents to flow. Similarly, the output current feed-forward term injected dc offsets and harmonics into the current reference, and due to the high bandwidth of the current controller, the inverter injects actual dc currents and harmonics. The inverter has a step-down delta-wye

transformer, and dc current in the transformer causes saturation of the magnetizing reactance, which results in very high peak currents. Magnetizing reactance saturation can easily result in currents large enough to cause an over-current trip.

Based on heuristic tuning of the experimental setup, it was found that an output current gain $H > 0.4$ caused the inverter to inject dc currents large enough to saturate the transformer and cause an overcurrent trip. Therefore, a gain of $H = 0.4$ was chosen. The output voltage feed-forward term also caused problematic dc offsets and harmonics. It was found that the current controller performance was satisfactory without output voltage feed-forward and decoupling terms, so they were eliminated.

The current controller PI gains were tuned heuristically to give the fastest response possible without causing instability. The virtual impedance and voltage controller gains were tuned heuristically, along with guidance from small-signal analysis of the inverter-generator lab microgrid.

A root locus plot is shown in Fig. 67 for sweeping output current feed-forward gain H from 0.9 to 0.2. Two primary eigenvalue pairs of interest are identified: $\lambda_{15,16}$, which based on participation factor analysis [32, 86] is primarily associated with the voltage controller states and generator stator and rotor currents, and $\lambda_{19,20}$, which is primarily associated with the generator electromechanical states and generator currents. From Fig. 67 it can be seen that the damping of the generator electromechanical mode $\lambda_{19,20}$ decreases with decreasing H, and the damping of two higher frequency modes (80 Hz & 100 Hz) increases with decreasing H.

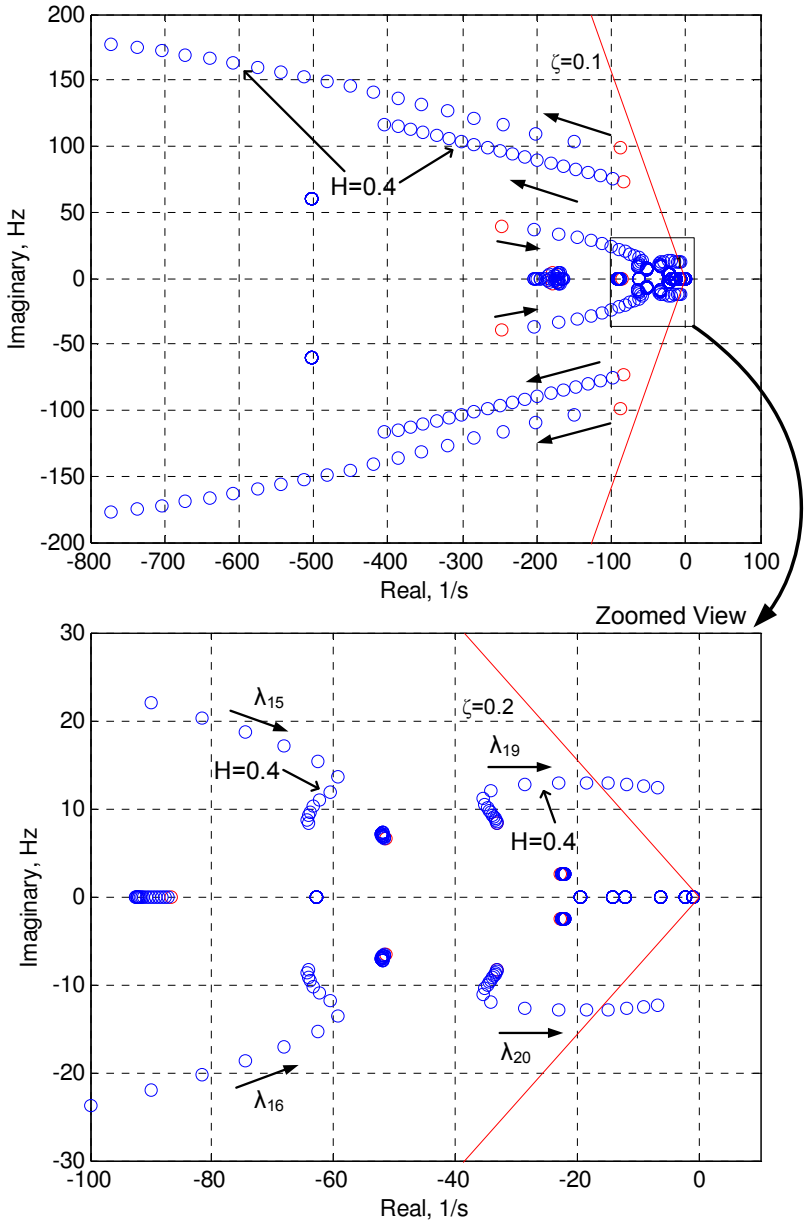

Fig. 67: Root locus for sweeping output current feed-forward gain *H* from 0.9 to 0.2, with zoomed view of low-frequency eigenvalues.

A root locus plot is shown in Fig. 68 for sweeping the voltage controller integral gain k_{iv} from 800 to 300. The voltage controller integral gain has a large effect on the voltage controller mode $\lambda_{15,16}$, and the generator electromechanical mode $\lambda_{19,20}$. The voltage controller proportional gain has little effect on any of the modes so a root locus plot is not shown. Note that in Fig. 67 – Fig. 68, $|Z_{VI}^{\,0}| = 0.1$ pu, $X_{VI}^{\,0}/R_{VI}^{\,0} = 1$, $H = 0.4$ pu, $k_{pv} = 0.05$ I_{pu}/V_{pu}, and $k_{iv} = 500$ $(I_{pu}/V_{pu})/s$, unless specified otherwise.

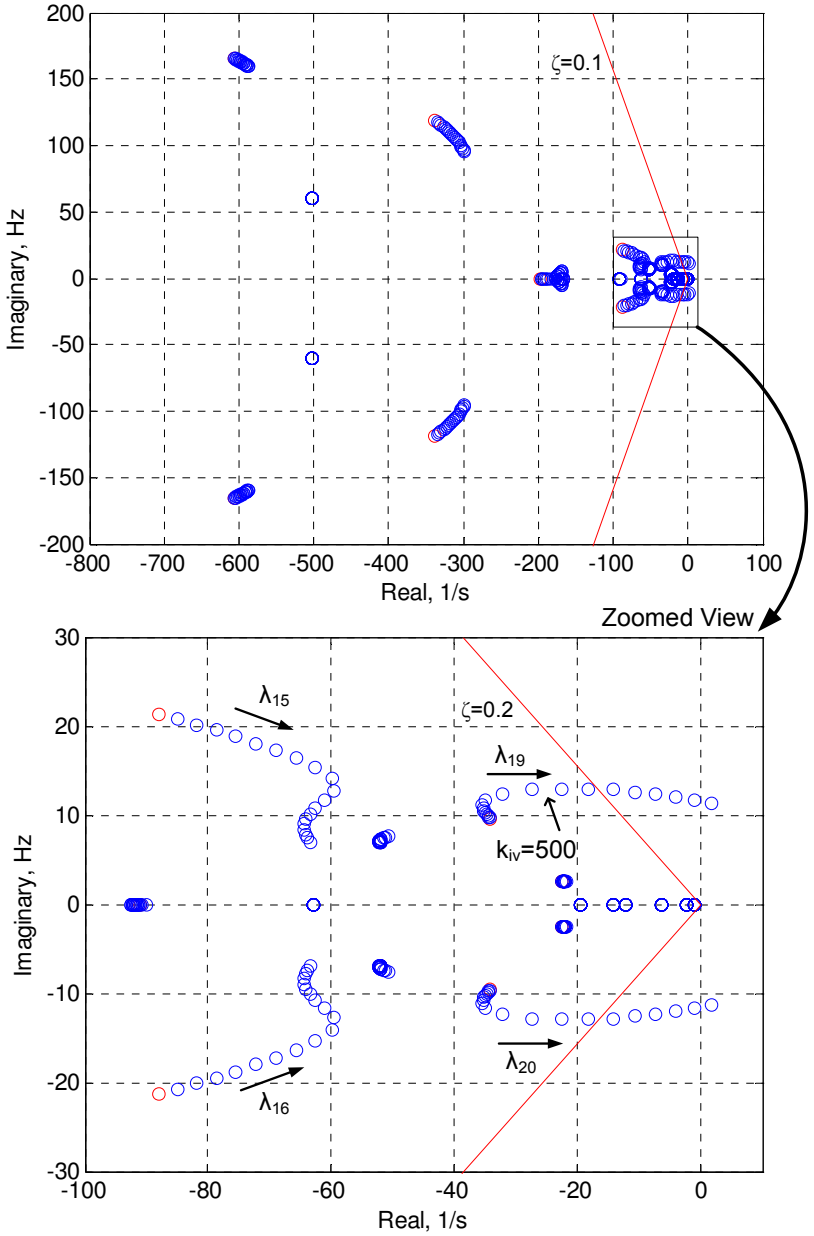

Fig. 68: Root locus for sweeping k_{iv} from 800 to 300.

Both the magnitude and X/R ratio of Z_{VI}^{0} impact stability. It has been well documented that a low X/R ratio causes coupling between the real and reactive power control loops, sometimes causing instability [13, 18, 20]. The root locus plot in Fig. 69 shows the system eigenvalue trajectories when sweeping X_{VI}^{0}/R_{VI}^{0} with a fixed $|Z_{VI}^{0}|$. As X_{VI}^{0}/R_{VI}^{0} goes from highly inductive to highly resistive, damping of the voltage controller mode increases and damping of electromechanical mode decreases.

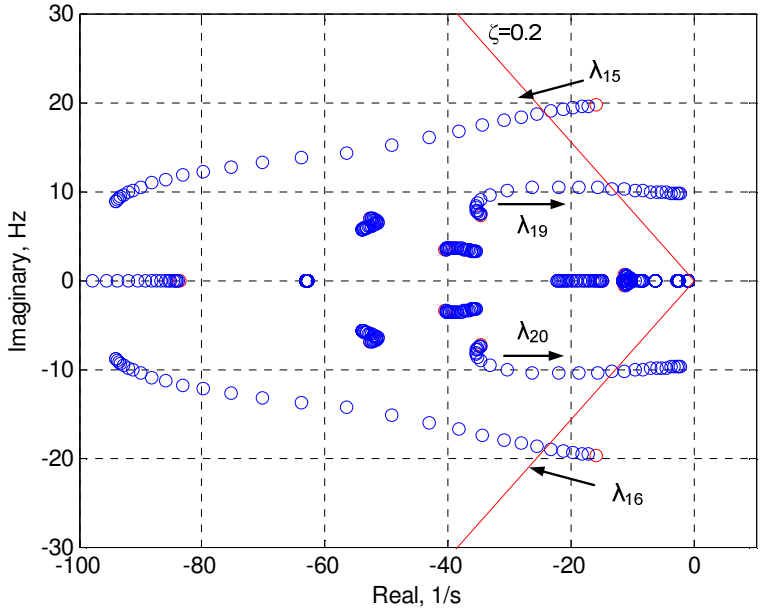

Fig. 69: Root locus for sweeping X_{VI}^{0}/R_{VI}^{0} from 10 to 0.1 (with $|Z_{VI}^{0}| = 0.1$ pu).

The root locus plot in Fig. 70 shows the eigenvalue trajectories when sweeping $|Z_{VI}^{0}|$ with X_{VI}^{0}/R_{VI}^{0} fixed. As $|Z_{VI}^{0}|$ is decreased, $\lambda_{19,20}$ in Fig. 70 become unstable. A compromise between damping of the voltage controller and generator electromechanical mode is chosen at $|Z_{VI}^{0}| = 0.1$ pu and $X_{VI}^{0}/R_{VI}^{0} = 1$.

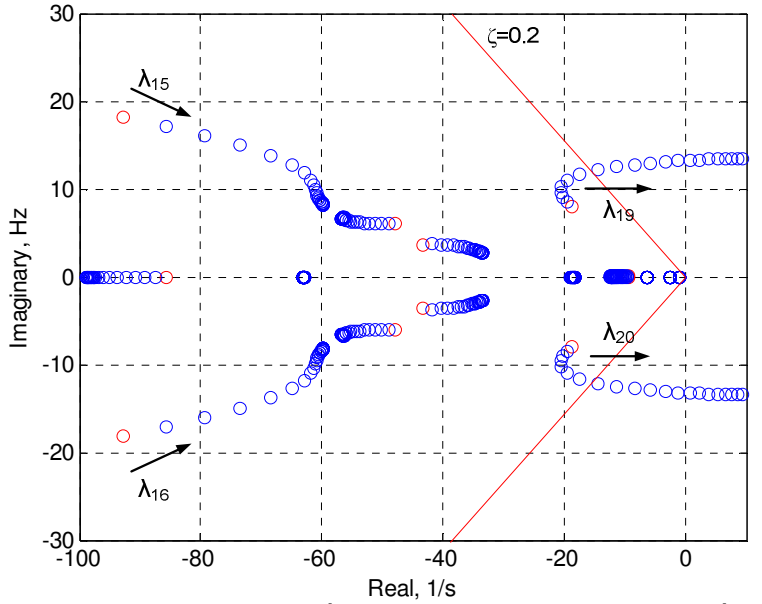

Fig. 70: Root locus for sweeping $|Z_{VI}^{0}|$ from 0.15 pu to 0.01 pu (with $X_{VI}^{0}/R_{VI}^{0} = 1$).

Small-signal analysis was also performed to compare stability with transient virtual impedance vs. normal virtual impedance for Z_{VI}^{0}. However, there were no

significant differences for any of the eigenvalues of interest, thus no plots are included. The multi-loop dq inverter control parameters are summarized in Table 7.

Table 7: Multi-loop DQ Inverter Control Parameters

Parameter	**Value**
Voltage PI proportional gain, k_{pv}	0.05 I_{pu}/V_{pu}
Voltage PI integral gain, k_{iv}	500 (I_{pu}/V_{pu})/s
Output current feed-forward gain, H	0.4 I_{pu}/I_{pu}
Current PI proportional gain, k_{pc}	0.5 V_{pu}/I_{pu}
Current PI integral gain, k_{ic}	500 (V_{pu}/I_{pu})/s
Nominal virtual resistance, R_{VI}^{0}	0.0707 pu
Nominal virtual inductance, L_{VI}^{0}	0.0707/(2π60) pu
Transient VI cutoff frequency, $\omega_{c,hpf}$	2*2π rad/s
Inverter filter inductor impedance	0.035 + j0.528 Ω
Inverter transformer leakage + cable impedance (measured)	0.25 + j0.15 Ω
Generator cable impedance (measured)	0.04 + j0.01 Ω

It is very interesting to note that small-signal analysis shows that too high of a virtual impedance X/R ratio causes insufficient damping of a voltage controller mode, and it is only very low X/R ratios (<0.5) that cause stability problems. This is the case in this experimental low-voltage microgrid with relatively low X/R ratio of connecting impedances (see Table 7). This indicates that with proper selection of virtual impedance, normal voltage and frequency droop may work acceptably in low voltage microgrids even with fairly low X/R ratios. However, X/R ratio is important, and microgrid designers need to pay attention to coupling impedances, particularly with multi-loop voltage control.

6.4.2. **Virtual Impedance and Initial Power Sharing**

In the single-loop inverter control with virtual impedance (Fig. 47), the virtual impedance is added directly to the inverter dq voltage command, v_{idq}*, but in the multi-loop dq inverter control the virtual impedance is added to the output voltage reference, v_{odq}*. The bandwidth of the virtual output impedance is limited by the bandwidth of the voltage control loop. The virtual output impedance therefore does not make a significant impact on the initial part of the output impedance step response, since the step response

contains high frequency components. For the single-loop inverter control, since the virtual impedance is directly applied to the inverter voltage command, it does impact the initial part of the output impedance step response, and therefore impacts the initial power sharing.

The effectiveness of virtual impedance on changing initial power sharing for multi-loop dq control is shown in Fig. 71. It can be seen that the virtual impedance has minimal impact on the initial power sharing (i.e. approximately first cycle) with multi-loop control.

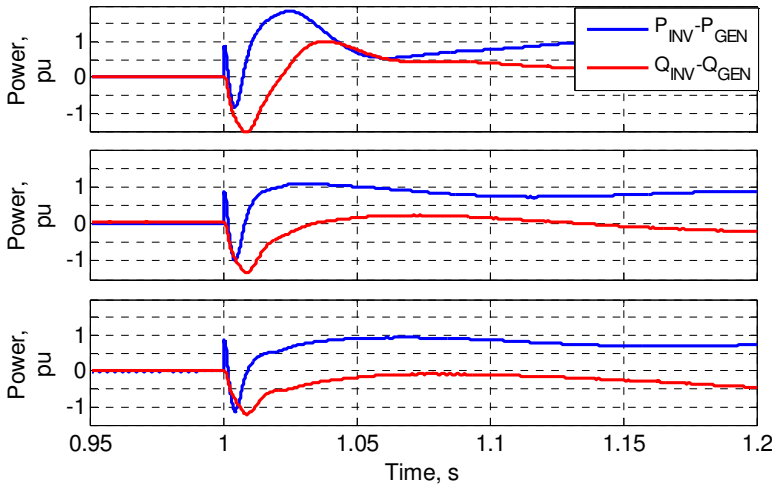

Fig. 71: Initial power sharing with multi-loop dq control for different values of virtual impedance ($|Z_{VI}^0| = 0.1$, $|Z_{VI}^0| = 0.2$, $|Z_{VI}^0| = 0.3$ – top to bottom, all with $X_{VI}^0/R_{VI}^0 = 1$), showing that virtual impedance does not impact initial power sharing as it does for single-loop control.

6.4.3. Transient Droop

The same transient voltage and frequency droop given by (55) and (56) can be used with multi-loop control to improve the transient power sharing. However, multi-loop control stability is significantly more sensitive to virtual impedance and transient droop gains than single-loop control. Significant oscillations begin to occur as the transient droop gains are increased, or as the virtual impedance is decreased. Simulations of varying the transient voltage and frequency droop gains are shown in Fig. 72. It can be seen that as the transient droop is increased the power sharing error decreases, but poorly damped oscillations develop. Small-signal analysis in Section 0 provides more

information about how the transient droop gains and virtual impedance impact those oscillatory modes.

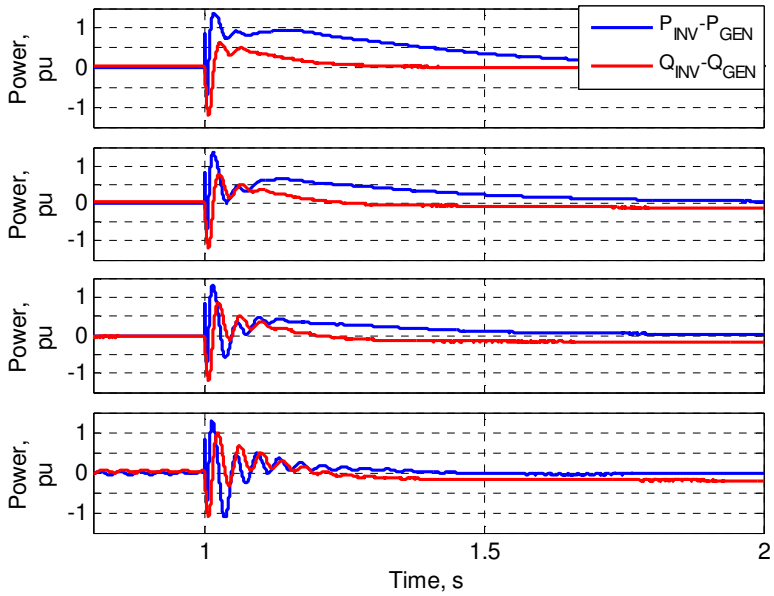

Fig. 72: Real and Reactive power sharing error for varied m_{P2} and m_{Q2} (0 Hz, 0 pu; 1 Hz, 0.1 pu; 2 Hz, 0.2 pu; 3 Hz, 0.3 pu – top to bottom, with multi-loop control, and $|Z_{VI}^0| = 0.15$ and $X_{VI}^0/R_{VI}^0 = 3$).

The power sharing mean squared errors are shown in Table 8 for the multi-loop control simulations in Fig. 72. Again, as transient droop increases, MSE_P and MSE_Q decrease, while MSE_V and MSE_f increase. In terms of transient load sharing, the case with m_{P2} = 2 Hz and m_{Q2} = 0.2 pu is identified as the best case, as it shows significant improvement in MSE_P and MSE_Q over the base case, but does not exhibit excessively oscillatory behavior. Again, the generator emulation case has the best MSE_P and MSE_Q but relatively large voltage and frequency dips.

Table 8: Power sharing MSE vs. transient droop for multi-loop control.

$Z_{VI}^{\,0}$	m_{P2} (Hz)	m_{Q2} (pu)	MSE_P	MSE_Q	MSE_V (x10^{-3})	MSE_f	V_{min} (pu)	f_{min} (Hz)
$\lvert Z_{VI}^{\,0}\rvert = 0.1$, $X_{VI}^{\,0}/R_{VI}^{\,0} = 1$	0	0.0	0.319	0.147	1.63	0.075	0.810	58.55
$\lvert Z_{VI}^{\,0}\rvert = 0.15$, $X_{VI}^{\,0}/R_{VI}^{\,0} = 3$	**0**	**0.0**	**0.297**	**0.120**	**1.76**	**0.074**	**0.830**	**58.63**
"	1	0.1	0.130	0.093	2.55	0.150	0.819	58.03
"	**2**	**0.2**	**0.058**	**0.062**	**3.44**	**0.258**	**0.795**	**57.30**
"	3	0.3	0.043	0.068	4.29	0.377	0.775	56.62
Generator Emulation (Fig. 42)			0.005	0.007	4.80	0.462	0.81	57.81

Finally, simulations of the base case and the case with both transient voltage and frequency droop are shown in Fig. 73 and Fig. 74 to allow a visual comparison of the effectiveness of the transient droop terms.

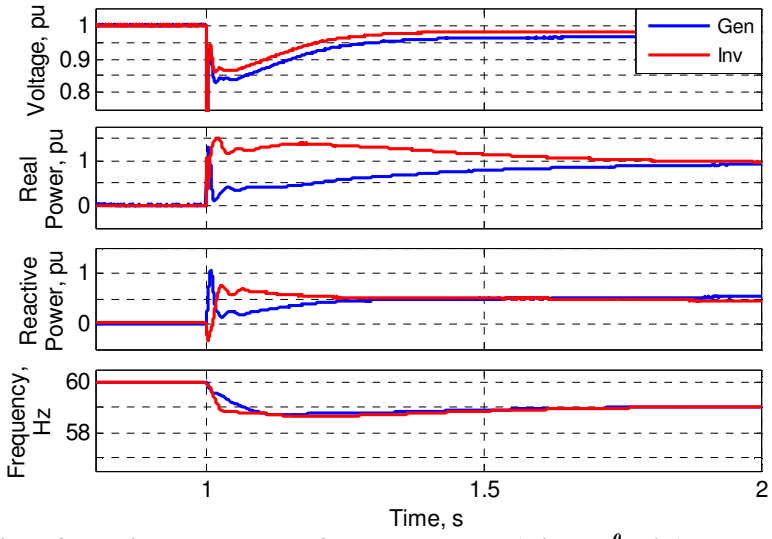

Fig. 73: Simulation of transient voltage and frequency droop (with $Z_{VI}^{\,0}$ = 0.15 pu, $X_{VI}^{\,0}/R_{VI}^{\,0}$ = 3, m_{P2} = 0 Hz, m_{Q2} = 0.0 pu).

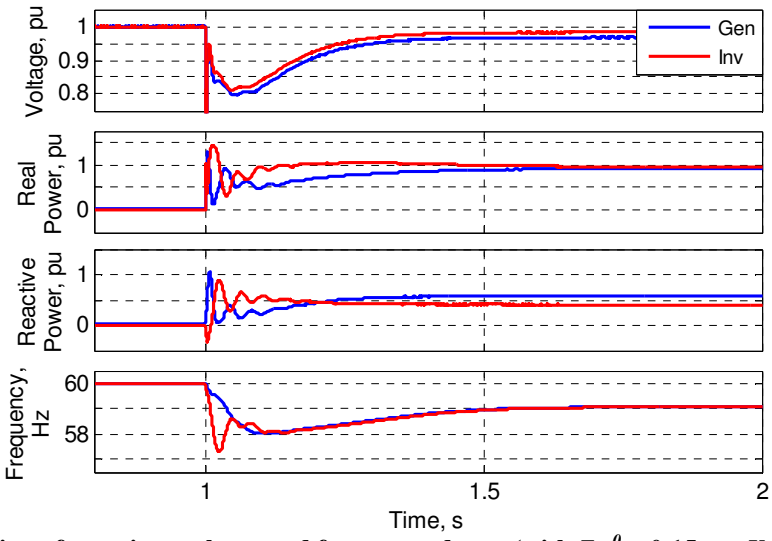

Fig. 74: Simulation of transient voltage and frequency droop (with Z_{VI}^{0} = 0.15 pu, X_{VI}^{0}/R_{VI}^{0} = 3, m_{P2} = 2 Hz, m_{Q2} = 0.2 pu).

6.4.4. Small-Signal Analysis

Small-signal analysis shows that the stability of multi-loop dq control is sensitive to virtual impedance. The simulations in Section 6.4.3 also showed that significant oscillations were caused by values of transient droop that did not cause problems with single-loop control. The impact of varying m_{P2} and m_{Q2} on closed-loop system eigenvalues is shown in Fig. 75, where m_{P2} and m_{Q2} are varied simultaneously. Note that in this section $|Z_{VI}^{0}|$ = 0.15 pu and X_{VI}^{0}/R_{VI}^{0} = 3, unless specified otherwise. From Fig. 75 it can be seen that a ~25 Hz mode pair becomes poorly damped. Based on participation factor analysis, this mode pair is primarily associated with the inverter's voltage regulator and the generator's stator and rotor currents. When varying m_{P2} and m_{Q2} separately (not shown), this mode is seen to be influenced more by m_{Q2} than m_{P2}. In Fig. 76 the impact of varying the virtual impedance with fixed values of transient droop is shown. As the virtual impedance magnitude decreases, the voltage controller mode damping decreases, and eventually becomes unstable.

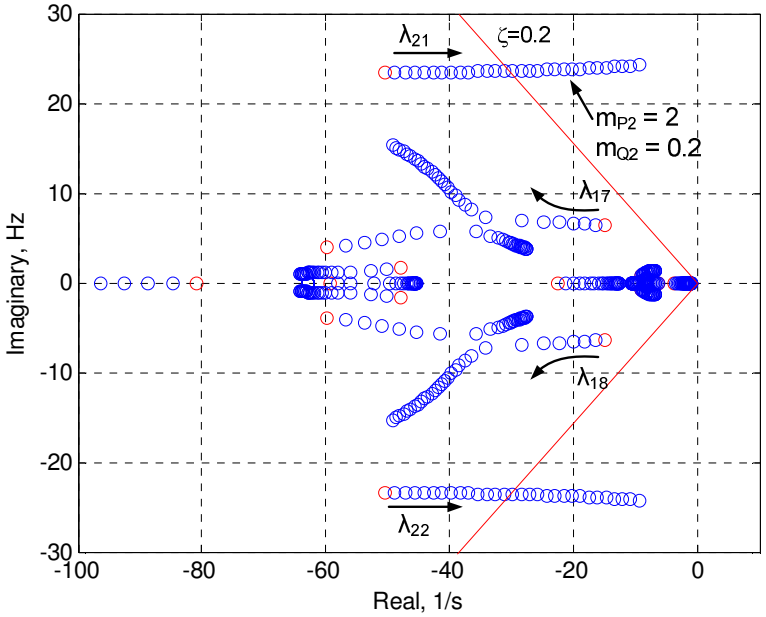

Fig. 75: Eigenvalue trajectories with multi-loop control when simultaneously sweeping m_{P2} from 0 Hz to 3 Hz and m_{Q2} from 0 pu to 0.3 pu.

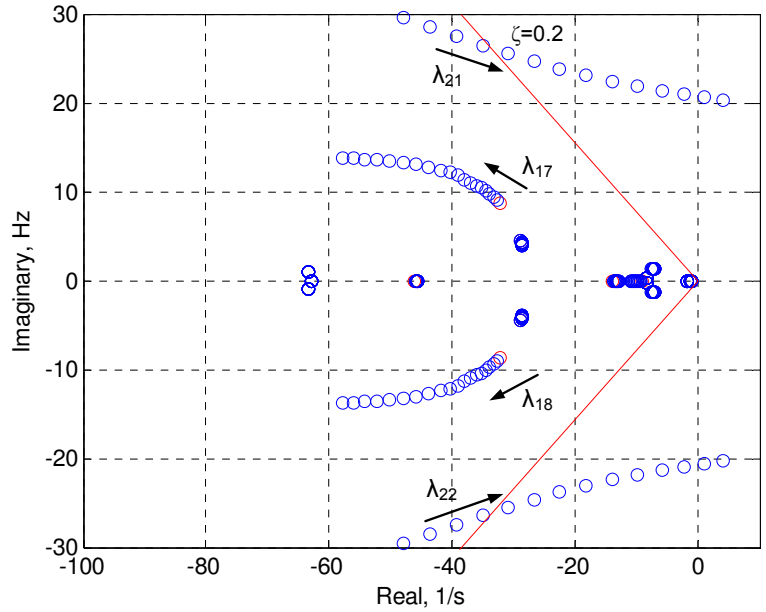

Fig. 76: Eigenvalue trajectories with multi-loop control when sweeping $|Z_{VI}^{\ 0}|$ from 0.3 pu to 0.1 pu (with $X_{VI}^{\ 0}/R_{VI}^{\ 0}$ = 3, m_{P2} = 2 Hz, and m_{Q2} = 0.2 pu), showing sensitivity to virtual impedance.

As discussed in Section 6.4.1.2, virtual impedance does not affect the initial power sharing significantly. However, it does have a significant impact on damping of important oscillatory modes. In single-loop control, virtual impedance can be chosen to control the initial power sharing ratio, without causing any significant small-signal

stability concerns. For multi-loop control, virtual impedance should be chosen based on damping of important modes rather than on controlling the initial power sharing ratio.

The impact of the transient voltage droop high-pass filter cutoff frequency ω_{c3} on small-signal stability is shown in Fig. 77. It can be seen that the modes of concern ($\lambda_{21,22}$ and $\lambda_{17,18}$) are affected minimally by the transient droop time constant. The modes that are affected by the transient droop time constant are the overdamped modes related to the reactive power and AVR state variables, which take longer to settle for a larger transient droop time constant. The plot for sweeping the transient frequency droop high-pass filter cutoff frequency ω_{c2} is similar to Fig. 77, and is not shown.

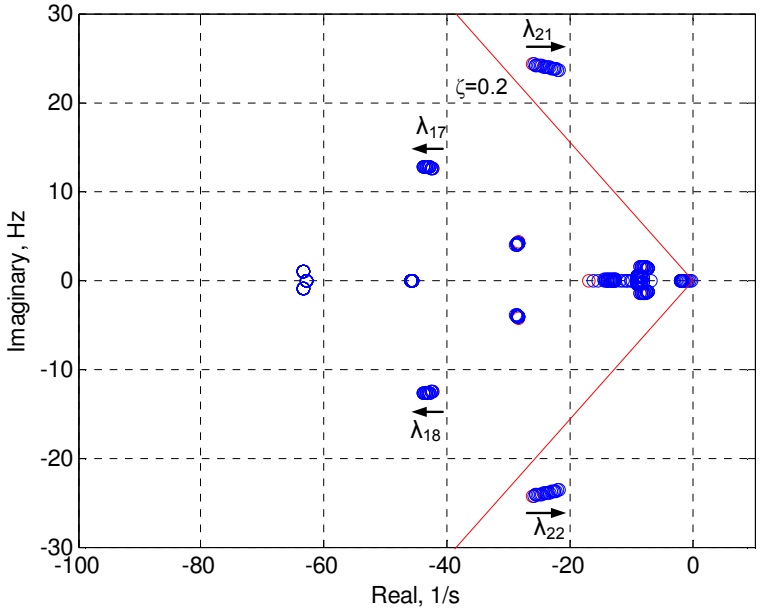

Fig. 77: Eigenvalue trajectories with multi-loop control when sweeping ω_{c3} from 5 Hz to 0.1 Hz, showing that the transient voltage droop time constant has little impact on stability.

6.5. Limitations on Voltage and Frequency Transients

In practical systems, there are typically limits on depth of voltage and frequency transients that may be specified by applicable standards or agreements between the customer and manufacturers. For example, relevant standards on maximum percentage voltage and frequency dip during load application and rejection for backup power systems are outlined in [87], and examples of power quality standards for Department of

Defense applications are [88, 89]. Commonly used techniques to meet stringent voltage and frequency dip requirements in backup power systems include sequencing of loads and oversizing generator sets. Microgrid designers may face similar requirements depending on their intended application. This chapter proposes methods to improve transient load sharing, and thus reducing peak rating requirements of inverters, at the expense of increased voltage and frequency transients. However, the voltage and frequency transients with the proposed methods typically approach that of a system with only synchronous generators. This work does not address how to meet any particular power quality standard, because power quality requirements are highly application specific. Instead this work develops techniques to allow microgrid designers control over the transient load sharing characteristics of inverters and generators, and control over the tradeoff between power quality and power sharing. In cases with stringent power quality requirements, the transient droop techniques in this chapter may not be applicable.

It is intuitive that voltage transients are important, because many types of loads are interrupted by under-voltage. However, frequency transients are not always critical. For example, rectifier loads in datacenters are not inherently sensitive to frequency, but they are sensitive to over or under voltage conditions. Rotating machinery may be sensitive to frequency transients though. For an induction machine (IM) that is connected prior to a load transient, the induction machine will tend to slow down during a voltage dip due to a decrease in electromagnetic torque. A larger frequency dip will also tend to slow down the induction machine, and speed it back up when the frequency recovers. The power the induction machine requires to speed back up will be greater with a greater frequency dip. To demonstrate the effect of transient droop on an induction motor load, a simulation is performed where a 5 hp induction motor load is online, and 75 % load step is applied, with and without transient voltage and frequency droop. These simulations are shown in Fig. 78, and use single-loop control with m_{P2} = 3 Hz and m_{Q2} = 0.3 pu. It can be

seen that the induction machine draws a larger torque as it speeds back up with transient droop enabled. However, the impact of the induction motor recovery is not significant in this case.

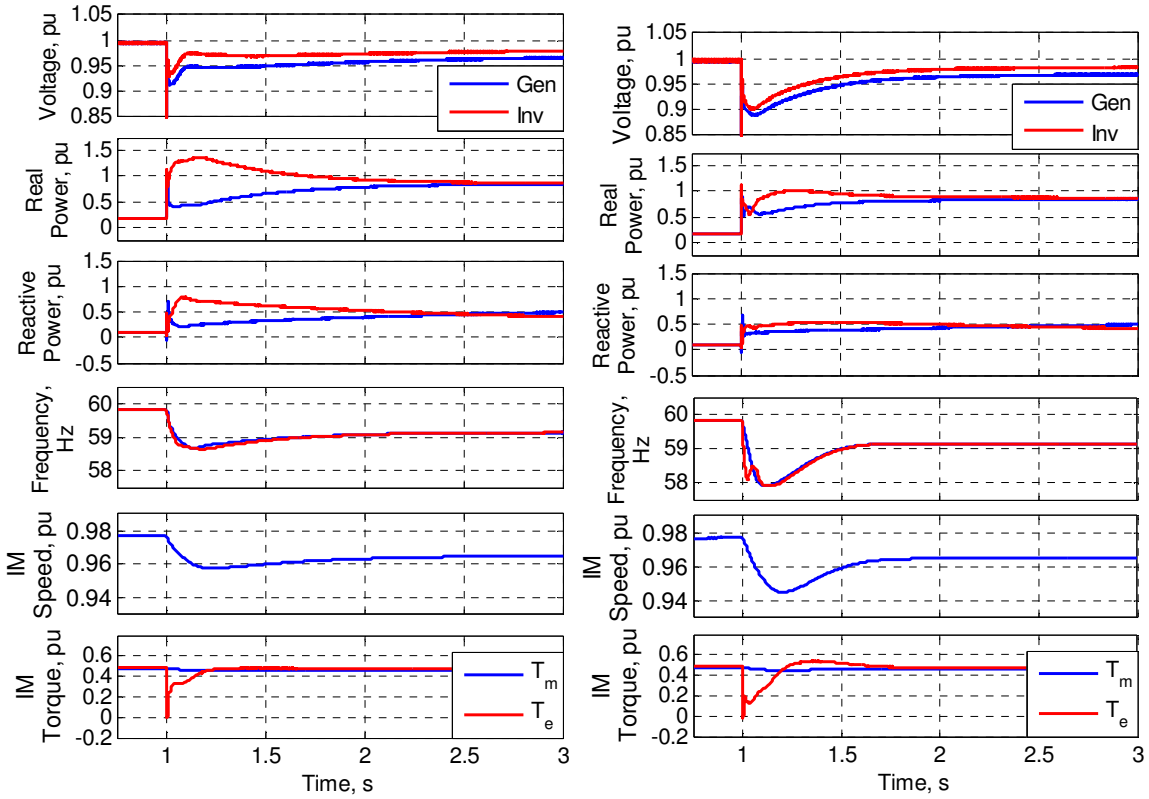

Fig. 78: Simulation of load step with 5 hp induction motor online, without (left) and with (right) transient droop.

In the case of induction motor starting, the frequency dip is not important, as the slip is nearly unity regardless of whether the microgrid frequency dips to 59 Hz or 57 Hz. Voltage dip matters during induction motor starting because the voltage dip decreases starting torque. In the case of larger induction motors with small rated slip, the impact of frequency transients and the corresponding recovery inrush may be more significant, because smaller changes in speed cause larger changes in torque (along the torque-speed curve). In conclusion, it is anticipated that voltage transients will have a more significant impact than frequency transients, even in the case of rotating machinery loads.

6.6. Experimental Results

6.6.1. Single-Loop Control

The single-loop dq control of with transient voltage and frequency droop has been tested on the experimental setup in Fig. 46. Fig. 79 and Fig. 80 show the measured instantaneous (unfiltered) real and reactive power for varied virtual impedance magnitude and X/R ratios. The measured results show that virtual impedance is effective in reducing the initial power sharing ratio. For varied X_{VI}^{0}/R_{VI}^{0}, simulations showed better damping of oscillations after the initial load step, but this is obscured by the 120 Hz ripple in the power measurement (caused by negative sequence current being exchanged between the inverter and generator).

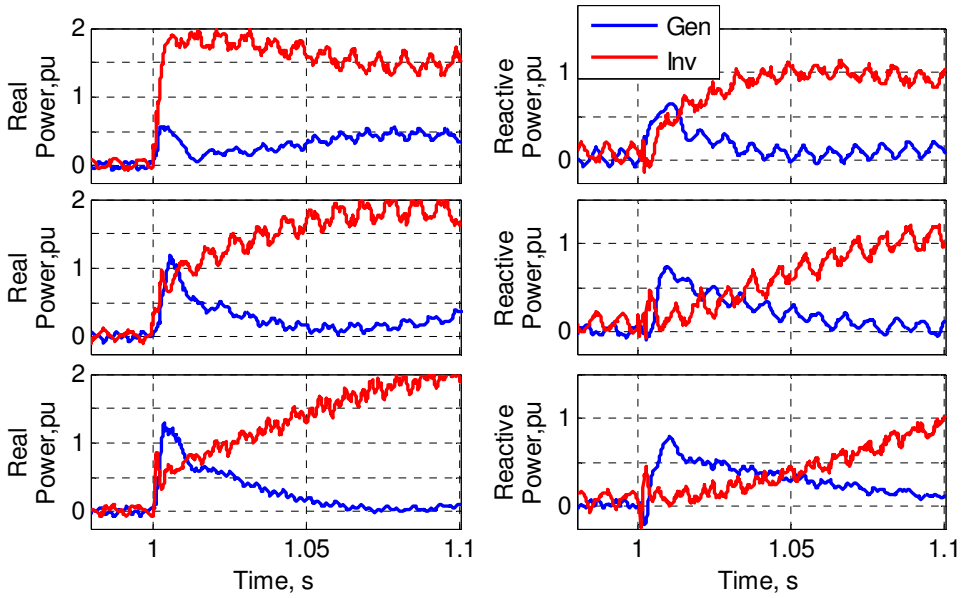

Fig. 79: Initial power sharing with varied virtual impedance magnitude (top to bottom - $|Z_{VI}^{0}|$ = 0 pu, 0.15 pu, and 0.3 pu, with X_{VI}^{0}/R_{VI}^{0} = 3).

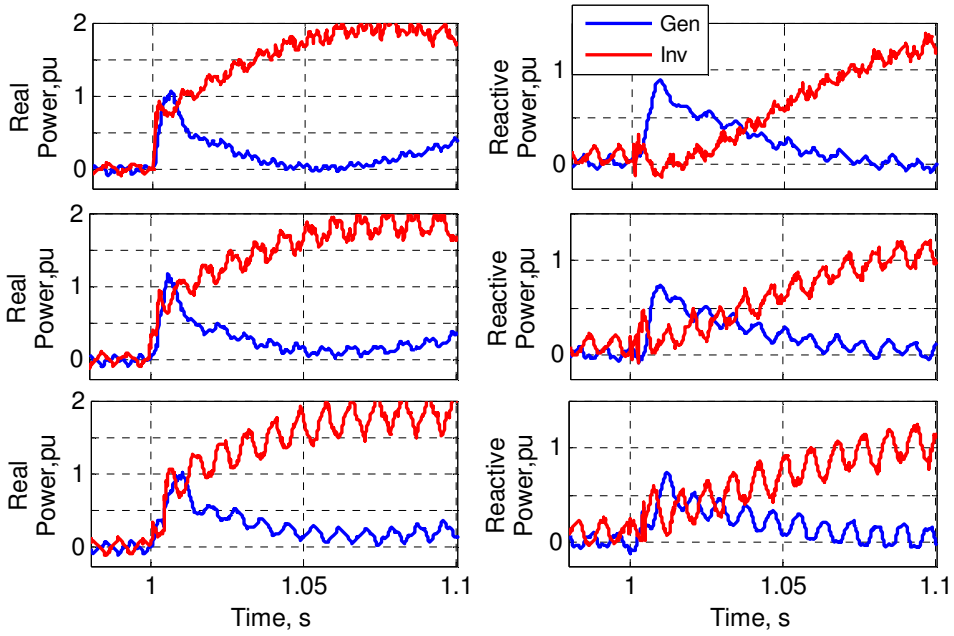

Fig. 80: Initial power sharing with varied X_{VI}^0/R_{VI}^0 (top to bottom - X_{VI}^0/R_{VI}^0 = 1, 3, and 1/0, with $|Z_{VI}^0|$ = 0.15 pu).

Fig. 81 shows the measured real and reactive power sharing error for various values of the transient droop time constant. The same trend emerges as with the simulation results in Section 6.2.2: as the transient droop time constant increases (i.e. the high-pass filter cutoff frequency decreases), the power sharing error decreases and then overshoots. A small transient droop time constant is ineffective at improving the transient load sharing, but an excessively large time constant causes the generator to pick up more of the load transiently. Note that the power traces in Fig. 81 are filtered to eliminate the 120 Hz component in the power measurement so that multiple traces can be placed together for easy visual comparison.

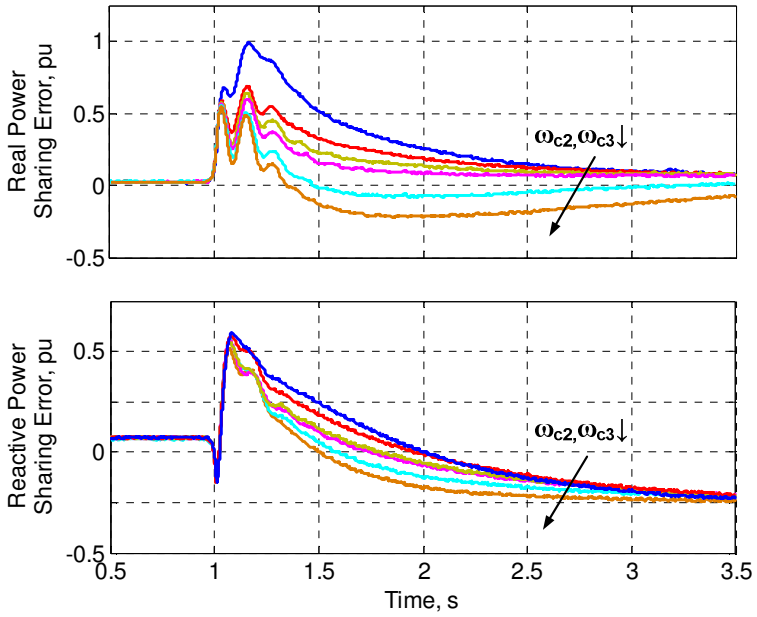

Fig. 81: Measured real and reactive power sharing error for varied transient droop time constant (ω_{c2}= ω_{c3}= 5 Hz, 2 Hz, 1.5 Hz, 1.25 Hz, 1 Hz, 0.75 Hz, and 0.5 Hz – top to bottom, with m_{P2} = 3 Hz, m_{Q2} = 0.3 pu, with $|Z_{VI}^{0}|$ = 0.15 pu and X_{VI}^{0}/R_{VI}^{0} = 3).

The real and reactive power sharing error for multiple values of transient voltage and frequency droop gain are shown in Fig. 82. As the transient droop gains are increased, the transient power sharing error is decreased. The results are similar to the simulations, except that the damping of the electromechanical mode, seen in the power oscillations, is worse in the experimental results.

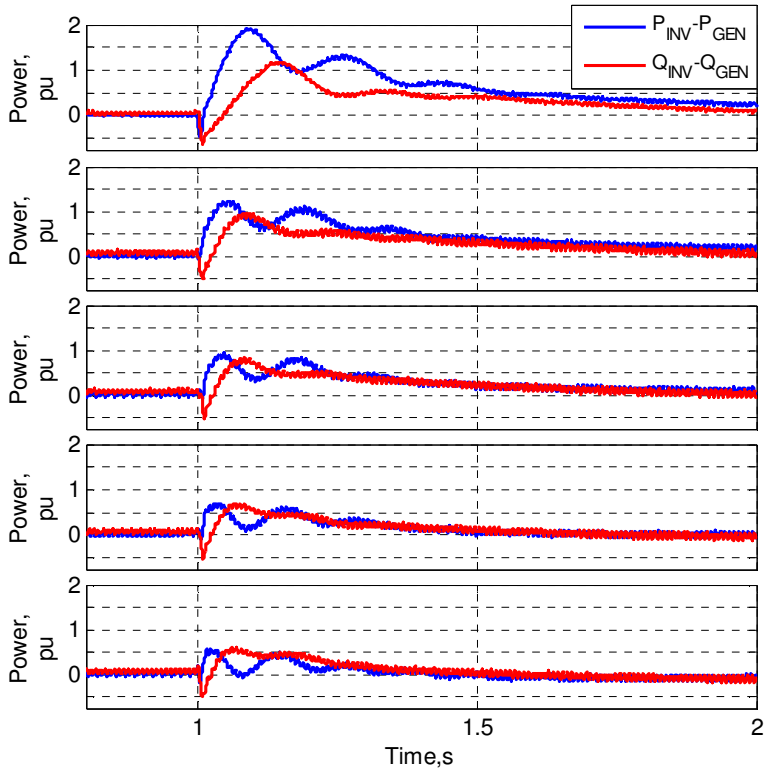

Fig. 82: Real and Reactive power sharing error for varied m_{P2} and m_{Q2} (0 Hz, 0 pu; 1 Hz, 0.1 pu; 2 Hz, 0.2 pu; 3 Hz, 0.3 pu ; 4 Hz, 0.4 pu – top to bottom, with $|Z_{VI}^{0}|$ = 0.15 pu and X_{VI}^{0}/R_{VI}^{0} = 3).

Finally, the measured results are shown for the base case, without virtual impedance or transient droop, in Fig. 83. The results with virtual impedance and transient droop are shown in Fig. 84, where it can be seen that the power sharing has been improved at the expense of increased voltage and frequency transients.

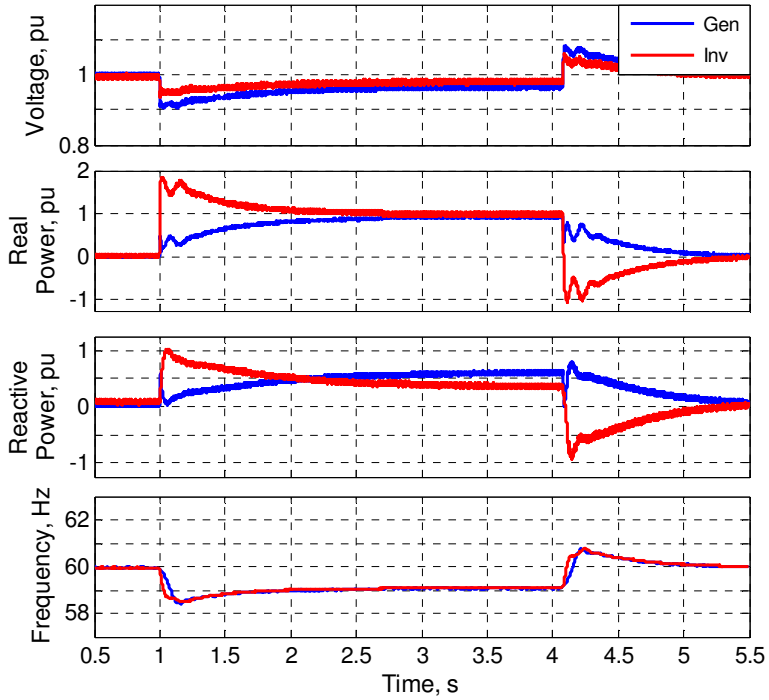

Fig. 83: Measurement of base case ($|Z_{VI}|$ = 0 pu, m_{P2} = 0 Hz, m_{Q2} = 0 pu).

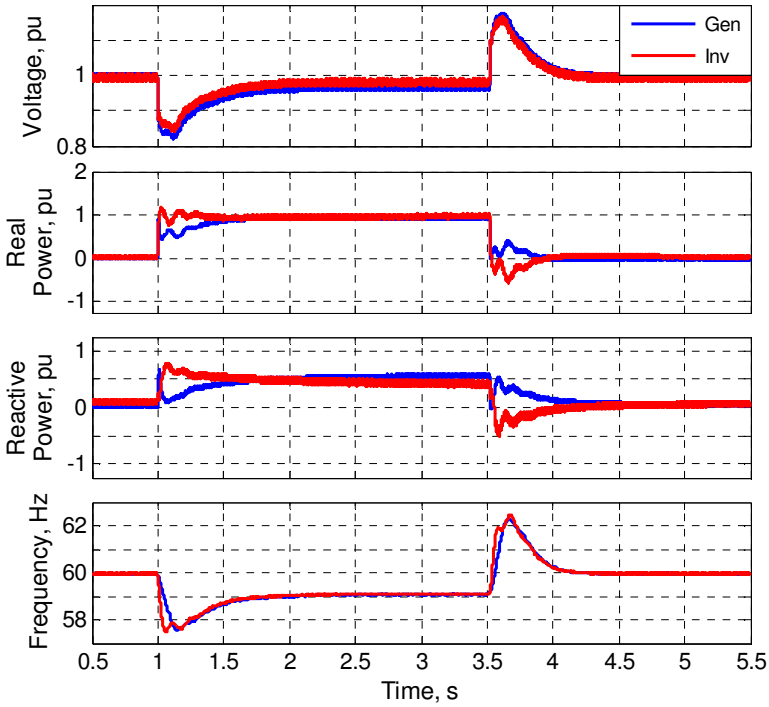

Fig. 84: Measurement of transient voltage and frequency droop ($|Z_{VI}|$ = 0.15 pu, X_{VI}^0/R_{VI}^0 = 3, m_{P2} = 3 Hz, m_{Q2} = 0.3 pu).

6.6.2. **Multi-Loop Control**

The multi-loop dq control with transient voltage and frequency droop has been tested on the experimental setup in Fig. 46. Multiple values of transient voltage and frequency droop gain were tested. Fig. 85 shows the measured real and reactive power sharing error for multiple values of m_{P2} and m_{Q2}, and shows that with larger transient droop gains the power sharing error is smaller and decays more quickly. Various values of transient droop time constant were tested, but since the results are similar to single-loop control, the results are not shown.

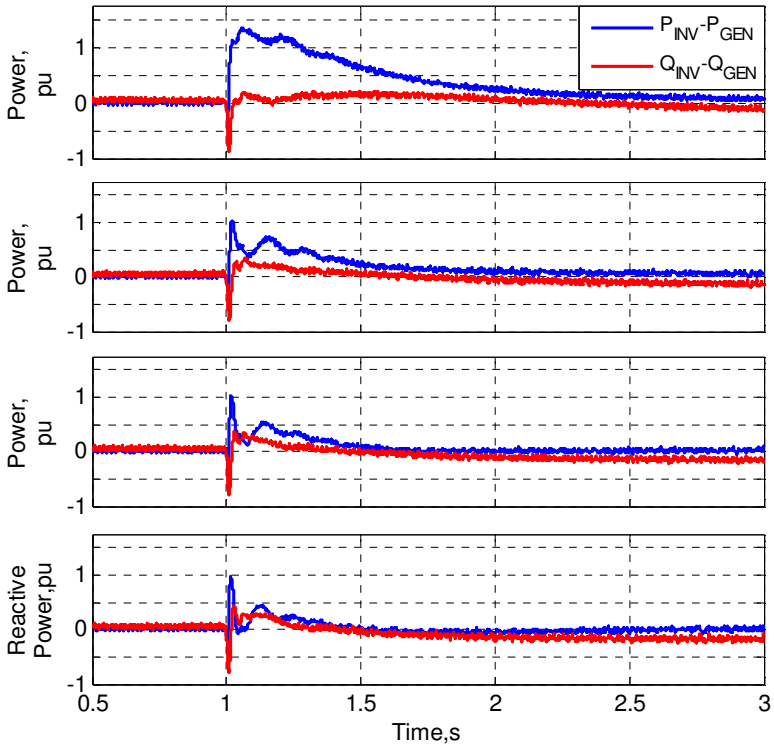

Fig. 85: Measured real and reactive power sharing error for varied m_{P2} and m_{Q2} (0 Hz, 0 pu; 2 Hz, 0.2 pu; 3 Hz, 0.3 pu; 4 Hz, 0.4 pu – top to bottom).

Finally, the complete measurement results are shown with and without transient droop, in Fig. 86 and Fig. 87. The real power sharing is improved significantly, but the improvement to the reactive power sharing is less significant. The improved power sharing comes at the expense of increased voltage and frequency dip.

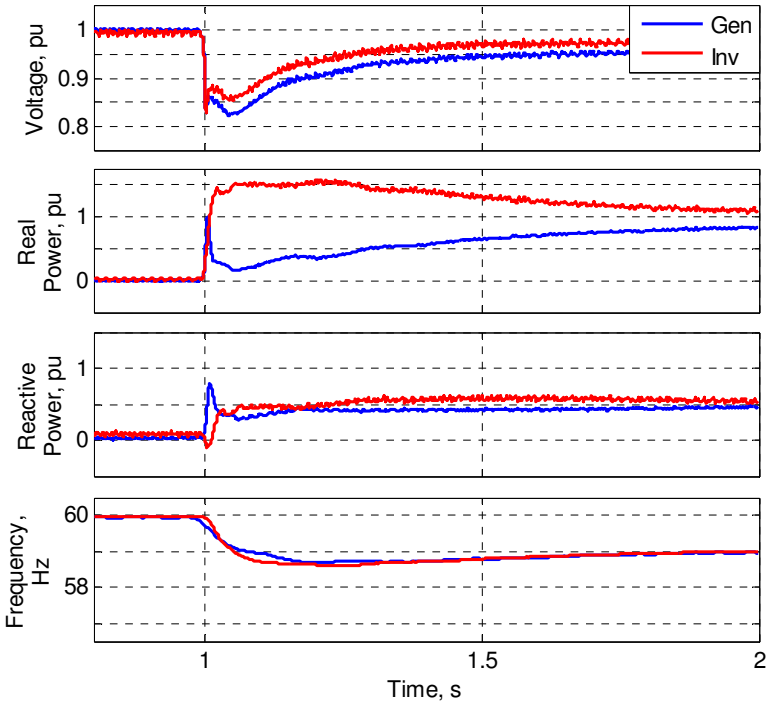

Fig. 86: Measured results without transient voltage and frequency droop ($|Z_{VI}| = 0.15$ pu, $X_{VI}^0/R_{VI}^0 = 3$, $m_{P2} = 0$ Hz, $m_{Q2} = 0.0$ pu).

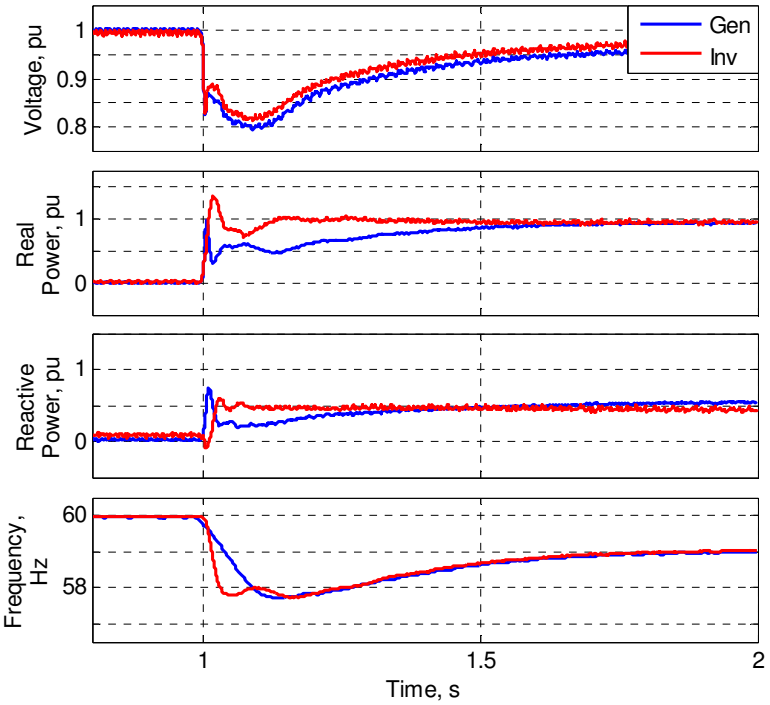

Fig. 87: Measured results of transient voltage and frequency droop ($|Z_{VI}| = 0.15$ pu, $X_{VI}^0/R_{VI}^0 = 3$, $m_{P2} = 3$ Hz, $m_{Q2} = 0.3$ pu).

Note that the measurement results traces are filtered eliminate the higher order harmonics in the measurement data, to facilitate visual comparison. The filter used is a 1st order Butterworth low-pass filter with a 180 Hz cutoff frequency, used as a zero-phase filter (MATLAB function 'filtfilt', which filters the data in forward and then reverse directions).

6.7. Chapter Conclusion

The use of transient droop and virtual impedance allows microgrid designers to control the inverter-generator transient power sharing characteristics, and to choose where the inverter-generator microgrid lies on the spectrum of power sharing vs. power quality. This chapter has introduced transient voltage and frequency droop, whereby the inverter has a larger droop slope during transients. With transient voltage and frequency droop, the inverter voltage and frequency sag further during transients, causing the generator to pick up more of the load step. The impact of transient droop on small-signal damping has been evaluated, and it has been shown that increasing transient droop gains decreases system damping. Multi-loop control is more sensitive than single-loop control to transient droop gains. It has been shown that virtual impedance can be used to control the initial power sharing with single-loop control, but virtual impedance has limited impact on initial power sharing with multi-loop control. The impact of virtual impedance on initial power sharing is not very significant compared to impact of transient droop on remainder of transient. Transient droop has a larger impact on transient power sharing than virtual impedance. However, virtual impedance does have a significant impact on damping of oscillatory modes. In general, it is preferable to choose the transient droop gains to improve the transient power sharing, and to choose virtual impedance based on damping of oscillatory modes.

The overall effectiveness of virtual impedance and transient droop on improving transient power sharing characteristics can be observed in the experimental results for

single-loop control with and without transient droop and virtual impedance, repeated here in Fig. 88. It is useful to compare the results of virtual impedance and transient droop to that of generator emulation (from Section 5.2), which is shown here again in Fig. 89 for comparison. The base case results in the smallest voltage and frequency deviations, but the worst transient power sharing. Virtual impedance and transient droop result in significantly improved transient load sharing, at the expense of power quality. Finally, generator emulation results in equal transient load sharing at the expense of the largest voltage & frequency transients (note that the generator emulation results are for a 75 % load step, whereas the virtual impedance and transient droop results are for a 100 % load step).

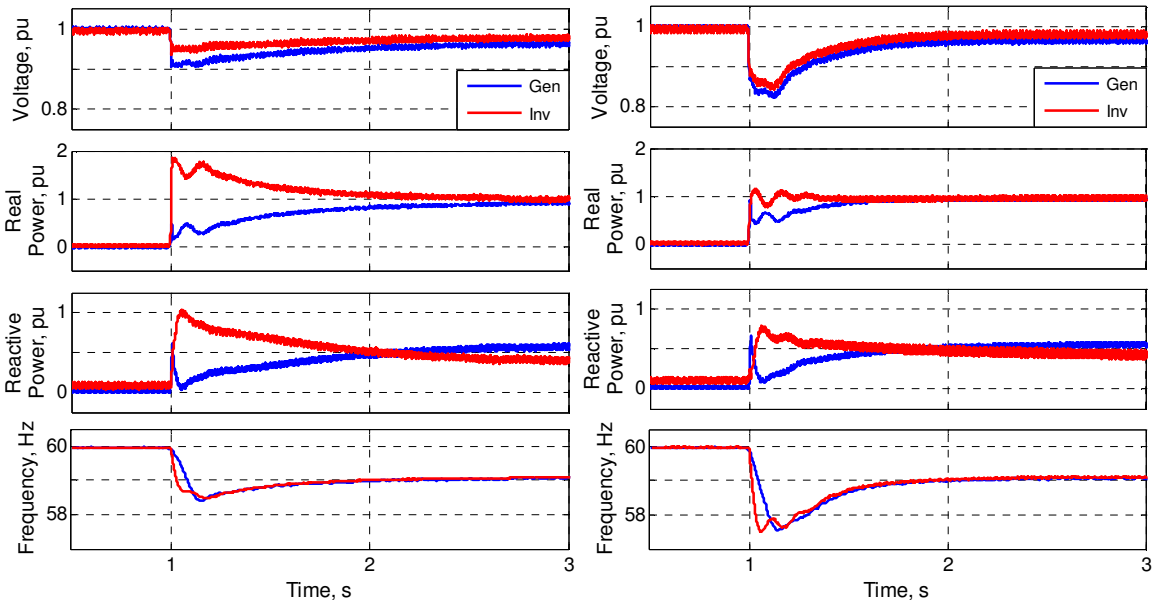

Fig. 88: Effectiveness of virtual impedance and transient droop on improving transient power sharing (Left: base case, Right: with virtual impedance and transient droop).

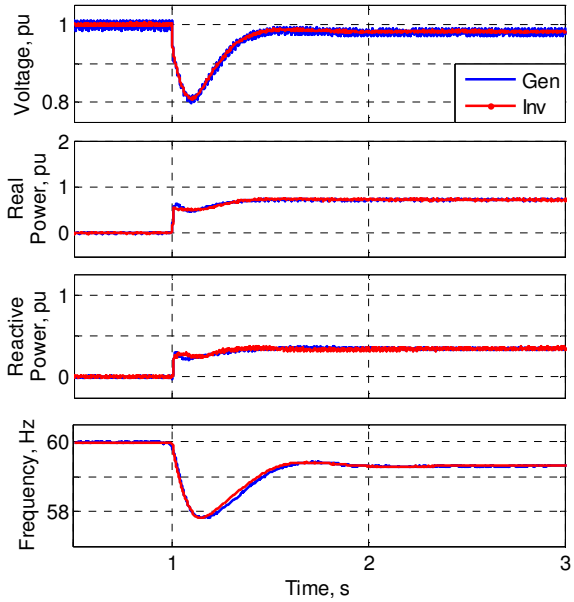

Fig. 89: Equal transient load sharing with generator emulation.

CHAPTER 7: VIRTUAL IMPEDANCE CURRENT LIMITING

Modifying the inverter controls to improve the transient load sharing has been demonstrated, but this comes at the expense of increased voltage and frequency transients. Instead of trying to improve the transient load sharing by effectively slowing down the inverter, it would often be preferable to fully utilize the inverter by allowing it to provide as much support as possible and simply current limit when necessary. This takes advantage of the fast response characteristics of the inverter to improve power quality, as well as protecting the inverter during faults.

This chapter describes that when grid-supporting-grid-forming inverters current limit during overloads when in parallel with synchronous generators, the use of simple current reference saturation limiters can cause instability. When the current reference saturates, the voltage controller is effectively disabled and loses control. The voltage and current controllers then wind up as the inverter and generator frequencies deviate, and the system can become unstable.

When operating a voltage controlled inverter in parallel with other voltage sources such as a synchronous generator, current limiting is not just as simple as limiting the current magnitude. It is important to address the interactions between the inverter and generator, and how the inverter enters and exits current limiting mode. Out of [19, 20, 34, 39, 69, 90-92], only [34, 90, 91] address how to exit current limiting, and [90, 91] only consider a single inverter with a bolted fault, for which entering and exiting current limiting is very straight forward. Reference [34] addresses current limiting with inverters and synchronous generators, but uses an overly complicated control scheme.

This chapter examines the current limiting characteristics of multi-loop grid-supporting-grid-forming inverter controls, specifically looking at current limiting during overloads caused by poor transient load sharing with synchronous generators.

7.1. Current Limiting Methods

Current limiting is accomplished differently in single-loop and multi-loop voltage control. Current limiting in single-loop voltage control methods is generally accomplished by reducing the voltage magnitude when the current exceeds a threshold, through a pre-defined I-V droop relationship [90], or by a current limiting PI controller [69]. In multi-loop voltage control methods, the two main current limiting methods are to either limit the current reference [34, 91, 92], or to reduce the voltage reference with a virtual impedance [19, 20, 39]. These methods are illustrated in Fig. 90. This chapter focuses on current limiting with multi-loop control.

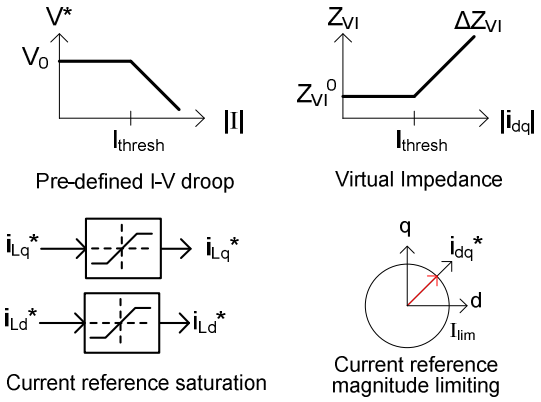

Fig. 90: Current limiting methods.

Current reference limiting can either saturate the reference to fixed upper and lower limits, or limit the magnitude of the dq current vector. With current reference magnitude limiting, if the magnitude of the dq current reference is greater than the maximum current reference magnitude I_{lim}, then the d and q current references are scaled by:

$$if\ \sqrt{{i_{Ld}}^{*2}+{i_{Lq}}^{*2}} > I_{\lim}: \begin{cases} i_{Ld}^{*} = i_{Ld}^{*} \dfrac{I_{\lim}}{\sqrt{{i_{Ld}}^{*2}+{i_{Lq}}^{*2}}} \\ i_{Lq}^{*} = i_{Lq}^{*} \dfrac{I_{\lim}}{\sqrt{{i_{Ld}}^{*2}+{i_{Lq}}^{*2}}} \end{cases}. \tag{65}$$

With current reference magnitude limiting, the current reference is less likely to be limited, since the magnitude of the current reference is limited to I_{lim} instead of limiting each reference to +/- $I_{lim}/\sqrt{2}$. Also, with reference magnitude limiting, the angle of the current reference is allowed to change, such that the voltage controller is not *completely* disabled during current limiting.

The multi-loop voltage control in Fig. 91 (same as Fig. 66, except only using proportional droop) has inherent current limiting ability due to the use of current regulators. Assuming the current regulators have sufficiently high bandwidth, the current can be limited simply by limiting the current reference, i_{Ld}* and i_{Lq}*.

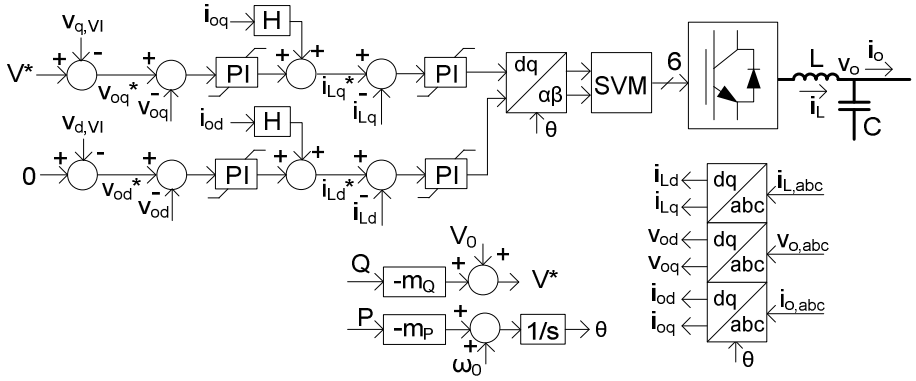

Fig. 91: Multi-loop dq grid-supporting-grid-forming control.

With current controlled inverters, i.e. grid-feeding control, the phase-lock-loop (PLL) tracks the grid voltage phase angle and aligns of the dq transformation angle with the grid voltage, such that the d and q axis currents correspond to reactive and real current, respectively. The multi-loop grid-supporting-grid-forming strategy in Fig. 91 aligns the q-axis with the output voltage by setting the d-axis voltage reference to zero and the q-axis voltage reference to the desired voltage magnitude. In a grid-feeding inverter the PLL maintains phase angle alignment even during current limiting (except for some transient error). However, with grid-supporting-grid-forming control, the output of the voltage regulator(s) saturate once current limiting starts, and the voltage regulators are not necessarily able to keep the q-axis aligned with the output voltage (or grid

voltage). While the current magnitude is effectively controlled, the alignment of the d and q-axis are not maintained. This allows the phase angle to drift, and if another voltage source is present with a different frequency, such as a generator whose frequency is transiently dipping following a load step, the frequencies may diverge causing the dq voltages to wind up. This problem is illustrated through a simulation in Section 7.2.

Reference [34] uses a hybrid between grid-forming and grid-feeding control, and thus may not suffer from the instability described above. In [34] the dq transformation angle is provided by a PLL as in grid-feeding control, but there are extra regulation loops that attempt to drive the frequency and phase angle to that given by the droop frequency (similar to grid-supporting-grid-forming control). Since the PLL tracks the output voltage phase angle, during current limiting the inverter dq transformation angle should not drift from the output voltage angle. However, the control in [34] is very complex, with many extra regulation loops. The control proposed in this work has the advantage of significantly reduced complexity.

7.2. Current Reference Saturation Instability

The response of the baseline controls (without current limiting) to the application of a 21 kW, 0.9 power factor linear load is shown in Fig. 92. The inverter uses the control in Fig. 91 and the generator uses the control in Fig. 29. The inverter initially picks up most of the load step, and the current reaches 1.89 pu. Note that |idq| in the bottom trace is the dq inductor current magnitude, $\sqrt{i_{Ld}{}^2 + i_{Lq}{}^2}$.

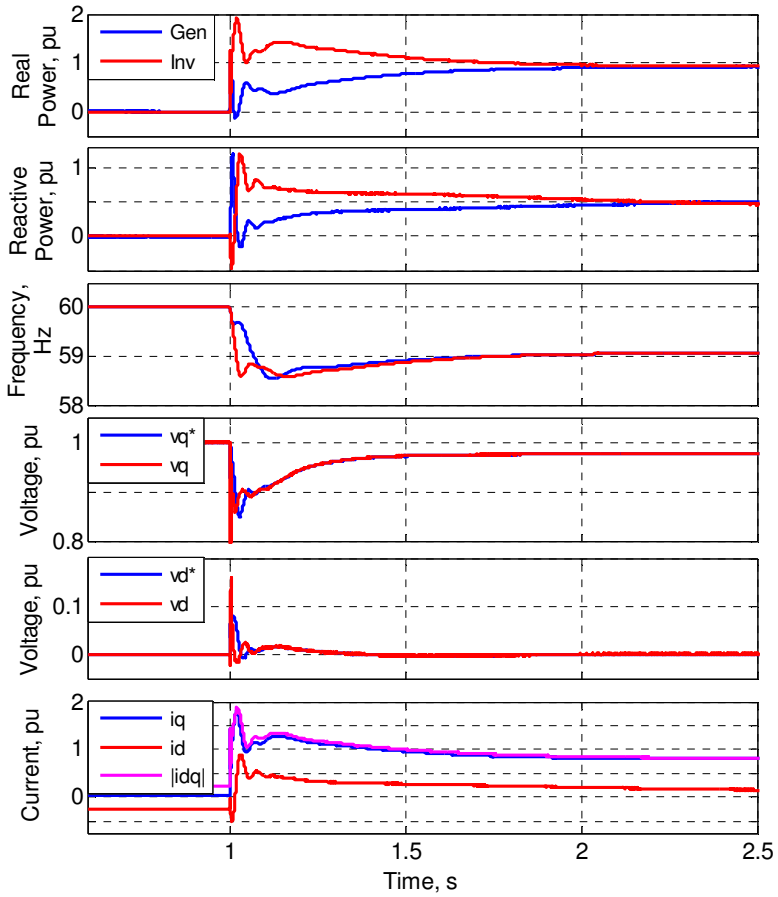

Fig. 92: Simulation of base case response to application of 21 kW, 0.9 power factor load without current limiting.

In Fig. 93 the same load step is applied, except with the current reference saturation limiters set at +/-1.06 pu ($I_{lim} = \sqrt{1.06^2+1.06^2} = 1.5$ pu). The q-axis current limit saturates first, and as the q-axis voltage drifts, the output voltage alignment drifts and the d and q axis currents no longer correspond to real and reactive power. This causes the generator voltage and frequency to change. As the inverter and generator frequency deviate, the inverter d and q-axis voltage begin to wind up and oscillate at a frequency equal to the difference between the generator and inverter frequency. As the sign of the d and q axis voltage error changes, the current reference flip-flops between positive and negative limit, and the voltage regulators never regain control.

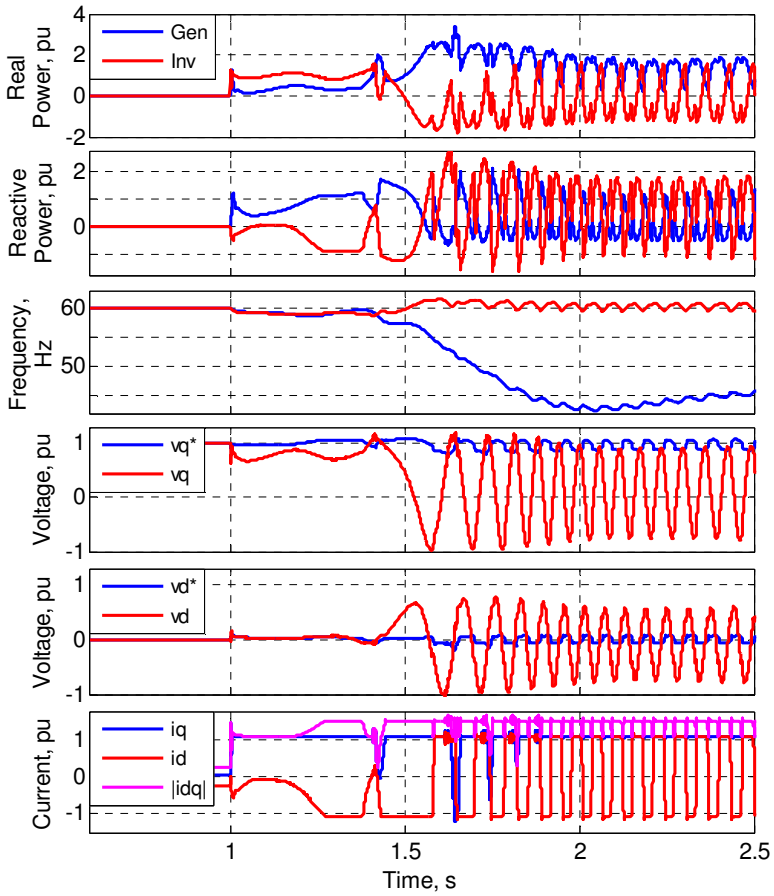

Fig. 93: Simulation of response to application of 21 kW, 0.9 power factor load with current limiting, showing instability caused by current reference saturation limiters.

The use of current reference magnitude limiting instead of simple current reference saturation does not cause the same instability shown in Fig. 93 for the same load step. This is primarily because the q-axis is allowed to reach nearly 1.5 pu before saturating, and the voltage controller is able to regain control quickly. However, in the next chapter it is shown that current reference magnitude limiting suffers from the same instability during fault current limiting. A different method that avoids disabling the voltage controller is needed, and is found in virtual impedance current limiting.

7.3. Virtual Impedance Current Limiting

Virtual impedance can be used to increase the inverter's output impedance during transients and thereby limit the current [19, 20, 39]. While normal current limiting works by limiting the current reference, virtual impedance current limiting works by reducing

the voltage reference, thereby preventing the voltage controller from commanding an excessively large current reference. During current limiting the voltage controller output does not saturate, and the instability observed in Fig. 93 can be avoided.

When the current magnitude exceeds a threshold, additional virtual impedance is added. The total virtual impedance is given by (66), and consists of a nominal virtual impedance, R_{VI}^{0}, and L_{VI}^{0}, plus a current limiting virtual impedance, ΔR_{VI} and ΔL_{VI}. This is the same as in [19]. The expressions for ΔR_{VI} and ΔL_{VI} are given in (67)-(68), where $k_{p,Rvi}$, $\Delta X/R$, and I_{thresh} are the current limiting virtual resistance proportional gain, current limiting virtual impedance X/R ratio, and current limiting threshold, respectively. $\Delta X/R$ is used to set the ratio $\omega\Delta L_{VI}/\Delta R_{VI}$.

$$R_{VI} = R_{VI}^{0} + \Delta R_{VI}\,,\;\; L_{VI} = L_{VI}^{0} + \Delta L_{VI} \tag{66}$$

$$\Delta R_{VI} = \max\left(k_{p,Rvi}\left(\sqrt{i_{Ld}{}^{*2} + i_{Lq,ref}{}^{*2}} - I_{thresh}\right), 0\right) \tag{67}$$

$$\Delta L_{VI} = k_{p,Rvi}\left(\Delta X/R\right)/\omega \tag{68}$$

For current limiting, transient virtual impedance is undesirable because the virtual impedance voltage drop decays with the high-pass filter time constant. Therefore, in this work, transient virtual impedance is used for Z_{VI}^{0}, but normal (not high-pass filtered) virtual impedance is used for ΔZ_{VI}. The final expression used in this work for the virtual impedance voltage drop is given by (69) and (70). Note that (67)-(68) use i_{Ldq}* for the current magnitude calculation instead of i_{odq} because using i_{odq} was found to cause significantly more oscillatory behavior.

$$v_{d,VI} = R_{VI}^{0} i_{od}\, s/(s+\omega_{c,hpf}) - \omega L_{VI}^{0} i_{oq}\, s/(s+\omega_{c,hpf}) + \Delta R_{VI} i_{od} - \Delta\omega L_{VI} i_{oq} \tag{69}$$

$$v_{q,VI} = R_{VI}^{0} i_{oq}\, s/(s+\omega_{c,hpf}) + \omega L_{VI}^{0} i_{od}\, s/(s+\omega_{c,hpf}) + \Delta R_{VI} i_{oq} - \Delta\omega L_{VI} i_{od} \tag{70}$$

7.3.1. **Setting Current Limiting Gains**

It is recommended to choose the current limiting gains $k_{p,Rvi}$ and $k_{p,Rvi}$*$\Delta X/R$ based on limiting the current magnitude to a suitable level during a bolted fault. For a three-phase bolted fault, the virtual impedance voltage drop should equal the voltage

magnitude command, V_0, as given by (71), where I_{max} is the desired maximum current magnitude.

$$V_0 = I_{\max} Z_{VI} = I_{\max} \sqrt{R_{VI}{}^2 + (\omega_0 L_{VI})^2} \tag{71}$$

For given values of I_{max}, I_{thresh}, and $\Delta X/R$, (66)-(68), and (71) can be combined and solved for k_p, with the result given in (72). Note that when using transient virtual impedance for $Z_{VI}{}^0$, $R_{VI}{}^0$ and $L_{VI}{}^0$ should be omitted from (72) because the voltage drop associated with $Z_{VI}{}^0$ would decay to zero with the high-pass filter's time constant, causing the current to increase beyond I_{max}.

$$k_{p,Rvi} = \frac{-b + \sqrt{b^2 - 4ac}}{2a} \tag{72}$$

where,

$a = (I_{\max} - I_{thresh})^2 \left(1 + (\Delta X/R)^2\right)$,

$b = 2(I_{\max} - I_{thresh})\left(R_{VI}^0 + (\Delta X/R)\omega_0 L_{VI}^0\right)$, and

$c = (R_{VI}^0)^2 + (\omega_0 L_{VI}^0)^2 - V_0{}^2 / I_{\max}^2$.

7.3.2. **Small-Signal Analysis**

Small-signal analysis of the inverter-generator microgrid is used to investigate the limits on the magnitude and X/R ratio of ΔZ_{VI}. In the following small-signal analysis, the operating point is rated load, with a 0.8 power factor linear load. The root locus plot for sweeping $|\Delta Z_{VI}|$ with $\Delta X/R$ and $Z_{VI}{}^0$ fixed is shown in Fig. 94. With increasing magnitude of Z_{VI}, damping of the generator electromechanical mode, $\lambda_{19,20}$, decreases and eventually becomes unstable. As $|\Delta Z_{VI}|$ increases, another voltage controller mode, $\lambda_{17,18}$, moves towards the horizontal axis.

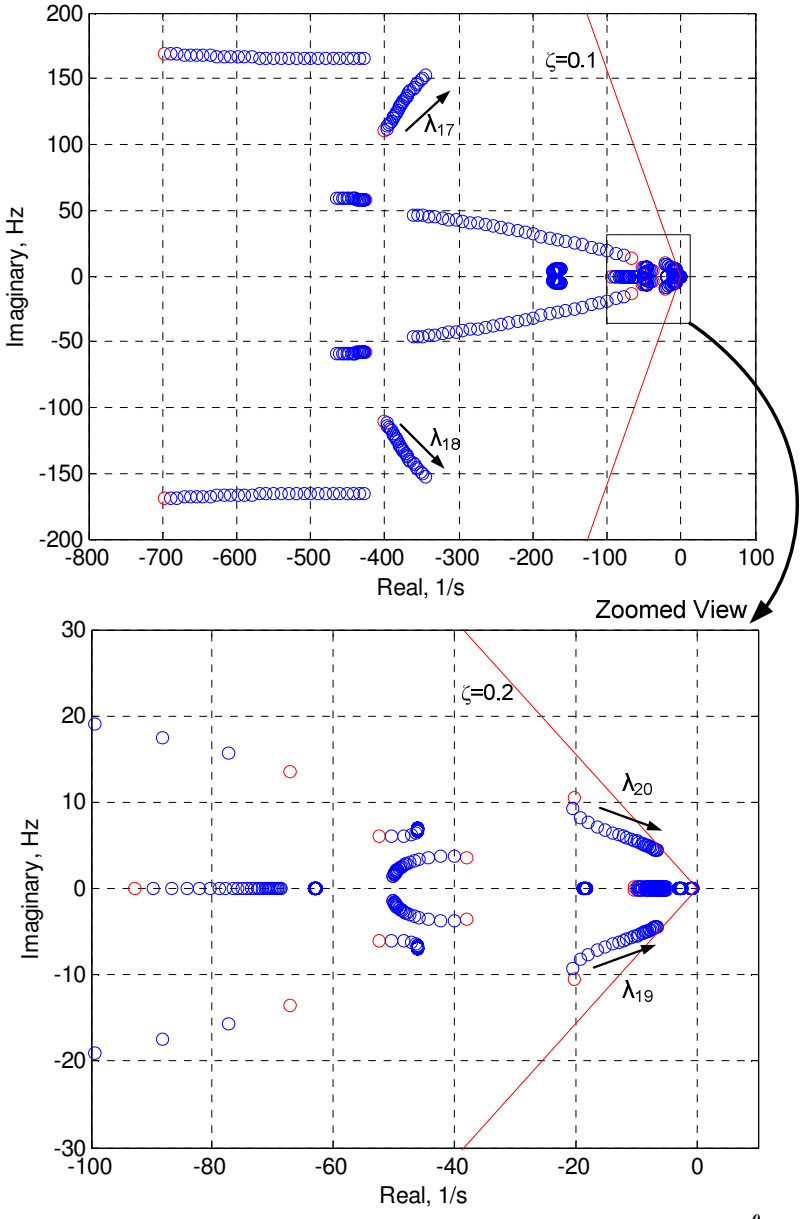

Fig. 94: Root locus for sweeping $|\Delta Z_{VI}|$ from 0 pu to 0.7 pu (with $\Delta X/R$ = 1, $|Z_{VI}^{0}|$ = 0.1 pu, and X_{VI}^{0}/R_{VI}^{0} = 1).

The root locus plot for sweeping $\Delta X/R$ with a fixed $|\Delta Z_{VI}|$ is shown in Fig. 95. As $\Delta X/R$ is increased from resistive to inductive, the damping of the electromechanical mode improves. However, the damping of the high frequency (~100 Hz – 150 Hz) voltage controller mode, $\lambda_{17,18}$, decreases. For larger ΔZ_{VI}, such as required when using a smaller I_{max} ($|\Delta Z_{VI}|$ is proportional to $1/I_{max}$), this high frequency voltage controller mode is problematic for inductive $\Delta X/R$.

The damping of the high frequency voltage controller mode will be seen to be very important during fault current limiting in Section 7.4.6, where inductive $\Delta X/R$ can cause poorly damped oscillations upon application and clearing of a fault.

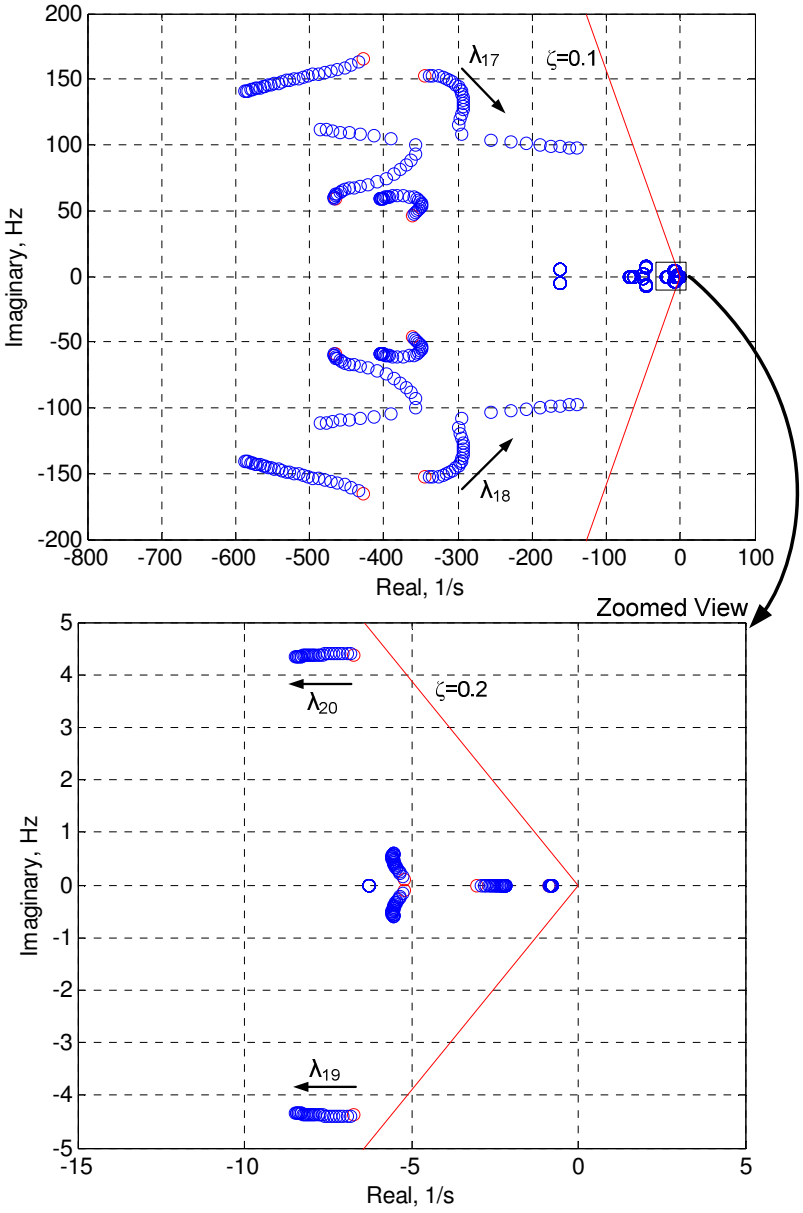

Fig. 95: Root locus for sweeping $\Delta X/R$ from 1 to 5 (with $|\Delta Z_{VI}| = 0.7$ pu).

7.3.3. Simulation

A simulation of the virtual impedance current limiting scheme is shown in Fig. 96 for the same load step as in Fig. 92. The virtual impedance increases when the current

magnitude exceeds 1 pu, and the current is reduced from a peak of 1.89 pu without current limiting (Fig. 92) to 1.2 pu with virtual impedance current limiting. The current limiting comes at the expense of increased voltage dip. The instability caused by current reference saturation limiters is prevented by the virtual impedance current limiting method by preventing the current references from saturating.

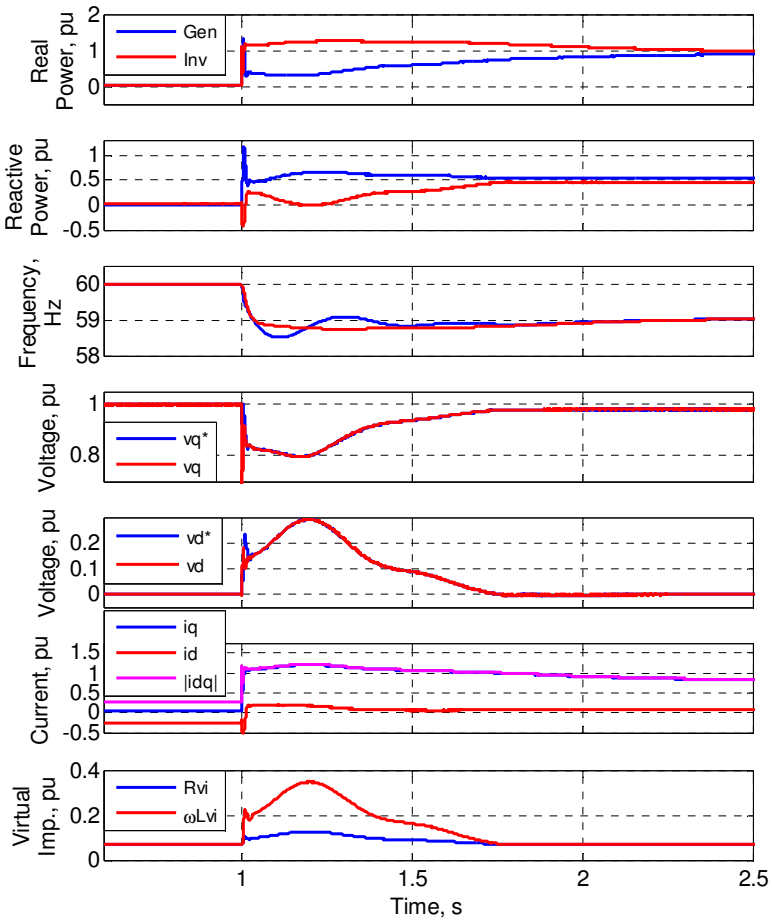

Fig. 96: Simulation of load step with virtual impedance current limiting (I_{max} = 1.5 pu, I_{thresh} = 1 pu, $\Delta X/R$ = 5).

The same simulation, with a less inductive $\Delta X/R$ is shown in Fig. 97. The current is still limited to a peak of 1.2 pu, but the main difference between the two simulations is that the reactive power sharing error is increased. This is because the larger resistive component creates a voltage drop from real power, and the increased voltage drop increases the reactive power sharing error.

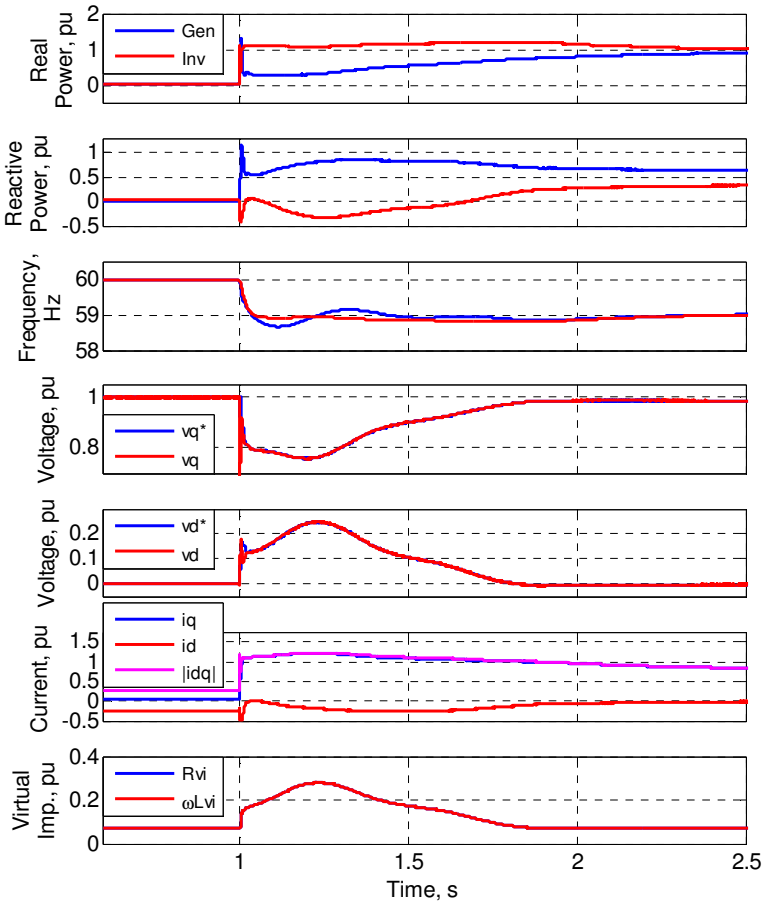

Fig. 97: Simulation of load step with virtual impedance current limiting (I_{max} = 1.5 pu, I_{thresh} = 1 pu, $\Delta X/R$ = 1).

7.3.4. Experimental Results

The proposed controllers have been tested on the experimental microgrid shown in Fig. 46. Experimental results are shown in Fig. 98, Fig. 99, and Fig. 100. All plots show instantaneous, unfiltered quantities. The data acquisition system has problems with picking up switching noise, and is primarily responsible for the significant harmonics present on the power and voltage traces.

Experimental results for the base case with constant Z_{VI}^{0} and no current limiting are shown in Fig. 98. The oscillations of the ~7 Hz electromechanical mode are apparent in the power and frequency traces.

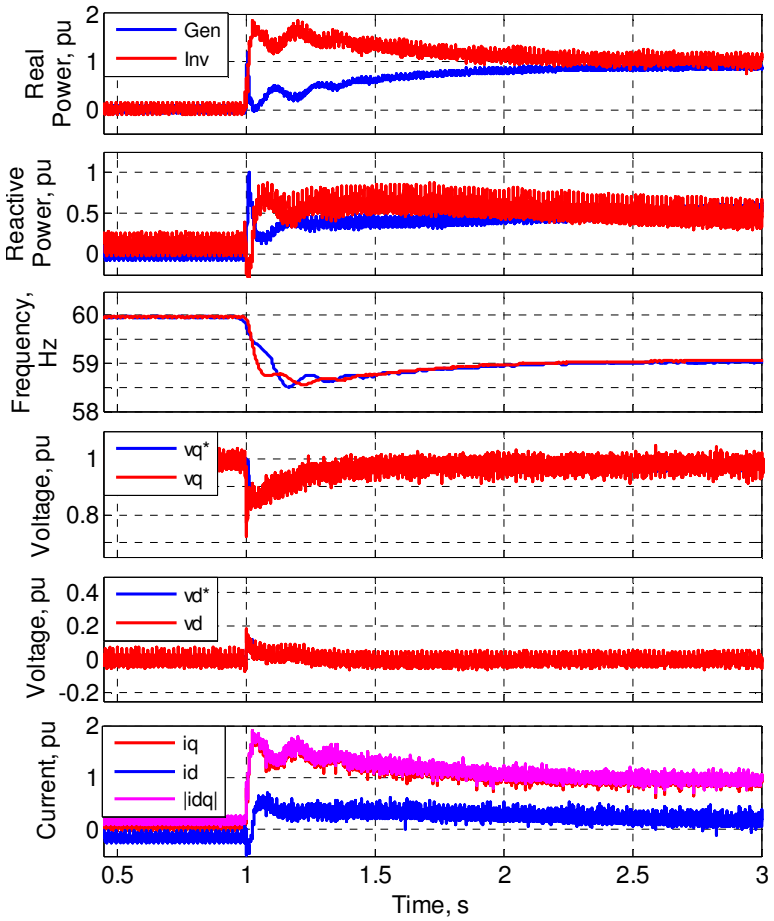

Fig. 98: Experimental results for base case without current limiting.

With simple saturation current limiting, shown in Fig. 99, the q axis voltage regulator current limits first, and when the inverter and generator frequency begin to deviate the voltage and current regulators wind up and become unstable.

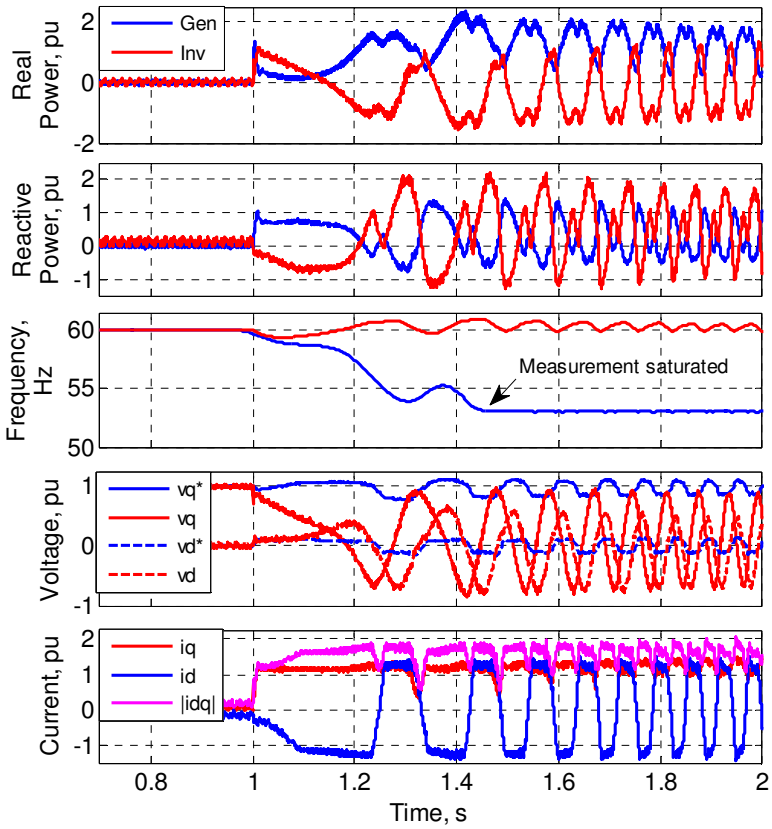

Fig. 99: Experimental results showing instability caused with simple current reference saturation limiting.

Virtual impedance current limiting is shown in Fig. 100. The virtual impedance is inserted when the current magnitude exceeds 1 pu, and reduces the q-axis voltage reference in order to limit the current. Virtual impedance is seen to be effective for current limiting during overloads caused by poor transient load sharing between grid-supporting-grid-forming inverters and synchronous generators.

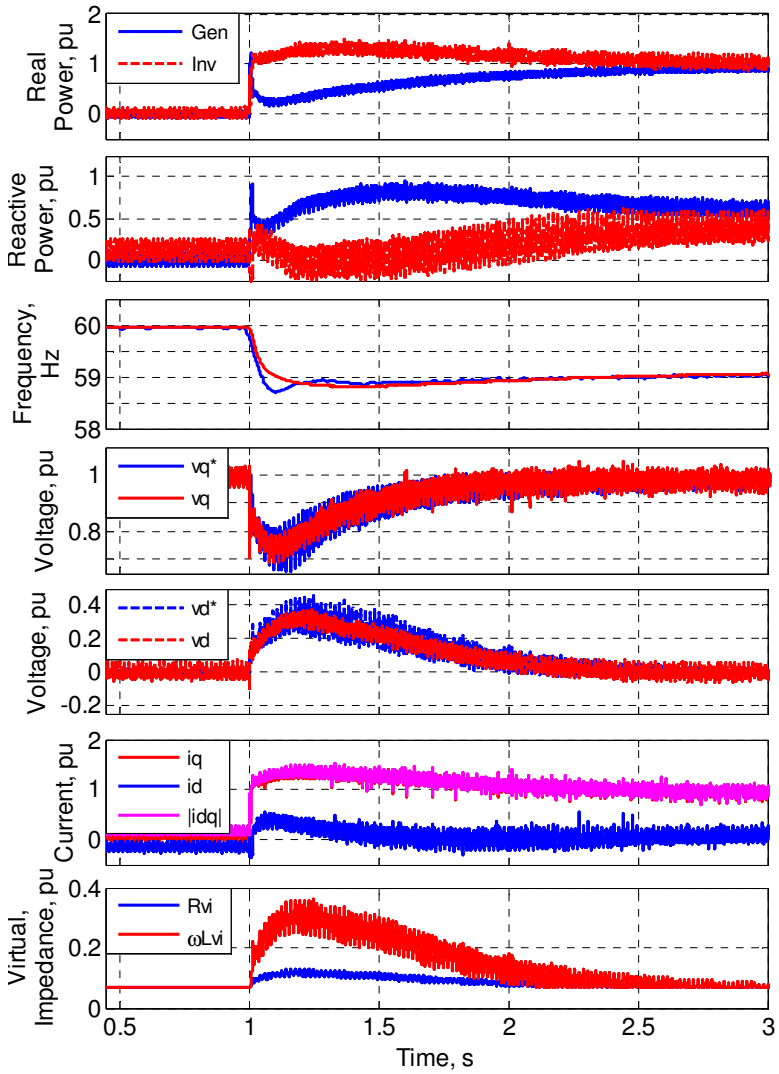

Fig. 100: Experimental results with virtual impedance current limiting showing that the current magnitude is limited and instability avoided (I_{max} = 1.5 pu, I_{thresh} = 1 pu, $\Delta X/R$ = 5).

7.4. Current Limiting During Faults

This section analyzes the performance of the proposed virtual impedance current limiting and conventional current limiting schemes during balanced faults in islanded mode. Current limiting during faults is very important, as any microgrid may be subject to faults. Overloads from poor transient load sharing could be avoided by limiting the size of load steps or selecting a sufficiently large inverter, but faults may occur in any application. Initial work on balanced faults is provided in this chapter, but many additional sub-topics are identified for future work.

7.4.1. **Current Reference Saturation**

The previous chapter showed that current limiting for grid-supporting-grid-forming control is challenging when in parallel with other voltage sources. When an inverter is by itself, entering and exiting current limiting is relatively simple. Once the short circuiting impedance is removed, the inverter just increases its voltage. However, when another grid-forming source is present, problems can occur, such as the reference-saturation induced instability described in Section 7.2. Fig. 101 shows a simulation of the laboratory microgrid, where a three-phase short circuit is applied in islanded mode, with the generator offline. In this simulation, multi-loop dq control is used with current-reference saturation at +/- 1.06 pu. When the fault is applied, the current reference saturates and current regulators limit the current. When the fault is removed, the voltage is restored without any problems, aside from some voltage overshoot.

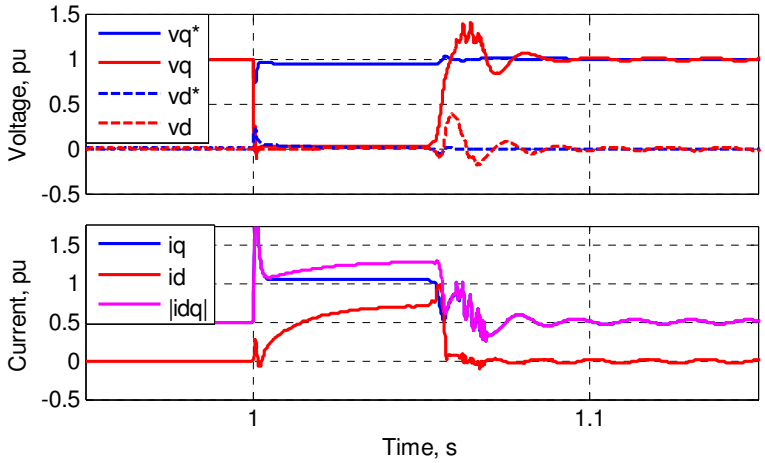

Fig. 101: Simulation of three-phase fault with only the inverter online with reference saturation limiting.

The same fault is simulated in Fig. 102, except with the generator online. When the fault is removed, the voltage regulators have trouble regaining control, and the current controllers inject large amounts of positive and negative real and reactive power, causing the voltage and frequency to deviate wildly. However, in this case, the system does eventually settle down (not shown).

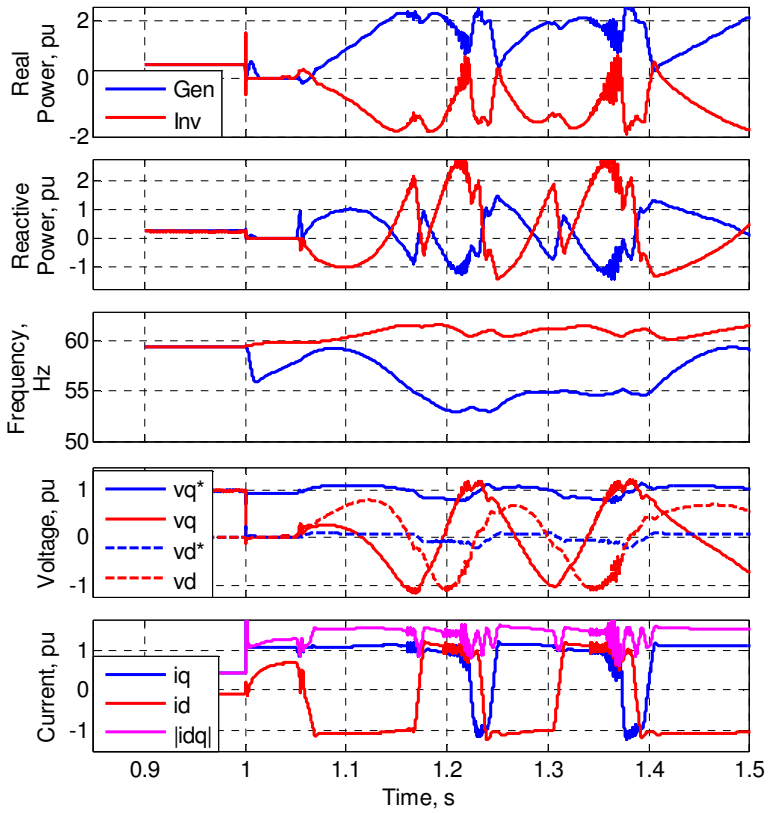

Fig. 102: Simulation of three-phase fault with both the inverter and generator online with reference saturation limiting.

Current reference magnitude limiting, where the magnitude of $|i_{Ldq}^*|$ is limited but the angle unchanged, provides better current limiting performance than simple reference saturation. The reference doesn't saturate as easily since the current reference magnitude is limited to I_{lim} instead of limiting each reference to +/- $I_{lim}/\sqrt{2}$ .Also, when the reference does saturate, the voltage regulator is not *completely* disabled since the angle of i_{Ldq}^* (i.e., atan(i_{Ld}^*/i_{Lq}^*)) can change. However, in the case of a fault, the current limiting easily becomes unstable, just like the simple reference saturation limiting. Fig. 103 shows a simulation of a three-phase fault with current reference magnitude limiting for a fault lasting 3 cycles (50 ms). The current reference magnitude is limited to 1.5 pu, and both the d and q current references are able to move around, but the inverter and generator frequencies still diverge, and the d and q axis currents and voltages still wind up. While the current limiting during overloads may often be satisfactory with current reference

magnitude limiting, the performance during recovery from a fault is typically unsatisfactory.

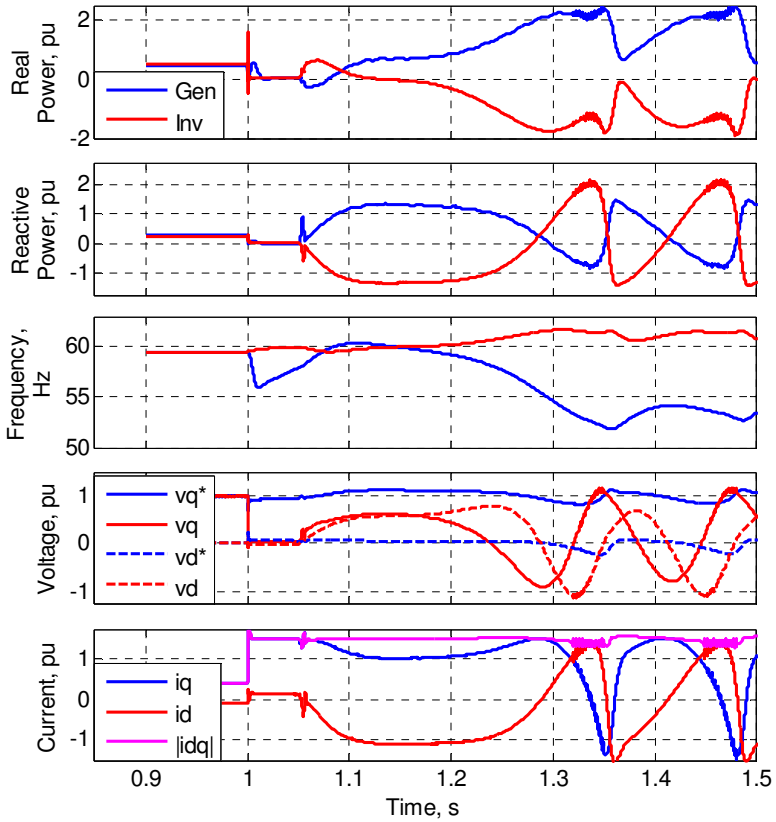

Fig. 103: Simulation of three-phase fault with both the inverter and generator online with reference magnitude limiting.

During faults, the generator speed changes, and when the voltage is restored, the generator and inverter phase angle may be misaligned. This is similar to the concept of critical clearing time in large grid-connected generators [93]. With large grid-connected generators, a fault causes a sudden decrease in electric output power due to a reduced voltage, and since the mechanical input power doesn't change quickly, the mechanical speed and the rotor angle increase. If the fault lasts too long and the rotor angle increases too far along the power angle curve, the rotor angle will continue to increase when the fault is cleared and the generator will lose synchronism. The basic concept of angle misalignment following fault clearing applies in the microgrid under consideration. However, some of the key assumptions in the critical clearing time derivations do not

apply: the mechanical input power cannot be assumed to be constant, and the inverter does not act as a stiff voltage source. With virtual impedance current limiting, the action of frequency droop and a large virtual impedance will help the inverter and generator regain angle alignment following fault clearing.

7.4.2. **Current Controller Overshoot**

When a fault occurs, a large voltage is initially imposed across the inverter's output filter inductor, causing the current to rise quickly. The current controller must quickly reduce the inverter voltage command to limit current overshoot. A couple things can reduce the current overshoot:

- Grid-voltage feed-forward in the current controller (see Fig. 8 in Section 2.2.5.4), such that the current controller only controls the voltage across the filter.
- Oversampling, and reducing PWM transport delay [94]. With triangular-carrier based PWM, the currents and voltages are normally sampled once per PWM period, and the new duty cycle is applied one PWM cycle later. Sampling twice per PWM period (at the carrier peak and minimum, and reducing the PWM transport delay to 1/2 cycle allows the current controller to respond more quickly.

Fig. 104 shows the simulated q-axis current overshoot with and without grid-voltage feed-forward in the current controller, for a three-phase bolted fault on the inverter's output. It can be seen that the current overshoot is reduced significantly by grid-voltage feed-forward. Only the q-axis current overshoots substantially since the q-axis voltage is near 1 pu prior to the fault, and the d-axis voltage is nearly zero. Fig. 105 shows the current overshoot for a fault with the controller sampling twice per PWM period, showing that the current overshoot is reduced significantly.

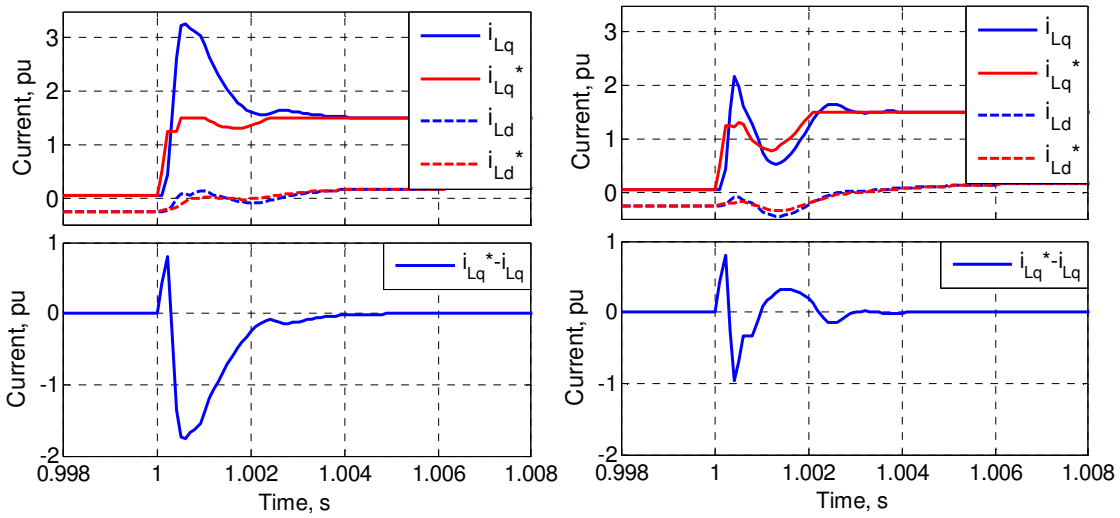

Fig. 104: Q-axis current overshoot without (left) and with (right) grid-voltage feed-forward.

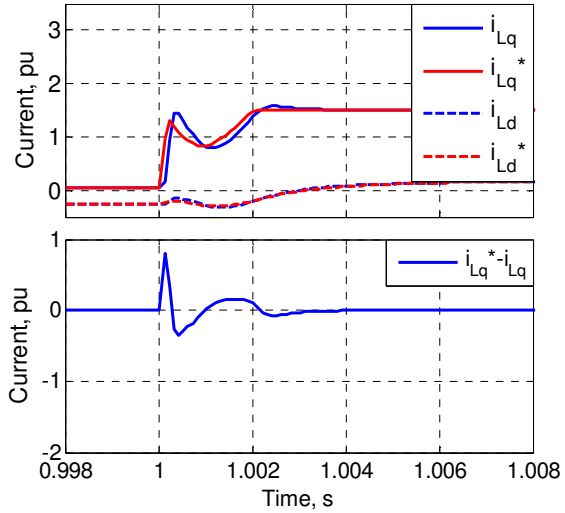

Fig. 105: Q-axis current overshoot with over-sampling and grid-voltage feed-forward.

In the experimental setup, there is a significant amount of noise in the feedback measurements due to a poorly designed data acquisition system, and the grid-voltage feed-forward causes significant problems by feeding forward noise. Also, the data acquisition system would need modification to allow sampling twice per PWM period. For these reasons, the grid-voltage feed-forward and oversampling methods have not been implemented in experiment or the remaining simulations. Therefore, a larger current overshoot occurs.

7.4.3. **Impact of ΔX/R and I_{max}**

In the case of a fault in islanded mode, when both the inverter and generator are online, the virtual impedance current limiting must do two things: 1) limit the current during the fault, and 2) limit the current after the fault is cleared and prevent unstable oscillations with the generator. The virtual impedance magnitude necessary to limit the fault current has been established in Section 7.3.1.

As discussed in Section 7.3.2, the current limiting X/R ratio, ΔX/R, impacts high frequency voltage controller modes. The high frequency modes only become poorly damped at large values of $|\Delta Z_{VI}|$, and are more problematic with faults than overloads due to the larger $|\Delta Z_{VI}|$ required to limit the current during faults. Damping of the high frequency voltage controller modes improves with decreasing ΔX/R, but low ΔX/R degrades the reactive power sharing during current limiting. It should be noted again that this high frequency voltage controller mode is also dependent on the voltage controller design and tuning.

The oscillations caused by inductive ΔX/R are more apparent during fault current limiting than overload current limiting due to the larger $|\Delta Z_{VI}|$ required for fault current limiting. Simulations of virtual impedance current limiting during faults show that ΔX/R is important for reducing these high frequency oscillations. However, the impact of ΔX/R on the damping of oscillations during faults is different than the small-signal analysis of large ΔZ_{VI} in Section 7.3.2, since this is a very different operating condition than the steady state operating condition around which the small-signal model is linearized.

To illustrate the impact of the current limiting virtual impedance X/R ratio on damping of this high frequency mode, simulations of a three-phase fault with both the generator and inverter online are performed. In both simulations, the current limiting virtual resistance gain, $k_{p,Rvi}$, is calculated with (72), using I_{thresh} = 1 pu and I_{max} = 1.5 pu. Fig. 106 shows a simulation of fault current limiting with ΔX/R = 5. Damping of the high

frequency mode is poor after application and clearing of the fault (behavior during the remainder of the fault recovery process will be shown later). Fig. 107 shows a simulation of fault current limiting with ΔX/R = 1. Damping of the high frequency mode is significantly improved.

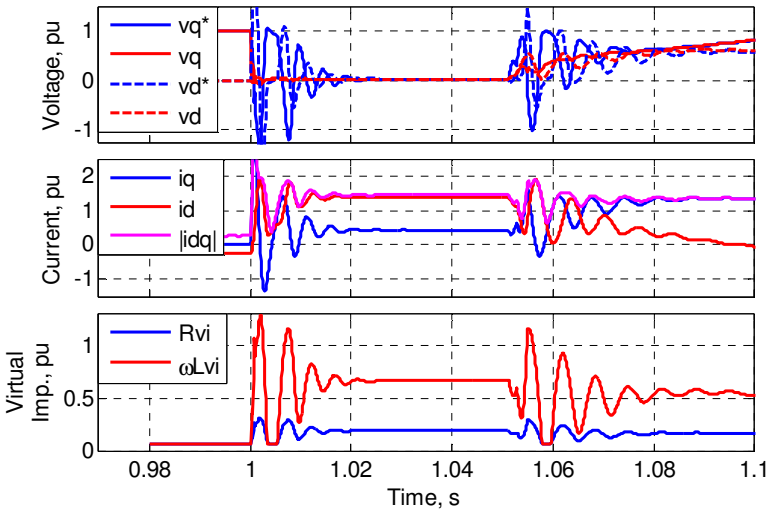

Fig. 106: Simulation of three-phase fault with ΔX/R = 5.

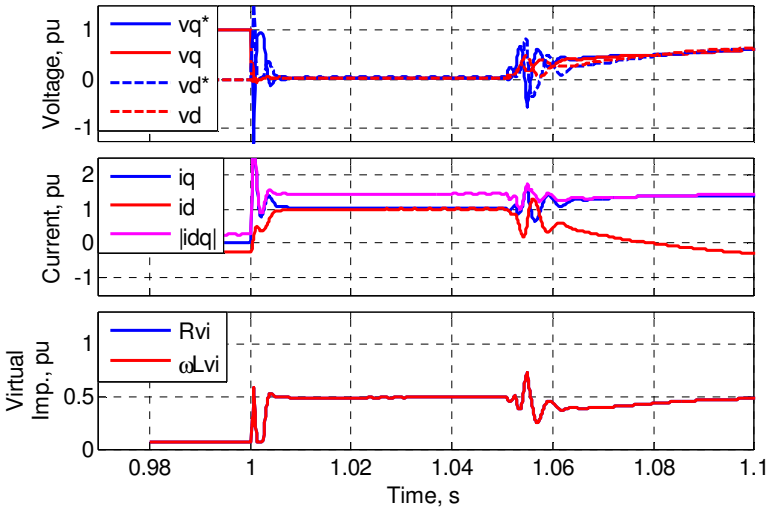

Fig. 107: Simulation of three-phase fault with ΔX/R = 1.

These high frequency oscillations are less problematic with larger I_{max}, since $|\Delta Z_{VI}|$ is proportional to $1/I_{max}$. If a larger I_{max} is tolerable, given the inverter's fault current capabilities, then a higher ΔX/R may be permissible. A higher ΔX/R is preferable for overload limiting, as it provides better damping of the generator electromechanical

mode and smaller reactive power sharing error. Fig. 108 shows a simulation of a three-phase fault with I_{thresh} = 1 pu, I_{max} = 2 pu, and ΔX/R = 5. Damping of the high frequency voltage controller mode is significantly improved compared to Fig. 106, where I_{max} = 1.5 pu. Note that in the remainder of this chapter, I_{thresh} = 1 pu, I_{max} = 1.5 pu, and ΔX/R = 1 are used ($k_{p,Rvi}$ = 0.943) due to satisfactory damping of the high frequency voltage controller mode and satisfactory damping of the electromechanical mode with lower I_{max}.

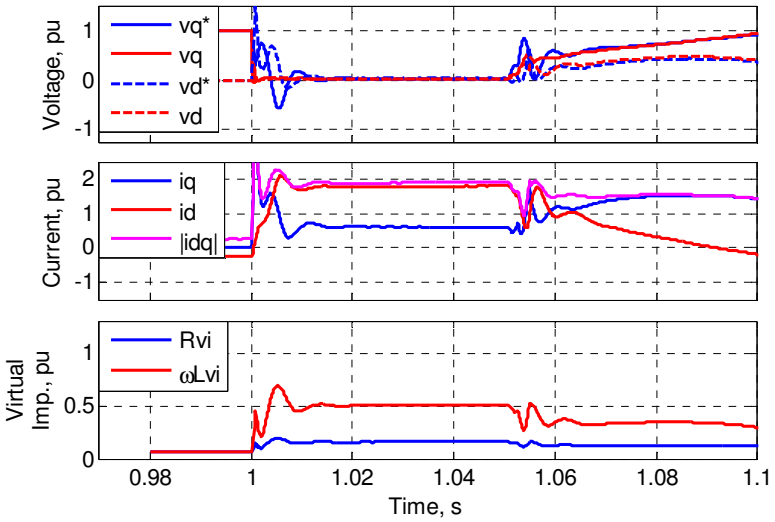

Fig. 108: Simulation of three-phase fault with ΔX/R = 5 and I_{max} = 2 pu.

7.4.4. Simulations

The performance of virtual impedance current limiting has been simulated for three-phase faults of various durations, and at different operating conditions. Faults within the microgrid would typically be cleared by normal overcurrent breakers, and thus would take 3 or more cycles to clear (as opposed to faults outside the microgrid which may be cleared within 1/2 cycle by a static switch). If the inverter is by itself, then the faults may take much longer to clear, or may not clear at all, due to the limited fault current capability of inverters [95]. Fault duration impacts the relative phase angle between the inverter and generator upon fault clearing. Fault duration also impacts the mechanical torque and field excitation upon fault clearing, since the mechanical torque and field excitation cannot be assumed to be constant due to the small size and relatively

fast speed of the generator's AVR and governor. The operating condition, specifically the load level, affects the load on the generator and inverter after the fault, and has a significant impact on the fault recovery.

Simulations were performed for faults at no load, with durations from 1 to 20 cycles, and at full load with durations of 1 to 12 cycles. The system recovers for all fault durations at no load, and faults of 1 to 7 cycles at full load. For faults of 8+ cycles at full load operating condition, the frequencies diverge and the system loses stability. This instability is discussed further in Section 7.4.5. Simulations of faults lasting 3 cycles and 8 cycles, at a no load operating point, are shown in Fig. 109. In both cases, there are large power, voltage, and frequency swings as the system settles down, but the system does finally reach steady state. The reactive power sharing takes longest to reach steady state following the fault. A large virtual impedance is required to limit the current after the fault is cleared. With the fault lasting 8 cycles, the generator and inverter are close to 180 degrees out of phase when the fault is cleared, as evidenced by the fact that v_q is negative when the fault is cleared, and that it swings through -1 pu before returning to 1 pu. For longer fault durations, power and frequency swings may last longer before the system settles down.

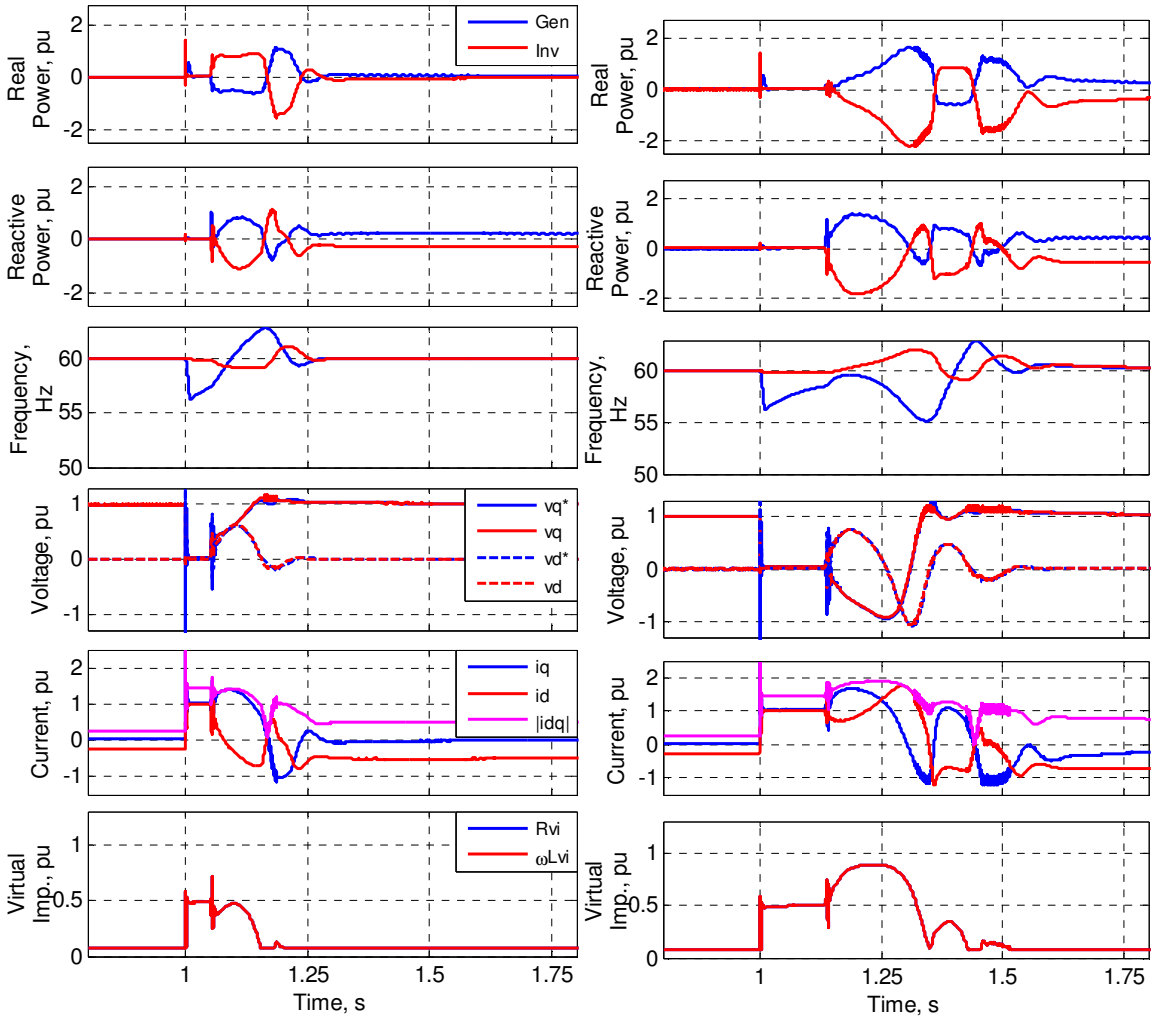

Fig. 109: Simulations of three-phase faults, lasting 3 cycles (left) and 8 cycles (right), at no load operating condition.

For faults at full load operating condition, swings in power, frequency, and voltage are also present. Reverse power conditions on the inverter are not as severe as in the no load case, since there is external load present and power swings between the inverter and generator do not necessarily cause reverse power on either source. At full-load operating condition, the system recovered for faults less than 8 cycles, but became unstable for faults lasting 8 or more cycles, as will be discussed further in Section 7.4.5.

Induction motor loads slow down during faults, and when the voltage is restored they can draw a large inrush. Depending on the severity and duration of the fault and the inertia and mechanical load, the speed of the machine and the inrush current upon fault

restoration will vary. A simulation is shown in Fig. 110 and Fig. 111 of a 6 cycle three-phase fault with a 5 hp induction motor and a 16 kW, 0.9 pf linear load. The induction motor has a fan-type load, where load torque is given by $T_m=0.5*\omega^2$. The induction motor slows down to 0.9 pu and then draws inrush as it speeds back up.

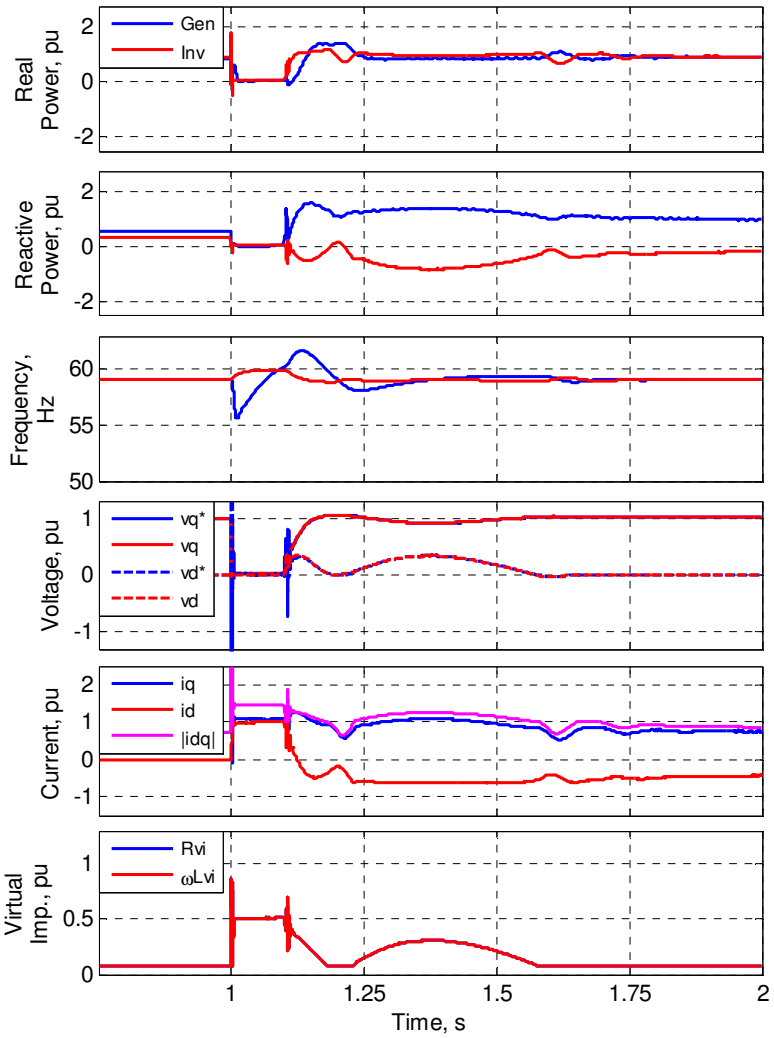

Fig. 110: Simulation of three-phase fault lasting 6 cycles, at full load operating condition with induction motor.

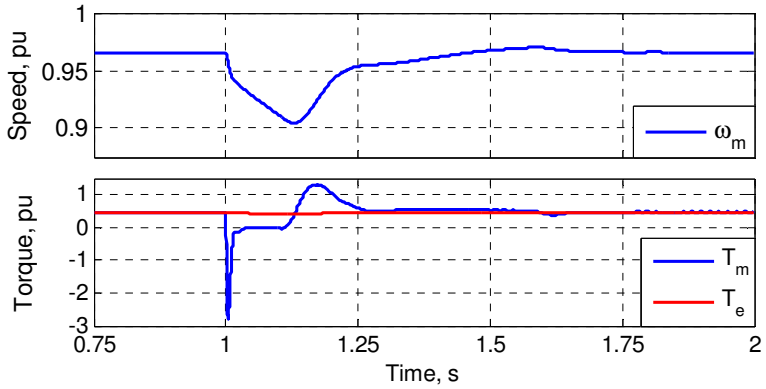

Fig. 111: Simulated induction motor speed and torque during three-phase fault.

The induction machine recovery inrush is not as large as the circulating reactive power between the inverter and generator. The current limiting action of the inverter means that the inverter will not be overloaded by induction motor recovery inrush, although it may delay recovery of the voltage. Fault recovery with various durations of faults and various operating conditions (RL load only vs. induction motor and RL load) were simulated, and it was found there were no significant differences with or without the induction motor.

Fault recovery with virtual impedance current limiting often results in large reverse power for the inverter and/or generator. Generator reverse power protection might trip during these faults, depending on the time delays and settings for the generator's reverse power protection. The large voltage and frequency swings could also trip the sources and/or loads offline. While the recovery transient *is* extreme, the system does reach steady state. A fault that takes 6+ cycles to clear would also interrupt many loads, so a rough recovery transient may not cause additional load interruptions.

7.4.5. **"Pole Slipping"**

With grid-connected synchronous generators, pole slipping is said to occur if the rotor angle goes beyond 180 degrees [96]. Pole-slipping typically results in large current and power swings that can damage the generator and cause line tripping. When a large current limiting virtual impedance is used, it is possible for "pole slipping" to occur,

where the inverter and generator frequencies diverge, and the d and q-axis voltages and currents wind up. Quotation marks are used here since “pole slipping” with inverters is not the same as pole slipping with synchronous generators. “Pole slipping” is similar to the current-reference saturation instability described in Section 7.2, except that the voltage regulator outputs do not saturate due to the virtual impedance current limiting action. “Pole slipping” is more likely to occur after faults than during overloads, due to the larger virtual impedance required to limit fault currents.

An example of a fault that results in “pole slipping” is shown in Fig. 112, where the inverter and generator are supply rated load prior to a three-phase fault lasting 8 cycles. After the fault is cleared, power swings occur, and are a function of the frequency difference, virtual impedance magnitude, and load. As the virtual impedance increases between 3.2 seconds and 3.4 seconds, the power decreases due to the angle of v_d and v_q changing, and then the generator speed slows down. Once the frequencies diverge, the dq voltages and currents wind up, and the microgrid does not recover.

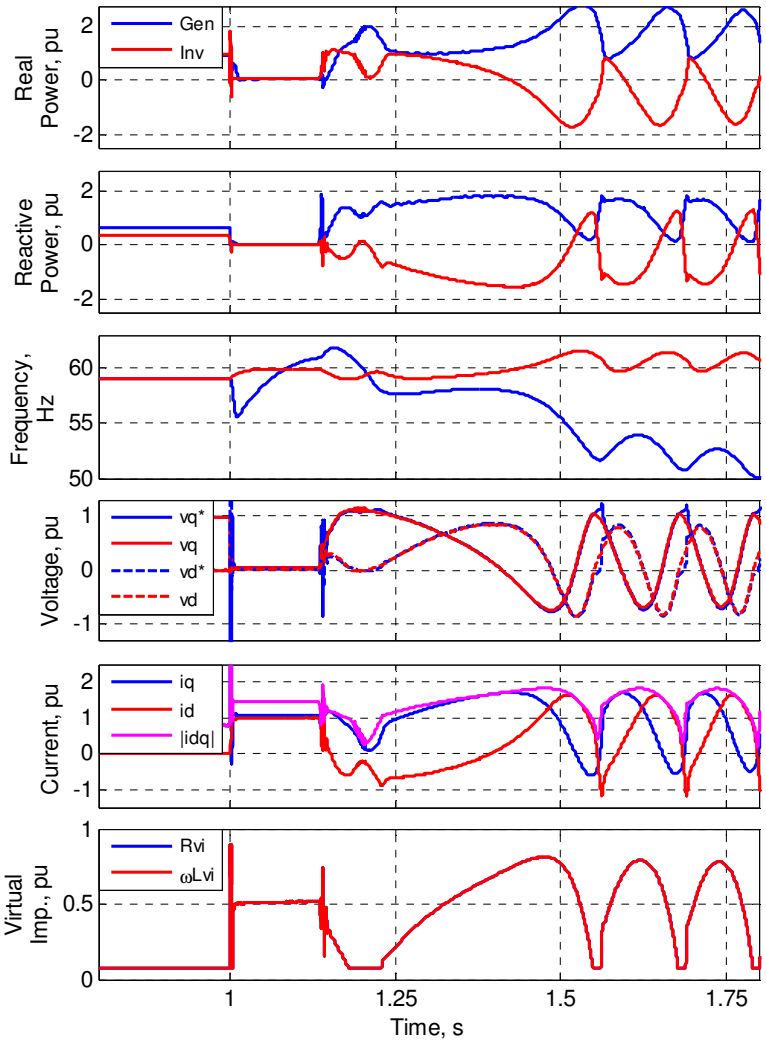

Fig. 112: Simulation of three-phase fault that causes "pole slipping".

During the fault, the generator speed initially decreases, then increases. The generator speed and torque are during the fault from Fig. 112 are shown in Fig. 113. The initial decrease in speed is due to the large electromagnetic torque (caused by the high initial fault current), and the machine's small inertia. The machine then accelerates because the mechanical input power is large prior to the fault. The mechanical input power does change significantly during the fault, however, due to the relatively fast governor.

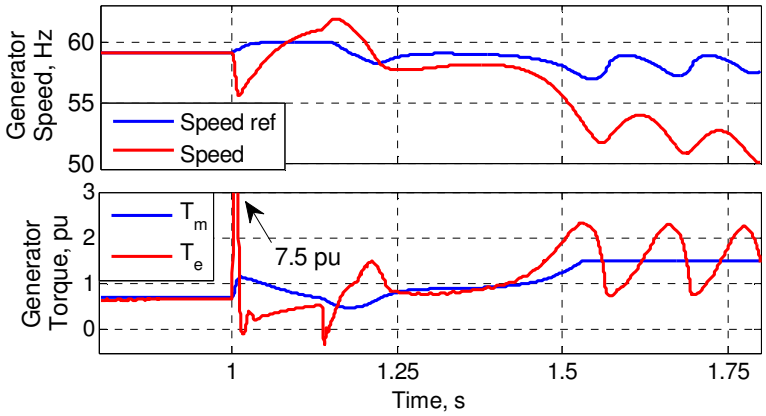

Fig. 113: Simulation of generator speed and torque during three-phase fault.

7.4.5.1. Maximum Current

When the inverter and generator voltages are significantly out of phase, the current can exceed I_{max}, the desired maximum current during a bolted fault used to calculate $k_{p,Rvi}$. If the inverter was 180 degrees out of phase with a stiff voltage source, the virtual impedance voltage drop would have to equal $2*V_0$. This would result in a current of $I_{thresh}+2*(I_{max} - I_{thresh})$. However, in a microgrid the voltage would typically be decreased significantly when the inverter and generator are out of phase due to the large currents being exchanged between the inverter and generator, and the current will be less than $I_{thresh}+2*(I_{max} - I_{thresh})$. In Fig. 112 the current magnitude reaches 1.8 pu, which is less than $I_{thresh}+2*(I_{max} - I_{thresh})$ (2 pu), but greater than I_{max} (1.5 pu).

7.4.5.2. Conditions for "Pole Slipping"

It is not possible to give definitive conditions of when "pole slipping" will or will not occur with virtual impedance current limiting, due to the complex and non-linear nature of the severe transients associated with "pole slipping". However, factors that influence the likelihood of encountering "pole slipping" can be identified. One of the basic causes of "pole slipping" is a basic characteristic of frequency regulation in grid-supporting-grid-forming control. When the generator experiences a load step, the frequency needs to swing (dip transiently) due to inertia and the governor response. Since

the inverter's frequency is given by power-frequency droop, the inverter does not necessarily let the generator's frequency swing, causing the inverter to assume more of the load. If the inverter begins to current limit, then the load must be assumed by the generator, and as the frequencies diverge, the inverter's dq voltages begin to wind up. Therefore, "pole slipping" is more likely to occur when the load is large. The following conditions have been identified that make "pole slipping" more likely to occur:

- Heavy load – generator frequency needs to swing but isn't allowed to by the inverter.
- Following faults vs. overloads, due to the higher ΔZ_{VI} required during faults.
- Faults that take a long time to clear, as this causes misalignment of the generator and inverter phase to be larger when the fault is cleared.
- Using smaller I_{max} – the inverter tends to provide less support to the generator, and uses larger ΔZ_{VI}.
- With lower $\Delta X/R$, because reactive power sharing is worse with lower $\Delta X/R$. Increasing $|\Delta Z_{VI}|$ tends to increase reactive power sharing error, which may lead to further increase of $|\Delta Z_{VI}|$.

The use of a transient droop during current limiting would be a logical attempt at letting the inverter frequency swing with the generator. However, due to the severe generator frequency swings following faults, transient droop during current limiting was found to have limited effectiveness. Transient droop during current limiting prevented "pole slipping" only in a limited number of situations, and thus does not justify the added complexity.

"Pole slipping" reveals a fundamental limitation of grid-supporting-grid-forming control in parallel with other grid-forming sources. With grid-feeding control, the inverter tracks the grid frequency, making the inverter much less likely to cause harmful interference as seen in "pole slipping" with grid-supporting-grid-forming control.

However, the types of conditions that cause "pole slipping", such as faults that take a long time to clear, are extreme conditions that would cause loss of load anyways.

7.4.6. **Unstable High Frequency Oscillations**

Simulations showed that increasing ΔX/R tends to cause poorly damped high frequency oscillations associated with the voltage controller. Simulations showed that these high frequency oscillations frequently become unstable immediately after fault application for ΔX/R greater than one. Factors affecting these oscillations included the value of ΔX/R, the value of I_{max}, system loading prior to fault application, and the fault resistance. Further investigation of these high frequency oscillations is recommended for future work.

Reactive power sharing is degraded further with low ΔX/R than high ΔX/R, as seen in Section 7.3.3, due to the impact of voltage drop across the virtual resistance. In experimental results, ΔX/R = 1 caused "pole slipping during" load steps. Therefore, a value of ΔX/R could not be found that worked for a wide range of load steps and a wide range of bolted faults. This necessitates either figuring out a way to avoid unstable high frequency oscillations with inductive ΔX/R, or transitioning from inductive ΔX/R (e.g. ΔX/R = 5) for overloads to lower ΔX/R (e.g. ΔX/R = 1) for faults. This topic is addressed in the future work section.

7.5. Chapter Conclusion

This chapter has analyzed current limiting performance of grid-supporting-grid-forming inverters in islanded microgrids. Current reference saturation can cause instability when current limiting during overloads and faults. When the current reference saturates, the voltage regulator is effectively disabled, and the system can lose stability. Current reference magnitude limiting is less likely to cause instability for overloads than simple d and q-axis saturation, but is likely to cause instability for faults.

Virtual impedance current limiting has been proposed to provide improved transient stability during overloads and faults. Virtual impedance current limiting works by reducing the voltage reference to prevent the voltage controller from commanding an excessively large current reference. A method has been proposed for setting the virtual impedance current limiting gains based on limiting the current to a specified value during a bolted fault. Stable current limiting during overloads caused by poor transient load sharing between inverters and generators has been demonstrated with the use of virtual impedance current limiting.

This chapter has also investigated the performance of virtual impedance current limiting during three-phase faults within the microgrid. During a fault, the generator and inverter phase angles deviate, causing large power swings upon fault clearing as the angles regain alignment. Despite the large swings while settling down, the system does usually settle down. In some cases, "pole slipping" occurs, where the inverter and generator frequency deviate, and instability occurs even though the inverter current reference does not saturate.

Virtual impedance current limiting allows for stable current limiting during a wide range of microgrid faults, unlike current reference saturation methods. However, virtual impedance does have some drawbacks: virtual impedance current limiting has a large number of degrees of freedom, which requires extra tuning effort. Virtual impedance limits the current gradually, and can become oscillatory if the virtual impedance is increased too quickly (i.e. $k_{p,Rvi}$ too large). Virtual impedance current limiting does not guarantee a maximum current (unlike reference saturation), which requires building in extra overhead in the inverter current rating. Finally, using a low I_{max} requires large $|\Delta Z_{VI}|$, which may cause extra oscillations. Despite the drawbacks, virtual impedance current limiting improves transient stability compared to traditional current limiting methods in grid-supporting-grid-forming inverters.

CHAPTER 8: CONCLUSIONS AND FUTURE WORK

This thesis has explored the difficulties encountered in operating grid-supporting-grid-forming inverters in parallel with synchronous generators. This work has specifically addressed mitigating transient overloads and providing stable current limiting during overloads and faults. While the problems associated with poor transient load sharing between inverters and generators could be solved by choosing an inverter large enough to support any possible transient, cost constraints may prevent microgrid designers from doing so. This research improves understanding of the transient interactions between grid-supporting-grid-forming inverters and generators, and provides microgrid designers control over the tradeoff between transient load sharing and power quality. The methods proposed in this thesis for mitigating inverter overloads will allow for more reliable and cost effective application of inverter based DER with synchronous generators in microgrids.

The cause of poor transient load sharing between grid-supporting-grid-forming inverters and synchronous generators has been identified as the differences between their respective frequency and voltage regulation characteristics. To improve transient load sharing, the inverter should allow the generator to swing – i.e. allow greater voltage and frequency transients. It was also shown that initial power sharing is a function of output impedances. By combining virtual output impedance with transient droop, the transient power sharing characteristics can be controlled. Nearly equal transient load sharing can be achieved at the expense of increased voltage and frequency dips.

In many situations it may be preferable to simply current limit the inverter during overloads instead of deliberately allowing power quality to be degraded to improve transient load sharing. However, simple current reference saturation methods are shown to cause instability during current limiting in some circumstances. When the current reference is saturated, the voltage regulator is essentially disabled, and the system can

lose stability. Virtual impedance current limiting is proposed to provide stable current limiting. Virtual impedance current limiting operates by reducing the voltage reference in order to prevent the voltage regulator from commanding an excessively large current reference. Virtual impedance current limiting significantly improves transient stability compared to simple current limiting methods, particularly in the case of faults, but cannot guarantee stability in all circumstances.

Performance during load transients and faults is more of a concern with voltage-controlled inverters than current-controlled (grid-feeding) inverters. Because voltage-controlled inverters attempt to regulate the output voltage, they are more easily overloaded during transients than current-controlled inverters, which track the output voltage and inject a specified current. Voltage-controlled inverters are particularly challenging when operating in parallel with other grid-forming sources that have different frequency regulation characteristics, due to the possibility of large power swings when the phase angles go out of alignment. However, the benefit of avoiding control mode transitions between grid-connected, islanded, and stand-alone mode motivates the use of grid-supporting-grid-forming control.

8.1. Contributions

The first part of this thesis fills an observed gap in the microgrid literature of distinguishing between what is technically feasible and how to derive economic value, and identifying barriers to adoption of inverter-based microgrids. The rest of this thesis finds solutions to issues encountered when operating synchronous generators and grid-supporting-grid-forming inverters together in islanded microgrids.

In summary, the main contributions from this research are:

- Analysis of microgrid value propositions and barriers to adoption of power-quality microgrids.

- Improved understanding of dynamic interactions between synchronous generators and grid-supporting-grid-forming inverters, and the tradeoff between transient load sharing and transient voltage and frequency regulation.
- Demonstration of a grid-supporting-grid-forming control with virtual impedance and transient droop to allow control over the degree of transient load sharing with synchronous generators.
- Virtual impedance current limiting for grid-supporting-grid-forming inverters to provide improved transient stability during overloads and faults when operating in parallel with synchronous generators.

Multiple publications have resulted from this work. A paper titled "Design considerations for microgrids with energy storage" was published in the *Energy Conversion Congress and Exposition* conference September 2012. The paper covered the material from Chapter 3. This paper received a Student Poster Presentation Award at the conference. This paper was submitted to *Transactions on Industry Applications / Industry Applications Magazine* under the revised title of "Design considerations for power quality microgrids," and was accepted for publication in the September/October 2014 edition of *Industry Applications Magazine*.

A paper titled "Transient load sharing between synchronous generators and inverters in islanded microgrids" was published in the *Energy Conversion Congress and Exposition* conference September 2012. This paper covered the material from Chapters 4 and 5. The paper was submitted to *Transactions on Industry Applications / Industry Applications Magazine* and was accepted for publication in the March/April 2014 edition of *Industry Applications Magazine*.

A paper titled "Virtual impedance current limiting for inverters in microgrids with synchronous generators" was published in the *Energy Conversion Congress and*

Exposition conference in September 2013. The paper covers the much of material from Chapter 7. This paper received a Student Oral Presentation Award at the conference.

8.2. Recommended Future Work

8.2.1. Impedance-Based Stability Analysis and Discrete-Time Analysis

Multi-loop grid-supporting-grid-forming inverter control is very sensitive to impedance. Eigenvalue analysis gives information about the impact of impedance and control parameters on system oscillations and damping, but has drawbacks: eigenvalues cannot be measured experimentally, and only dominant eigenvalues are visible in measurements. Using impedance-based analysis allows measurement of the input/output impedance of sources and networks, and the use of impedance-based stability criteria. Impedance based stability criteria allow experimental validation of stability margins.

Using discrete-time small-signal analysis instead of the continuous time analysis used in this thesis may provide more insight into the effects of PWM delays and control cycle delays on the virtual impedance current limiting controls.

8.2.2. Single-Loop vs. Multi-Loop Control

Single-loop grid-supporting-grid-forming control is not nearly sensitive to impedance and virtual impedance as multi-loop grid-supporting-grid-forming control. The sensitivity to impedance of multi-loop control, and the need for relatively high bandwidth of the outer voltage loop, is problematic for: 1) large inverters with low switching frequency (<= 3 kHz) 2) plug & play applications, where it is desired to add DER without having to redesign the entire system. However single-loop has some disadvantages: relatively poor performance with harmonics & unbalance, more challenging fault protection, and potentially worse voltage regulation & voltage quality than might be expected from a system competing with conventional power quality solutions. A thorough comparison of optimized implementations of multi-loop vs. single-

loop control would highlight the advantages and disadvantages of the two control strategies.

8.2.3. **Fault Current Limiting**

Current limiting virtual impedance X/R ratio ΔX/R has an impact on stability. Inductive ΔX/R was seen to cause high frequency oscillations in many situations, and lower values of ΔX/R were seen to degrade reactive power sharing and increase likelihood of "pole slipping." Future work should either find a way to avoid unstable high frequency oscillations with inductive ΔX/R, or a way to transition from inductive ΔX/R for overloads (to avoid pole slipping) to lower ΔX/R for faults (to avoid high frequency oscillations).

This thesis has investigated the performance of virtual-impedance current limiting during balanced three-phase faults. However, unbalanced faults are much more common than balanced faults. Unbalance creates a 120 Hz component in the synchronous dq frame, which can be regulated with proportional + integral + resonant (PIR) controllers or with separate positive and negative dq frames. Alternatively, proportional + resonant (PR) controllers can be used to regulate both positive and negative sequence in the stationary frame. The current reference, including the 120 Hz component, must be limited in the synchronous reference frame. In the stationary frame, anti-windup PR controllers should be used to limit the current reference without clipping the waveforms. Performance of virtual impedance during unbalanced faults is a topic that needs to be addressed.

In microgrids that have inverters with energy storage, fast-acting interconnection switches such as a static-switch would typically be used. In the case of grid-faults, the interconnection should typically open within 1/2 cycle, but sources should not trip offline if the interconnection switch takes longer than normal to open (e.g. 6+ cycles). Both

balanced and unbalanced grid-faults should be addressed, including the phase-jump often present with unbalanced grid-faults.

The virtual impedance current limiting method proposed in this work increases the current limiting virtual impedance proportionally. The use of other current limiting profiles should be investigated, such as an exponential virtual impedance term, to reduce overshoot beyond I_{max}.

8.2.4. **Impact of Different Load Types**

This research only focused on constant impedance loads. Constant power & constant current loads such as power electronic loads tend to de-stabilize systems. When constant power & constant current loads are present, it is important to consider them in stability analysis.

Sharing of harmonic and unbalanced loads in multi-inverter microgrids has been investigated in the literature. In the case of microgrids with inverters and generators, the relative sharing of harmonic & unbalanced loads should be considered. The impact of inverter virtual impedance will impact sharing of negative sequence and harmonic loads, but will also cause greater voltage distortion.

APPENDIX A: EXPERIMENTAL VALIDATION OF GENERATOR PARAMETERS

Based on consultation with PSCAD technical support, two different tests were performed to validate the d and q-axis generator datasheet parameters. By applying a resistive load step with a constant field voltage and comparing the measured and simulated d and q-axis voltages and currents, the q-axis transient parameters (X_q'' and T_{qo}'') may be estimated. The voltage is in phase with the q-axis prior to the load step, and since the current is in phase with the voltage for a resistive load, q-axis parameters dominate the resistive load step behavior. By applying a purely inductive load step with a constant field voltage, the d-axis transient parameters (X_q', X_q'', T_{do}', and T_{qo}'') may be estimated. Since the current is in quadrature with the voltage for an inductive load, the d-axis transient parameters will dominate the behavior for an inductive load step. The d-axis transient parameters should be tuned first with the inductive load step test, since the q-axis parameters influence the inductive load step less than the d-axis parameters influence the resistive load step. Once the transient reactances and time constants have been validated, X_d and X_q can be estimated from the steady state voltage and current for the resistive load step, since the power angle ($\text{atan}(v_d/v_q)$) will increase significantly for a resistive load.

Using resistive and inductive load steps to tune the datasheet parameters was preferred over the short-circuit test, because the current measurements saturated badly during the short circuit test, and the generator breaker tripped when the short-circuit test was performed at rated voltage. Also, the short circuit test gives d-axis parameters, while the method proposed by PSCAD support allows validation of both d and q-axis parameters.

Since the speed encoder signals were not directly measured, an alternative method of estimating the rotor angle was required to allow decomposition of measured voltages

and currents into d and q-axis values. The generator frequency measurement (from the variable frequency drive powering the induction motor) was integrated to give the angle, with an offset chosen to set the d-axis voltage to zero before the load step is applied (at no-load, the terminal voltage is in phase with the q-axis). Multiple load steps were recorded in the same dataset to ensure that the calculated d-axis voltage remained at zero at no-load in steady-state after each load step, giving confidence that the estimated dq transformation angle is accurate during the load step. To ensure that the simulated dq transformation matched the value calculated from measured data, the inertia and governor k_p were manipulated (small H, large k_p) to ensure simulated speed closely matched measured speed.

Resistive and inductive load step tests were performed on the experimental setup with the AVR disconnected and a DC power supply powering the exciter. The measured values were compared to simulation results, and the generator parameters were adjusted to match simulation with experiment. Fig. 114 and Fig. 115 and show the measured and simulated d and q-axis voltages and currents for the inductive and resistive load steps. In the inductive load step, the decaying 60 Hz oscillations in the d and q-axis currents are from the decaying dc offset associated with the inductive load step.

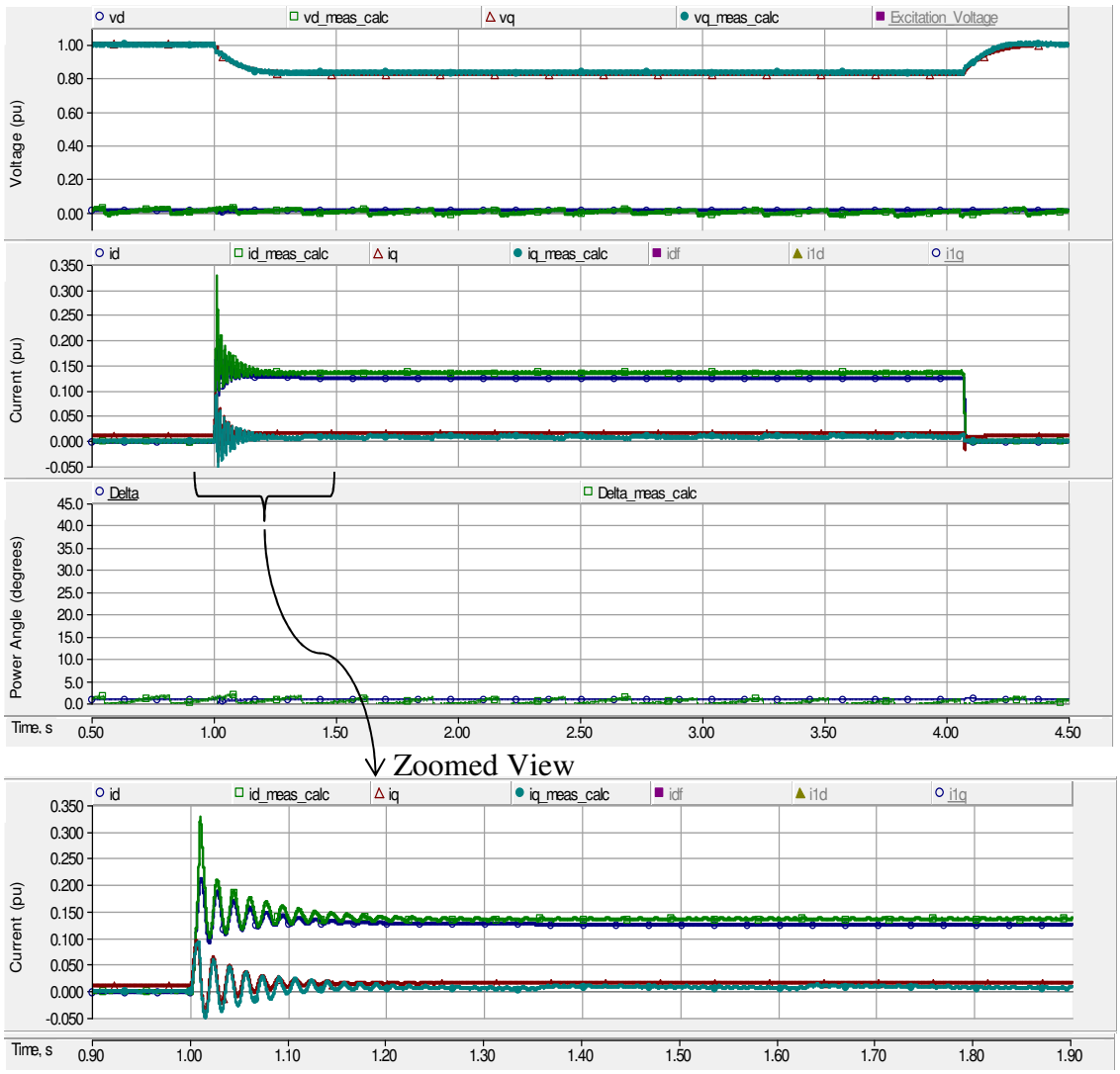

Fig. 114: Comparison of measured and simulated d and q-axis voltage and current for inductive load step using validated datasheet parameters.

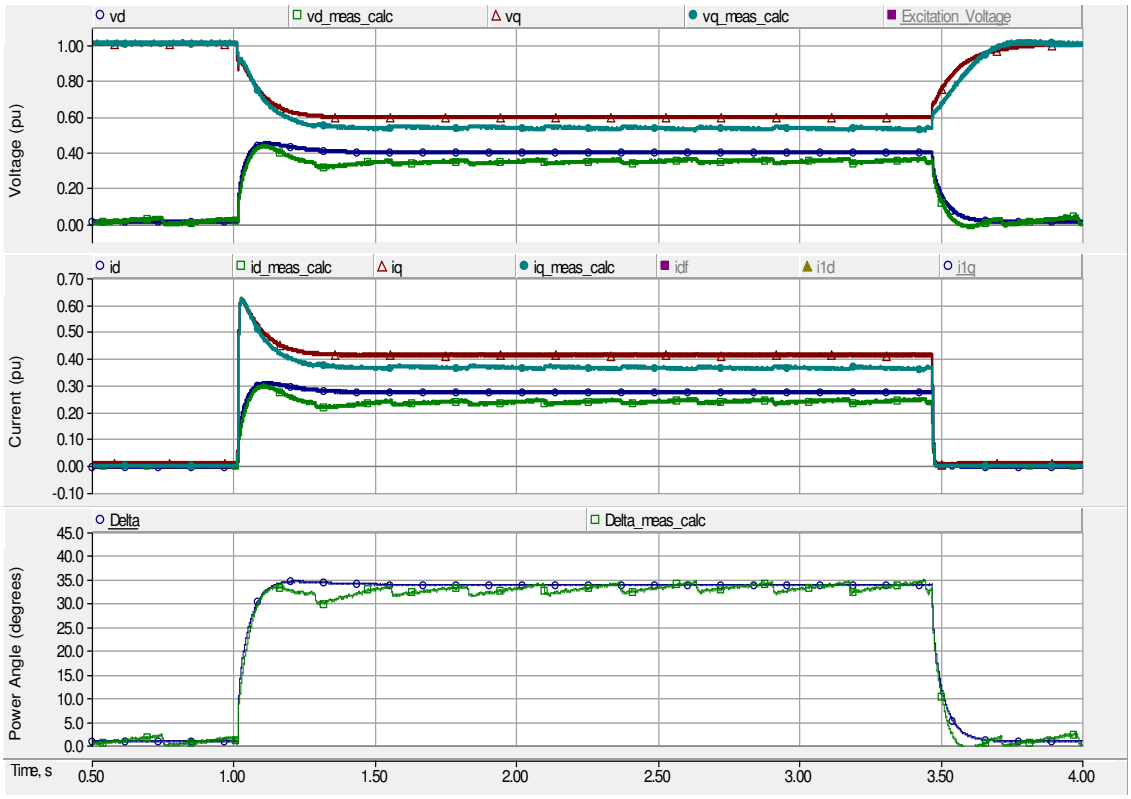

Fig. 115: Comparison of measured and simulated d and q-axis voltage and current for resistive load step using validated datasheet parameters.

Two sources of error are identified by certain dynamics not being modeled. The generator uses a brushless exciter with a rotating rectifier that feeds the field winding, so some of the field circuit dynamics are not modeled. D-axis saturation was not modeled in the simulated data, and applying a load step acts to change the d-axis mutual flux, causing a change in the saturation factor. Lack of d-axis saturation impacts the resistive load step test more than the inductive test, since the resistive load was larger. Modeling of d-axis saturation was investigated, but accurate representation of both the unsaturated behavior of the machine (from short circuit tests) and saturated behavior of the machine (i.e. tests in Fig. 114 and Fig. 115, and load steps with AVR enabled) was not successful. While the simulations do not match the measured data perfectly, the behavior without d-axis saturation modeled is satisfactory for this work.

The measured and simulated d and q-axis voltage and current using the original datasheet parameters are shown in Fig. 116 for an inductive load step, showing the degree

of error with the original d-axis datasheet parameters. The error in X_d can be seen by the excessive drop in simulated v_q, and the overly large T_{do}' can be seen by the much slower time constant of simulated v_q.

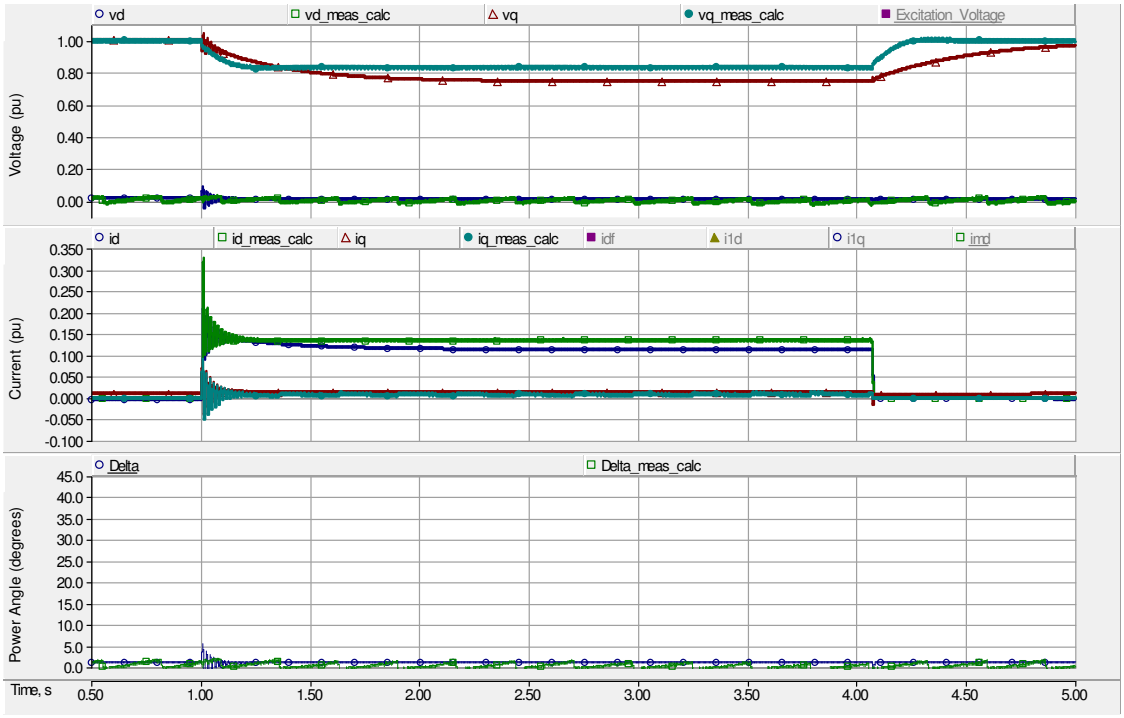

Fig. 116: Comparison of measured and simulated d and q-axis voltage and current for inductive load step using original datasheet parameters.

To experimentally validate the inertia and friction constants, the generator and induction motor were allowed to coast and a small load step was applied. By adjusting the friction constant, the rate of speed decay during the coasting period before load application could be matched. By adjusting the inertia constant, the rate of speed decay could be matched after applying the load step. Fig. 117 shows the comparison of simulated and measured speed and power used to validate the inertia and friction constants. A close match between simulation and measured speed indicates a good match between simulated and actual inertia and friction values.

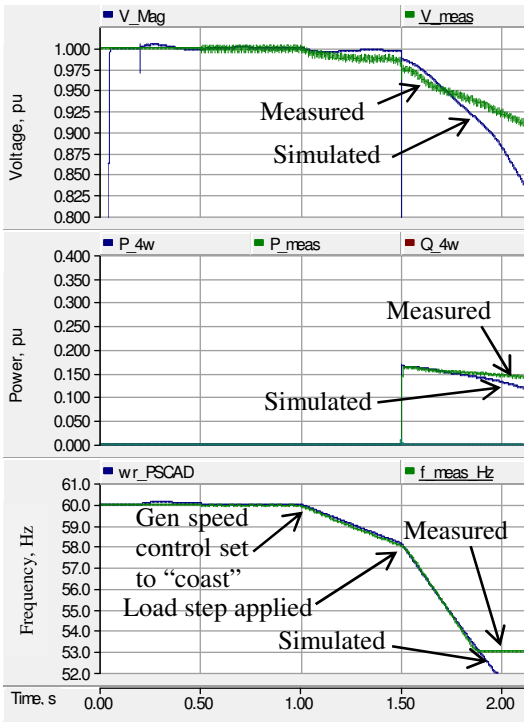

Fig. 117: Comparison of measured and simulated speed for validating inertia and friction constants.

The factory vs. experimentally validated datasheet parameters are shown in Table 9. The "Comment" column gives notes about the values in the "Datasheet" column.

Table 9: Generator Parameters from Datasheet vs. Validated Values

Parameter [42]	Datasheet	Expt. Validation	Comment
Base Power, S_{base}	18.8 kVA	18.8 kVA	Datasheet parameters given on 18.8 kVA (15 kW) base, but plotting uses 12.5 kW base.
Base Voltage, V_{base}	208 V	208 V	Datasheet parameters given for high-wye configuration (480 V), but stator reconfigured as low-wye (240 V) and ran at 208 V, so scaled datasheet parameters by $V_{base,old}/V_{base,new}$ = 240/208.
Unsaturated Reactance, X_d	2.267 pu	1.4 pu	
Unsaturated Transient Reactance, X_d'	0.140 pu	0.35 pu	
Unsaturated Sub-Transient Reactance, X_d''	0.119 pu	0.1 pu	
Unsaturated Reactance, X_q	1.360 pu	1.0 pu	X_q not given, so assume Xq = 0.6*X_d
Unsaturated Sub-Transient Reactance, X_q''	0.273 pu	0.3 pu	X_q'' not given, so calculated from X_2 (negative sequence reactance), X_2 = (X_d''+X_q'')/2 [42]
Open-Circuit Unsaturated Transient Time Constant, T_{do}'	0.47 s	0.1 s	
Open-Circuit Unsaturated Sub-Transient Time Constant, T_{do}''	0.0094 s	0.0094 s	
Open-Circuit Unsaturated Sub-Transient Time Constant, T_{q0}''	0.0016 s	0.045 s	T_{qo}'' not given, so assume T_q'' = T_d'' [42].
Stator Resistance, R_s	0.0504 pu	0.0504 pu	
Stator Leakage Reactance, X_l	0.052 pu	0.052 pu	X_l not given, so assume X_l = X_0 (zero sequence reactance)
Inertia Constant, H	- s	0.34 s	
Friction Constant, B	- pu	0.04 pu	

With the generator datasheet parameters validated, the governor and AVR gains were validated by applying small speed and voltage reference steps at no-load. Fig. 118 shows a comparison of measured and simulated speed for validation of governor gains. Fig. 119 shows a comparison of measured and simulated voltage for validation of AVR gains. Note that Fig. 118 and Fig. 119 are separate tests. There is some error in the tuning of the AVR gains because the AVR gains were actually tuned to match measured and simulated voltage during a load step, which is shown in Fig. 120. The discrepancy in the voltage during load rejection is primarily due to d-axis saturation being disabled in simulation.

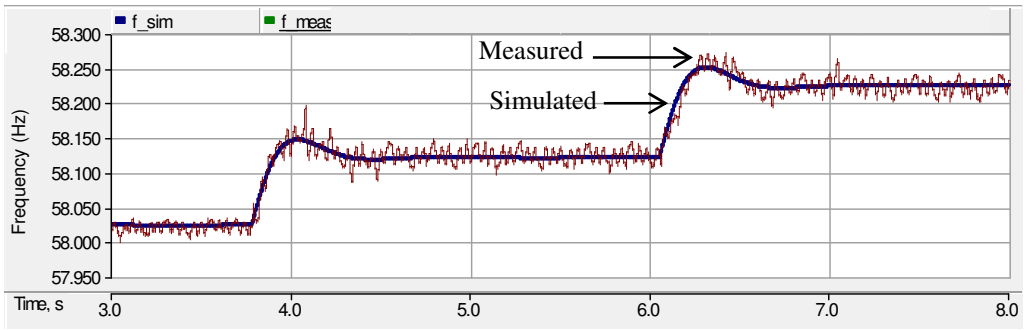

Fig. 118: Comparison of measured and simulated speed for validating governor gains.

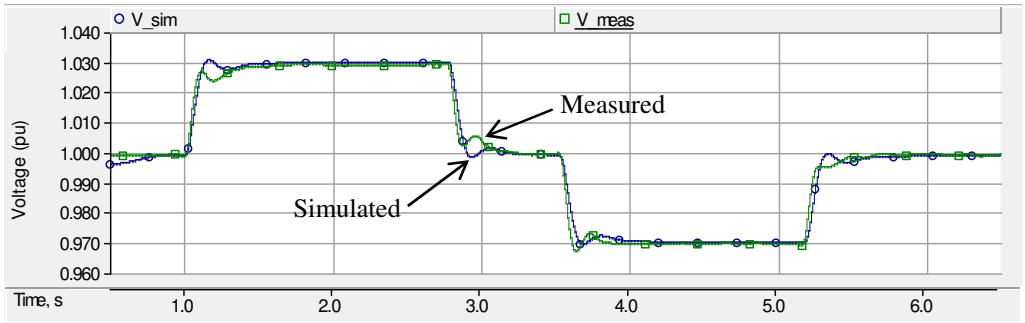

Fig. 119: Comparison of measured and simulated voltage for validating AVR gains.

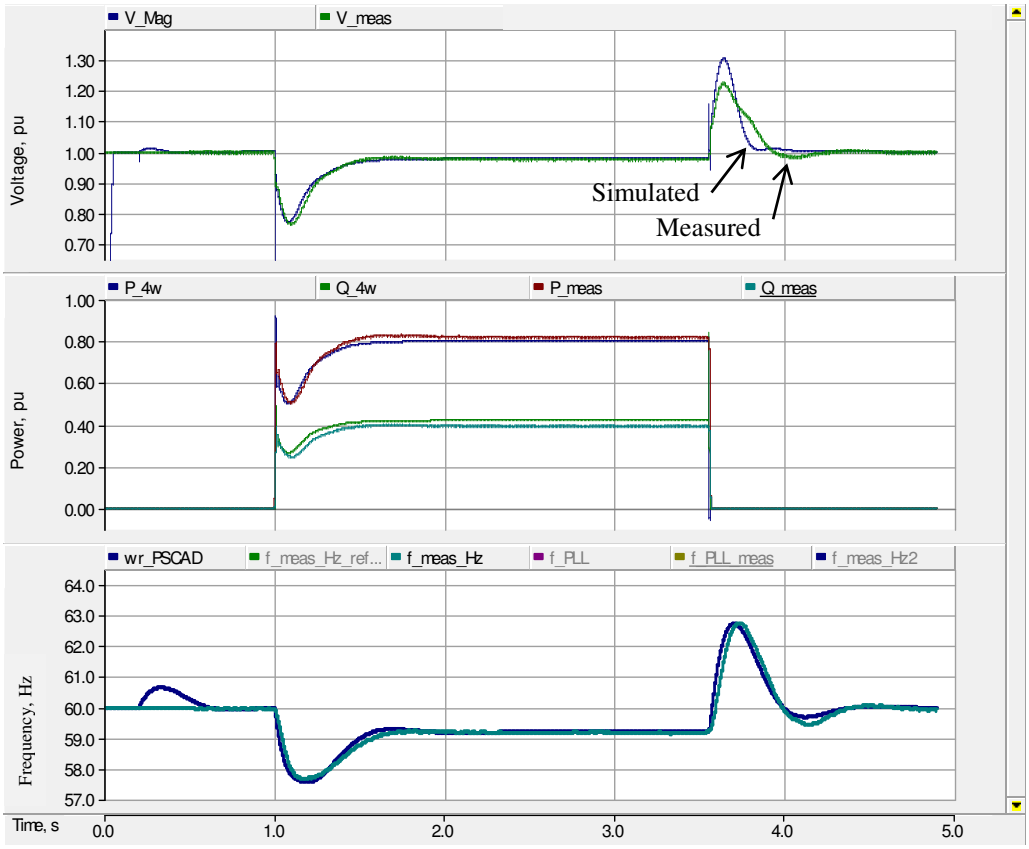

Fig. 120: Comparison of measured and simulated voltage for validating AVR gains.

REFERENCES

[1] H. B. Puttgen, P. R. MacGregor, and F. C. Lambert, "Distributed generation: Semantic hype or the dawn of a new era?," *IEEE Power and Energy Magazine,* vol. 1, pp. 22-29, 2003.

[2] P. Piagi and R. H. Lasseter, "Autonomous control of microgrids," in *Proc. Power Eng. Soc. General Meeting*, Montreal, Que., 18-22 June 2006.

[3] "DOE microgrid workshop report," U.S. Department of Energy, San Diego, CA, Aug. 30-31, 2011, [Online], Available: http://energy.gov/sites/prod/files/Microgrid Workshop Report August 2011.pdf.

[4] B. Kroposki, R. Lasseter, T. Ise, S. Morozumi, S. Papatlianassiou, and N. Hatziargyriou, "Making microgrids work," *IEEE Power and Energy Magazine,* vol. 6, pp. 40-53, 2008.

[5] N. Hatziargyriou, H. Asano, R. Iravani, and C. Marnay, "Microgrids," *IEEE Power and Energy Magazine,* vol. 5, pp. 78-94, 2007.

[6] R. H. Lasseter, "MicroGrids," in *Proc. Power Eng. Soc. Winter Meeting*, New York, NY, 27-31 Jan. 2002, pp. 305-308.

[7] F. Katiraei, R. Iravani, N. Hatziargyriou, and A. Dimeas, "Microgrids management," *IEEE Power and Energy Magazine,* vol. 6, pp. 54-65, 2008.

[8] A. L. Dimeas and N. D. Hatziargyriou, "Operation of a multiagent system for microgrid control," *IEEE Transactions on Power Systems,* vol. 20, pp. 1447-1455, 2005.

[9] H. Farhangi, "The path of the smart grid," *IEEE Power and Energy Magazine,* vol. 8, pp. 18-28, 2010.

[10] S. B. Van Broekhoven, N. Judson, S. V. T. Nguyen, and W. D. Ross, "Microgrid study: energy security for DoD installations," MIT Lincoln Laboratory, TR-1164, 18 June 2012, [Online], Available: http://serdp-estcp.org/content/download/15304/175087/version /3/file/MIT LL DoD Microgrid Study TR-1164 18Jun12.pdf.

[11] "Catalog of CHP technologies," U.S. Environmental Protection Agency, Dec. 2008, [Online], Available: http://www.epa.gov/chp/documents/catalog_chptech_full.pdf

[12] M. Pipattanasomporn, H. Feroze, and S. Rahman, "Multi-agent systems in a distributed smart grid: Design and implementation," in *Proc. IEEE PSCE '09*, Seattle, WA, 15-18 Mar. 2009.

[13] J. Rocabert, A. Luna, F. Blaabjerg, and P. Rodriguez, "Control of power converters in AC microgrids," *IEEE Transactions on Power Electronics,* vol. 27, pp. 4734-4749, 2012.

[14] K. De Brabandere, "Voltage and frequency droop control in low voltage grids by distributed generators with inverter front-end," Ph.D. Dissertation, Faculteit Ingenieurswetenschappen, K.U. Leuven, Belgium, 2006.

[15] M. C. Chandorkar, D. M. Divan, and R. Adapa, "Control of parallel connected inverters in standalone AC supply systems," *IEEE Transactions on Industry Applications,* vol. 29, pp. 136-143, 1993.

[16] M. Chandorkar, "Distributed uninterruptible power supply systems," Ph.D. Dissertation, Dept. Elect. Eng., Univ. of Wisconsin Madison, Madison, WI, 1995.

[17] L. Yun Wei and K. Ching-Nan, "An accurate power control strategy for power-electronics-interfaced distributed generation units operating in a low-voltage multibus microgrid," *IEEE Transactions on Power Electronics,* vol. 24, pp. 2977-2988, 2009.

[18] K. De Brabandere, B. Bolsens, J. Van den Keybus, A. Woyte, J. Driesen, and R. Belmans, "A Voltage and frequency droop control method for parallel inverters," *IEEE Transactions on Power Electronics,* vol. 22, pp. 1107-1115, 2007.

[19] J. He and Y. W. Li, "Analysis, design, and implementation of virtual impedance for power electronics interfaced distributed generation," *IEEE Transactions on Industry Applications,* vol. 47, pp. 2525-2538, 2011.

[20] J. M. Guerrero, J. Matas, L. G. de Vicuna, M. Castilla, and J. Miret, "Decentralized control for parallel operation of distributed generation inverters using resistive output impedance," *IEEE Transactions on Industrial Electronics,* vol. 54, pp. 994-1004, 2007.

[21] J. M. Guerrero, J. C. Vasquez, J. Matas, L. G. de Vicuna, and M. Castilla, "Hierarchical control of droop-controlled AC and DC microgrids; A general approach toward standardization," *IEEE Transactions on Industrial Electronics,* vol. 58, pp. 158-172, 2011.

[22] J. M. Guerrero, L. G. de Vicuna, J. Matas, M. Castilla, and J. Miret, "A wireless controller to enhance dynamic performance of parallel inverters in distributed generation systems," *IEEE Transactions on Power Electronics,* vol. 19, pp. 1205-1213, 2004.

[23] J. M. Guerrero, J. Matas, L. G. de Vicuna, M. Castilla, and J. Miret, "Wireless-control strategy for parallel operation of distributed-generation inverters," *IEEE Transactions on Industrial Electronics,* vol. 53, pp. 1461-1470, 2006.

[24] H. W. van der Broeck, H. C. Skudelny, and G. V. Stanke, "Analysis and realization of a pulsewidth modulator based on voltage space vectors," *IEEE Transactions on Industry Applications,* vol. 24, pp. 142-150, 1988.

[25] J. Restrepo, J. Aller, A. Bueno, V. Guzmán, and M. Giménez, "Generalized algorithm for pulse width modulation using a two-vectors based technique," *EPE Journal,* vol. 20, no. 2, pp. 30-39, 2011.

[26] P. C. Krause, O. Wasynczuk, and S. D. Sudhoff, *Analysis of Electric Machinery and Drive Systems*, 2nd ed. Piscataway, NJ: IEEE Press, 2002, ISBN: 047114326X.

[27] H. Fujita and H. Akagi, "The unified power quality conditioner: the integration of series and shunt-active filters," *IEEE Transactions on Power Electronics,* vol. 13, pp. 315-322, 1998.

[28] A. Timbus, M. Liserre, R. Teodorescu, P. Rodriguez, and F. Blaabjerg, "Evaluation of current controllers for distributed power generation systems," *IEEE Transactions on Power Electronics,* vol. 24, pp. 654-664, 2009.

[29] M. P. Kazmierkowski and L. Malesani, "Current control techniques for three-phase voltage-source PWM converters: a survey," *IEEE Transactions on Industrial Electronics,* vol. 45, pp. 691-703, 1998.

[30] D. N. Zmood, D. G. Holmes, and G. H. Bode, "Frequency-domain analysis of three-phase linear current regulators," *IEEE Transactions on Industry Applications,* vol. 37, pp. 601-610, 2001.

[31] S. K. Chung, "A phase tracking system for three phase utility interface inverters," *IEEE Transactions on Power Electronics,* vol. 15, pp. 431-438, 2000.

[32] N. Pogaku, M. Prodanovic, and T. C. Green, "Modeling, analysis and testing of autonomous operation of an inverter-based microgrid," *IEEE Transactions on Power Electronics,* vol. 22, pp. 613-625, 2007.

[33] Y. Mohamed and E. F. El-Saadany, "Adaptive decentralized droop controller to preserve power sharing stability of paralleled inverters in distributed generation microgrids," *IEEE Transactions on Power Electronics,* vol. 23, pp. 2806-2816, 2008.

[34] M. A. Zamani, A. Yazdani, and T. S. Sidhu, "A control strategy for enhanced operation of inverter-based microgrids under transient disturbances and network faults," *IEEE Transactions on Power Delivery,* vol. 27, pp. 1737-1747, 2012.

[35] L. Poh Chiang and D. G. Holmes, "Analysis of multiloop control strategies for LC/CL/LCL-filtered voltage-source and current-source inverters," *IEEE Transactions on Industry Applications*

vol. 41, pp. 644-654, 2005.

[36] R. Lasseter and M. Erickson, "Integration of battery-based energy storage element in the CERTS microgrid " University of Wisconsin-Madison, Oct. 2009, [Online], Available: http://certs.lbl.gov/certs-der-pubs.html.

[37] H. Nikkhajoei and R. H. Lasseter, "Distributed generation interface to the CERTS microgrid," *IEEE Transactions on Power Delivery,* vol. 24, pp. 1598-1608, 2009.

[38] J. M. Guerrero, J. C. Vasquez, J. Matas, M. Castilla, and L. G. de Vicuna, "Control strategy for flexible microgrid based on parallel line-interactive UPS systems," *IEEE Transactions on Industrial Electronics,* vol. 56, pp. 726-736, 2009.

[39] C. A. Plet and T. C. Green, "A method of voltage limiting and distortion avoidance for islanded inverter-fed networks under fault," in *Proc. European Conference on Power Electronics and Applications (EPE)*, Birmingham, UK, Aug. 30-Sept. 1 2011.

[40] "Caterpillar Digital Voltage Regulator (CDVR): Specifications, System Operation,Testing, and Adjusting Guide," Caterpillar, Inc., RENR7941-01, May 2005.

[41] "DVR 2000E Technical Information," Marathon Electric Mfg. Corp., GPN019, Mar. 2006, [Online], Available: http://www.marathonelectric.com/generators/docs/manuals/GPN019WB.pdf.

[42] M. S. Sarma, *Electric Machines*, 2nd ed. St. Paul, MN: West, 1994, ISBN: 0534938434.

[43] "IEEE recommended practice for excitation system models for power system stability studies," *IEEE Std. 421.5-2005,* 2006.

[44] V. Friedel, "Modeling and simulation of a hybrid wind-diesel microgrid," Master's Thesis, School of Elect. Eng., Royal Inst. of Tech., Stockholm, Sweden, 2009.

[45] S. Roy, O. P. Malik, and G. S. Hope, "A k-step predictive scheme for speed control of diesel driven power plants," *IEEE Transactions on Industry Applications,* vol. 29, pp. 389-396, 1993.

[46] Z. Miao, A. Domijan, and L. Fan, "Investigation of microgrids with both inverter interfaced and direct AC-connected distributed energy resources," *IEEE Transactions on Power Delivery,* vol. 26, pp. 1634-1642, 2011.

[47] F. Katiraei and M. R. Iravani, "Power management strategies for a microgrid with multiple distributed generation units," *IEEE Transactions on Power Systems,* vol. 21, pp. 1821-1831, 2006.

[48] C. Il-Yop, L. Wenxin, D. A. Cartes, E. G. Collins, and M. Seung-Il, "Control methods of inverter-interfaced distributed generators in a microgrid system," *IEEE Transactions on Industry Applications,* vol. 46, pp. 1078-1088, 2010.

[49] R. H. Lasseter and P. Paigi, "Microgrid: a conceptual solution," in *Proc. IEEE-PESC '04*, Aachen, Germany, 20-25 June 2004, pp. 4285-4290.

[50] J. A. P. Lopes, C. L. Moreira, and A. G. Madureira, "Defining control strategies for microgrids islanded operation," *IEEE Transactions on Power Systems,* vol. 21, pp. 916-924, 2006.

[51] S. Krishnamurthy, "On the modeling and control of wound field synchronous machine based gensets for operation in a microgrid environment," Ph.D. Dissertation, Dept. Elect. Eng., Univ. of Wisconsin Madison, Madison, WI, 2008.

[52] S. Krishnamurthy, T. M. Jahns, and R. H. Lasseter, "The operation of diesel gensets in a CERTS microgrid," in *Proc. Power & Energy Soc. General Meeting*, Pittsburgh, PA, 20-24 July 2008.

[53] M. Dewadasa, A. Ghosh, and G. Ledwich, "Dynamic response of distributed generators in a hybrid microgrid," in *Proc. Power & Energy Soc. General Meeting*, Detroit, MI, 24-29 July 2011.

[54] T. L. Vandoorn, B. Meersman, J. D. M. De Kooning, and L. Vandevelde, "Directly-coupled synchronous generators with converter behavior in islanded microgrids," *IEEE Transactions on Power Systems,* vol. 27, pp. 1395-1406, 2012.

[55] F. Katiraei, M. R. Iravani, and P. W. Lehn, "Micro-grid autonomous operation during and subsequent to islanding process," *IEEE Transactions on Power Delivery,* vol. 20, pp. 248-257, 2005.

[56] L. Yunwei, D. M. Vilathgamuwa, and L. Poh Chiang, "Design, analysis, and real-time testing of a controller for multibus microgrid system," *IEEE Transactions on Power Electronics,* vol. 19, pp. 1195-1204, 2004.

[57] C. A. Hernandez-Aramburo, T. C. Green, and N. Mugniot, "Fuel consumption minimization of a microgrid," *IEEE Transactions on Industry Applications,* vol. 41, pp. 673-681, 2005.

[58] "IEEE guide for design, operation, and integration of distributed resource island systems with electric power systems," *IEEE Std. 1547.4-2011,* 2011.

[59] N. Jayawarna and M. Barnes, "Assessing marginal value of stage 2 microgrids," in *Proc. Power & Energy Soc. General Meeting*, Minneapolis, MN, 25-29 July 2010.

[60] D. Divan, R. Schneider, and D. Bielinski, "Industrial-strength sag correction," Power Quality Mag., Mar. 2002, [Online], Available: http://ecmweb.com/power-quality-archive/industrial-strength-sag-correction.

[61] D. Divan, A. Bendre, W. Kranz, and R. Schneider, "Dual source dynamic sag correctors-a cost effective topology for enhancing the reliability of dual source systems," in *Proc. IAS Annual Meeting*, Salt Lake City, UT, 12-16 Oct. 2003, pp. 940-947.

[62] D. D. Sabin, "An assessment of distribution system power quality," Electric Power Research Institute, EPRI TR-106294-V2, May 1996.

[63] W. E. Brumsickle, R. S. Schneider, G. A. Luckjiff, D. M. Divan, and M. F. McGranaghan, "Dynamic sag correctors: cost-effective industrial power line conditioning," *IEEE Transactions on Industry Applications,* vol. 37, pp. 212-217, 2001.

[64] A. Prasai and D. M. Divan, "Zero-energy sag correctors - optimizing dynamic voltage restorers for industrial applications," *IEEE Transactions on Industry Applications,* vol. 44, pp. 1777-1784, 2008.

[65] S. Karve, "Three of a kind [UPS topologies, IEC standard]," *IEE Review,* vol. 46, pp. 27-31, 2000.

[66] M. Ton and B. Fortenbury, "High performance buildings: data centers UPS," Dec. 2005, [Online], Available: http://hightech.lbl.gov/documents/UPS/Final_UPS_Report.pdf.

[67] L. Giuntini, "Harmonics reduction in high-efficiency operation of double-conversion UPS," in *Proc. European Conference on Power Electronics and Applications (EPE)*, Birmingham, UK, 30 Aug.-1 Sept. 2011.

[68] S. Guoqiao, X. Dehong, and Y. Xiaoming, "A novel seamless transfer control strategy based on voltage amplitude regulation for utility-interconnected fuel cell inverters with an LCL-filter," in *Proc. IEEE-PESC '06*, Jeju, Korea, 18-22 June 2006.

[69] S. Barsali, M. Ceraolo, P. Pelacchi, and D. Poli, "Control techniques of dispersed generators to improve the continuity of electricity supply," in *Proc. Power Eng. Soc. Winter Meeting*, New York, NY, 27-31 Jan. 2002, pp. 789-794.

[70] W. Fei, J. L. Duarte, and M. A. M. Hendrix, "Grid-interfacing converter systems with enhanced voltage quality for microgrid application - concept and implementation," *IEEE Transactions on Power Electronics,* vol. 26, pp. 3501-3513, 2011.

[71] J. Rocabert, G. M. S. Azevedo, A. Luna, J. M. Guerrero, J. I. Candela, and P. Rodriguez, "Intelligent connection agent for three-phase grid-connected microgrids," *IEEE Transactions on Power Electronics,* vol. 26, pp. 2993-3005, 2011.

[72] "Electric Power SpecSizer," Version 2.7.0, Caterpillar Inc., [Online], Available: http://www.cat.com/powergeneration/specsizer.

[73] "Technical reference – grid connect operation – Capstone Model C30 and C60/C65," Capstone Turbine Corporation, [Online], Available: www.capstoneturbine.com.

[74] "Technical Reference – Capstone Model C60/C65 Electrical," Capstone Turbine Corporation, [Online], Available: www.capstoneturbine.com.

[75] S. Schoeng, "Energy storage systems cost update," Sandia National Laboratories, SAND2011-2730, Apr. 2011, [Online], Available: http://prod.sandia.gov/techlib/access-control.cgi/2011/112730.pdf.

[76] "Application guide – Capstone Model C65 Hybrid UPS," Capstone Turbine Corporation, [Online], Available: www.capstoneturbine.com.

[77] R. H. Lasseter, "Smart distribution: Coupled microgrids," *Proceedings of the IEEE,* vol. 99, pp. 1074-1082, 2011.

[78] S. Grubic, B. Amlang, W. Schumacher, and A. Wenzel, "A high-performance electronic hardware-in-the-loop drive-load simulation using a linear inverter (LinVerter)," *IEEE Transactions on Industrial Electronics,* vol. 57, pp. 1208-1216, 2010.

[79] S. Lentijo, S. D'Arco, and A. Monti, "Comparing the dynamic performances of power hardware-in-the-loop interfaces," *IEEE Transactions on Industrial Electronics,* vol. 57, pp. 1195-1207, 2010.

[80] Q. Zhong and G. Weiss, "Synchronverters: Inverters that mimic synchronous generators," *IEEE Transactions on Industrial Electronics,* vol. 58, pp. 1259 - 1267, 2010.

[81] M. Torres and L. A. C. Lopes, "Inverter-based virtual diesel generator for laboratory-scale applications," in *Proc. IEEE-IECON'10*, Glendale, AZ, 7-10 Nov. 2010, pp. 532-537.

[82] H. P. Beck and R. Hesse, "Virtual synchronous machine," in *Proc. Electrical Power Quality and Utilisation*, Barcelona, Spain, 9-11 Oct. 2007.

[83] *PSCAD/EMTDC User Manual*. Version 4.7, Manitoba HVDC Research Centre.

[84] C.-T. Lee, C.-C. Chu, and P.-T. Cheng, "Quantitative analysis of system parameters asymmetry on droop-controlled converters," in *Proc. IEEE-ECCE'12*, Raleigh, NC, 15-20 Sept. 2012.

[85] F. Katiraei, M. R. Iravani, and P. W. Lehn, "Small-signal dynamic model of a micro-grid including conventional and electronically interfaced distributed resources," *Generation, Transmission & Distribution, IET,* vol. 1, pp. 369-378, 2007.

[86] P. Kundur, *Power System Stability and Control*. New York: McGraw-Hill, 1994, ISBN: 007035958X.

[87] "Electric Power Applications, Engine & Generator Sizing - Application and Installation Guide," Caterpillar, Inc., LEBE5294-02, 2008.

[88] "Military Standard: Definitions of Tactical, Prime, Precise, and Utility Terminologies for Classification of the DOD Mobile Electric Power Engine Generator Set Family," *MIL-STD-1332B,* 1973.

[89] "Military Standard: Aircraft Electric Power Characteristics," *MIL-STD-704F,* 2008.

[90] M. S. Moon and R. W. Johnson, "DSP control of UPS inverter with over-current limit using droop method," in *Power Electronics Specialists Conference, 1999. PESC 99. 30th Annual IEEE*, 1999, pp. 552-557 vol.1.

[91] M. N. Marwali and A. Keyhani, "Control of distributed generation systems-Part I: Voltages and currents control," *IEEE Transactions on Power Electronics,* vol. 19, pp. 1541-1550, 2004.

[92] C. A. Plet, M. Brucoli, J. D. F. McDonald, and T. C. Green, "Fault models of inverter-interfaced distributed generators: Experimental verification and application to fault analysis," in *Proc. Power & Energy Soc. General Meeting*, Detroit, MI, 24-29 July 2011.

[93] A. Bergen, *Power Systems Analysis*, 1st ed. Englewood Cliffs, NJ: Prentice-Hall, 1986, ISBN: 0136878644.

[94] D. G. Holmes, T. A. Lipo, B. P. McGrath, and W. Y. Kong, "Optimized Design of Stationary Frame Three Phase AC Current Regulators," *IEEE Transactions on Power Electronics,* vol. 24, pp. 2417-2426, 2009.

[95] T. Loix, T. Wijnhoven, and G. Deconinck, "Protection of microgrids with a high penetration of inverter-coupled energy sources," in *Integration of Wide-Scale Renewable Resources Into the Power Delivery System, 2009 CIGRE/IEEE PES Joint Symposium*, 2009, pp. 1-6.

[96] "Power swing and out-of-step considerations on transmission lines," IEEE PES PSRC WG D6, July 19, 2005, [Online], Available: http://www.pes-

psrc.org/Reports/Power Swing and OOS Considerations on Transmission Lines F..pdf.